A bioengineered 3D model to study the crosstalk between mammary epithelial cells and fibroblasts

Mariana Mendes Martins Coelho

Dissertation for the Degree of Master of Science in Bioengineering at Faculdade de Engenharia da Universidade do Porto and Instituto de Ciências Biomédicas Abel Salazar da Universidade do Porto

U.PORTO FEUP FACULDADE DE ENGENHARIA UNIVERSIDADE DO PORTO
U.PORTO INSTITUTO DE CIÊNCIAS BIOMÉDICAS ABEL SALAZAR UNIVERSIDADE DO PORTO
3S INSTITUTO DE INVESTIGAÇÃO E INOVAÇÃO EM SAÚDE UNIVERSIDADE DO PORTO
INEB Instituto de Engenharia Biomédica

A bioengineered 3D model to study the crosstalk between mammary epithelial cells and fibroblasts

Mariana Mendes Martins Coelho

Dissertation for the Degree of Master of Science in Bioengineering at Faculdade de Engenharia da Universidade do Porto and Instituto de Ciências Biomédicas Abel Salazar da Universidade do Porto

Supervisor: Cristina Barrias

Co-supervisors: Sílvia Bidarra and Sara Neves

June 2019

U.PORTO FEUP FACULDADE DE ENGENHARIA UNIVERSIDADE DO PORTO

U.PORTO INSTITUTO DE CIÊNCIAS BIOMÉDICAS ABEL SALAZAR UNIVERSIDADE DO PORTO

3S INSTITUTO DE INVESTIGAÇÃO E INOVAÇÃO EM SAÚDE UNIVERSIDADE DO PORTO

INEB Instituto de Engenharia Biomédica

“Tell me and I forget.
Teach me and I remember.
Involve me and I learn.”

- Benjamin Franklin

This page was intentionally left in blank

AGRADECIMENTOS

Gostaria de agradecer, em primeiro lugar, à Cristina Barrias, que me acolheu no grupo assim que lhe perguntei se podia fazer a tese por cá, e me ajudou, com paciência infinita, de outubro a julho. É um prazer trabalhar com e para uma G*roup Leader* como a Cristina, cheia de ideias e com vontade de as pôr em prática, e que não descarta nenhuma sugestão vinda de mentes ainda tão pequeninas no mundo da ciência, como é a minha. Vi em si uma líder, mas também uma amiga e conselheira, não só para o trabalho no laboratório, mas também para decisões futuras. Obrigada por todos os conselhos, votos de confiança e tentativas de suavizar o meu negativismo ou inseguranças. Obrigada por acreditar desde o início que conseguiríamos construir este modelo e por dizer sempre "vais ver, vai ficar fantástico!".

Não podem faltar agradecimentos às minhas duas co-supervisoras: Sara Neves e Sílvia Bidarra. Sara, foste a minha primeira amiga no laboratório. Obrigada por me introduzires a todo o pessoal da melhor maneira, e de me introduzires àquela que se tornaria na minha melhor amiga dentro do laboratório 107. A nossa querida impressora 3D! Ajudaste-me a desfazer o "bicho de 7 cabeças" que a *printer* se estava a tornar, e ensinaste-me a compreendê-la e trabalhar com ela da melhor maneira possível. À Sílvia, muito obrigada pela paciência de santa que teve comigo, desde os primeiros dias passados em frente à câmara de fluxo a ouvir as minhas perguntas demasiado básicas, aos últimos, passados em frente ao confocal à procura "da célula perfeita!". Ensinou-me que por muitos erros que se cometa na bancada, depois de feito, é impossível voltar atrás, e que por isso o melhor é mesmo continuar em frente, sempre de cabeça erguida. Às duas, quero agradecer todo o *input* valioso que foram dando ao longo deste processo, e toda a ajuda que disponibilizaram sempre que precisei. Sem vocês teria sido, literalmente, impossível apresentar todo este trabalho.

Um agradecimento especial aos colegas de trabalho, que foram acompanhando o meu progresso. Obrigada pela contribuição de cada um, com soluções inovadoras para resolver qualquer problema que surgisse, ou com sorrisos e palavras de encorajamento. Um obrigada especial à Tália, pela gigante ajuda e constante boa disposição, e pelo carinho pela sua "Lurdinhas". Obrigada ao Carlos, o espanhol mais português, pela amizade, pelas discussões científicas e por ser incansável sempre que lhe pedi ajuda ou conselhos. Obrigada à Patrícia, pela ajuda no desenvolvimento do trabalho e por todos os conselhos e sugestões para torná-lo o mais robusto possível. E obrigada a todos os restantes, à Mariana Neves, à Filipa, ao Marco, aos Daniéis, ao Rúben, ao Tiago… Por tornarem o laboratório num local divertido e para o qual foi sempre bom vir trabalhar.

Não menos importante, quero agradecer a todos aqueles que iniciaram e completaram este percurso de 5 anos comigo… Ao pessoal de Bio, que "sofreu" tudo em conjunto, desde as primeiras frequências, às monografias, relatórios e finalmente à tese. Às amigas que vão ficar no coração, Filipa e Maria; às parceiras de sebentas e estudo, Lena e Patrícia; à direção do NEB, Paulo Maia e Marianita; aos parceiros de laboratório, de bancada e de carteira, Margarida, Silveira, Sara e Raio. Ajudaram a tornar o curso na experiência mais transversal, mais interessante e, atrevo-me a dizer, mais divertida e diversa que tive até hoje.

Por último, um obrigada em maiúsculas à minha família e aos meus amigos de sempre. Pai e mãe, dois pilares tão diferentes mas tão complementares entre si. Ao pai, pela racionalidade e pela dedicação cega à nossa família; à mãe, pelo miminho e pela força que sempre transmitiu e continua a transmitir. Aos dois, pela vontade em compreender a ciência que faço, e em festejar todos os meus sucessos mais do que eu própria. À minha irmã e minha melhor amiga, obrigada por existires e por me ensinares a ser melhor pessoa todos os dias. À titi, ao Pedro, ao tio e aos avós, à Cuka e à Branquita, obrigada por serem a melhor família de sempre e por serem a fonte de toda a força que tenho para seguir este meu caminho. Aos amigos, Cascais, Inês, Rafa, Rita, Carlos, Pedro, João, Marta, Maria e a todos os outros que estiveram presentes nos últimos 5 anos: obrigada pela vossa amizade.

Em Filosofia aprendemos que o ser humano é um ser social, que é com e para os outros. Nada faz mais sentido para mim do que esta frase. Obrigada a todos os que rodeiam este ser social que sou eu própria e que asseguram cada passo, cada decisão, que suavizam cada derrota e celebram cada vitória. Esta vitória é só mais uma, estou certa de que mais virão entretanto.

The research described in this thesis was financially supported by:

Project 3DEMT funded by POCI via FEDER (POCI-01-0145-FEDER-016627) and by FCT via OE (PTDC/BBB-ECT/2518/2014).

ABSTRACT

Breast tissue is a highly complex tissue, which undergoes various morphological and functional alterations throughout a woman's life. The breast is composed by mammary gland epithelial cells and a variety of stromal cell types, which interact in several different ways, depending on internal and external stimuli. Improved knowledge on this crosstalk would enable a better understanding of both healthy and pathological dynamic alterations of breast tissue.

Most studies in breast tissue and breast cancer have been developed in simplistic 2D models, which greatly fail to recapitulate natural cellular microenvironments. Others have been made in complex *in vivo* models, which raise ethical concerns, are more expensive and difficult to use, and may fail to reproduce some processes/mechanisms occurring in humans. Therefore, the use of "intermediate" 3D *in vitro* models that mimic several features of native tissues, stands up as a promising alternative.

In this work, we aimed at developing an advanced 3D *in vitro* model, incorporating multiple components of breast tissue, namely stromal cells and their extracellular matrix (ECM) and parenchymal epithelial cells. For this purpose, porous alginate scaffolds were produced by-design using extrusion-based 3D printing and, on a first stage, were populated with human mammary fibroblasts. After testing different culture parameters, optimal scaffolds were developed, where fibroblasts were able to adhere, spread and produce endogenous ECM, providing acceptable coverage of the scaffold fibers, without obstructing the pores. On a second stage, mammary gland epithelial cells were embedded in a gel precursor solution, which filled the scaffold's pores, forming a hydrogel inside. Along time, these cells underwent epithelial morphogenesis forming typical mammary acinar-like structures. This generated a heterotypic co-culture model that partially recapitulates stromal-parenchymal interactions in breast tissue.

In a variation of the model, scaffolds populated by fibroblasts were decellularized. In the future, this setting can be alternatively used for studying direct interactions between fibroblast-derived ECM and mammary gland epithelial cells. Preliminary tests were made aiming at developing miniaturized versions of the printed scaffolds, which can be used for improving the throughput of modeling and analysis.

Validation of the heterotypic model included the discrimination of both cell types, after recovery from dissolved alginate hydrogels, using cell type-specific markers and flow cytometry. After future optimizations, discriminating the different cell populations will allow for cell sorting and a more detailed analysis of cells after culture, namely at gene and protein levels. Such techniques will allow to investigate the crosstalk between mammary epithelial and stromal cells in more detail, which may provide important insights into physiological and pathological processes.

Collectively, results from this work represent an important step towards the development of a new 3D *in vitro* model for studying stromal-parenchymal interactions in breast tissue, both under physiological and pathological conditions, with clear implications in both regenerative medicine and cancer treatments.

This page was intentionally left in blank

CONTENTS

LIST OF FIGURES

This page was intentionally left in blank

LIST OF TABLES

LIST OF EQUATIONS

This page was intentionally left in blank

LIST OF ABBREVIATIONS

2D – two-dimensional

3D – three-dimensional

ALG – alginate (unpurified)

(calcein) AM – (calcein) acetoxymethyl

BF – bright field

BM – basement membrane

BSA – bovine serum albumin

CAD – computer-aided design

Ca^{2+} – calcium ion

$CaCl_2$ – calcium chloride

$CaCO_3$ – calcium carbonate

CAFs – cancer-associated fibroblasts

CDM – cellular-derived matrix

CLSM – confocal laser scanning microscopy

CO_2 – carbon dioxide

dECM – decellularized extracellular matrix

DMEM – Dulbecco's Modified Eagle Medium

DMSO – dimethyl sulfoxide

DNA – deoxyribonucleic acid

DNAse – deoxyribonuclease

ECM – extracellular matrix

EDC – 1-ethyl-3-(3-dimethylaminopropyl)-carbodiimide

EDTA – 2,2',2'',2'''-(ethane-1,2-diyldinitrilo)tetraacetic acid

EGF – epidermal growth factor

EMT – epithelial-to-mesenchymal transition

Ex/em – excitation/emission

FACS – flow-assisted cell sorting

FBS – fetal bovine serum

FC – flow cytometry

FN – fibronectin

GAGs – glycosaminoglycans

GDL – D-glucono-delta-lacton

H – hour(s)

hASCs – human adipose-derived stem cells

HBSS – Hank's balanced salt solution

hMECs – human mammary epithelial cells

hMFs – human mammary fibroblasts

MEFs – mouse embryonic fibroblasts

MES – 2-(N-morpholino)ethanesulfonic acid

Min – minute(s)

Na^+ – sodium ion

NaCl – sodium chloride

NH_4OH – ammonium hydroxide

NHS – N-hydroxysuccinimide

ON – overnight

P-ALG – purified alginate

PBS – phosphate buffered saline

Pen-Strep – penicillin-streptomycin

PFA – paraformaldehyde

pHEMA – polyhydroxyethylmethacrylate

PI – propidium iodide

RGD – arginine-glycine-aspartic acid

RNA – ribonucleic acid

Rpm – rotations per minute

RT – room temperature

S – second(s)

SDS – sodium dodecyl sulfate

SI – supplementary information

TCPS – tissue culture polystyrene

TDLU – terminal duct lobular unit

TGF-β – transforming growth factor beta

TME – tumor microenvironment

TNBC – triple negative breast cancer

This page was intentionally left in blank

INTRODUCTION

1. 3D cell culture models for *in vitro* research

In the human body, nearly all cells reside in a complex, three-dimensional (3D) fiber-intertwined network, with varied distribution of biochemical and physical signals [1]. Although virtually all cell types can be efficiently cultured on flat substrates, under appropriate conditions, more complex settings are fundamental to more closely recapitulate *in vivo* behavior [2]. A key player of the cell microenvironment is the extracellular matrix (ECM), a highly dynamic, non-cellular component of every tissue. The ECM is mainly composed of water, proteins and polysaccharides, although its composition varies with the type of tissue, with age and under pathological conditions, such as fibrosis and cancer. The ECM undergoes constant remodeling, supporting dynamic cell growth, organization and differentiation, thus allowing morphogenetic phenomena to occur [3,4].

The properties of the ECM depend on the presence and ratio of different components: ECM fibrous proteins, namely collagen, mostly produced by stromal fibroblasts, and elastin, contribute to its tensile strength, regulate cell adhesion and support chemotaxis and migration. More specialized proteins, namely fibronectin (FN) or laminin, are responsible for mediating specific cell-ECM interactions and crosstalk [4]. On the other hand, glycosaminoglycans (GAGs) play an important role in regulating tissue buffering, hydration and permeability, as well as in modulating viscoelastic properties [4].

It is currently well-established that the local microenvironment, or niche, of a cell is essential in regulating its behavior [5]. Thus, spatial-temporal changes in the ECM may strongly affect molecular/cellular mechanisms and induce significant alterations in normal cell function [6]. For example, in tumor development, aberrant behavior of cancer cells leads to loss of tissue organization and, in many cases, to an increase in stiffness, which will in turn affect cancer progression [7,8]. Changes in tumor ECM occur essentially due to a dynamic and bi-directional communication between cancer cells and matrix-producing stromal cells [4,5].

This highlights the importance of using advanced cell culture systems when studying biological processes, which may mimic relevant features of the microenvironment of native tissues, namely by taking into account the presence of the ECM and/or of different cell types.

1.1. 2D vs. 3D cell culture models: shifting the paradigm

Most studies on *in vitro* cultured cells published over the past years have been performed using 2D surfaces, generally presented as tissue culture polystyrene (TCPS) flasks, well-plates and dishes, mainly due to practical advantages, including ease of use [2]. However, these substrates present considerable limitations, and several studies report that 2D-growing cells do not behave as their *in vivo* counterparts, undergoing both genotypic and phenotypic alterations [3]. Cells cultured on flat surfaces typically grow as monolayers, mainly composed of stretched, proliferating cells, with forced polarity [9]. They are exposed to abnormal soluble factor gradients that induce distinct polarization on the cells' edges and bulk [10], promoting altered mechano-transduction and affecting intracellular signaling pathways and phenotypic fate [11]. While on an *in vivo* microenvironment cells are normally exposed to 3D gradients of soluble factors, nutrients and cytokines [12], 2D culture induces a quasi-homogeneous concentration of each of these molecules. This will have obvious influences on cell-cell and cell-ECM communication and their dynamic interactions. In turn, these will impact processes like differentiation, apoptosis, cell proliferation and metabolism. Cells cultured in 2D are normally confined to plane surfaces, making it hard to properly recapitulate native processes, namely cell migration and motility, with key roles during tumor invasion and metastization. In contrast, in 3D, cells are surrounded by matrix that creates a physical barrier, limiting cell movement [10,13]. In this sense, diverse studies have determined that cells in 3D behave closer to their native parental cells in a range of processes, such as the formation of breast acinar-like structures. This has been mimicked using different approaches, namely using 3D spheroid culture, or by evaluating the capacity of cells to migrate/invade across layers of ECM proteins or Matrigel™ [14]. Recapitulating, cells in 2D are not exposed to biologically relevant cell-cell and cell-ECM stimuli, and the abnormal interactions with the surrounding environment may induce meaningful alterations in 2D cultures [10,13,14].

On the other hand, *in vivo* studies using animal models such as mice or rats, still represent the golden standard for validation of most biological studies. These models present much higher complexity when compared to any *in vitro* mimic, allowing assessment of combined features of native processes occurring in the body. However, such models are also expensive, raise ethical concerns, and their use is extremely difficult to certify, as they are subject to strict regulation from the responsible authorities. This often results in studies with low numbers of replicates that may lack scientific rigor. So, they represent models with higher physiological relevance, but lower experimental tractability. Moreover, some processes occurring in animals may not resemble the original human condition. Therefore, whenever possible, the use of

animal models should be reduced/replaced by others, namely by advanced 3D *in vitro* models [15,16]. Hence, over the last years, 3D cell culture systems were introduced to bridge the gap between 2D monolayer cell culture and animal models.

The main goal of 3D culture models is to provide cells with a way to organize themselves into geometrically and biologically functional structures [14]. By adding a new dimension to *in vitro* studies, 3D models more closely resemble the *in vivo* tissue architecture, inducing more natural cellular responses and minimizing morphological and physiological variations [10,17]. This can be achieved either by using a physical 3D support (scaffold-based approach) or by inducing cells to self-assemble into multicellular structures (scaffold-free approach). In the next section an overview of scaffold-based approaches for 3D cell culture will be provided.

1.2. 3D models using scaffold-based approaches

Scaffold-based 3D cell culture platforms can be produced using biomaterials from either natural or synthetic sources, representing a popular strategy to provide cells with a more complex environment that better mimics a native tissue. Current biomaterials offer a wide range of features and properties, and their application in cell and tissue engineering has largely increased over the last years. Advanced biomaterials may be fine-tuned to play the role of an artificial ECM, and recapitulate the natural cell milieu, both in healthy and diseased tissue conditions. By providing adequate biochemical, biomechanical and structural support for a certain cell type, or combination of cells, a biomaterial may support/promote different cell processes, such as adhesion, growth, differentiation, and ultimately morphogenesis [18–21].

Apart from their therapeutic uses, biomaterials are nowadays also being widely used as ECM analogues, to study cell biology and pathophysiological processes *in vitro* [18,22]. Scaffold-based models can be very versatile and be tuned according to their specific application. 3D scaffolds for cell culture are generally based on polymers, ceramics, or combinations of these. Synthetic substrates present well-defined composition and mechanical properties, ensuring higher tunability and reproducibility. Naturally-derived scaffolds are often made of protein-based or polysaccharide-based materials, being more physiological but also presenting batch-to-batch variation [10,23].

Polymeric hydrogels are amongst the most popular materials used for scaffold fabrication. These can either be processed into micro-/macro-porous 3D scaffolds, where cells can be cultured “on top” (often considered as 2.5D conditions), or as softer nano-porous matrices, where cells can be entrapped and cultured inside (true 3D conditions) [18]. Hydrogels have high water content, are compliant and permeable, thus resembling the native ECM and

providing an adequate 3D microenvironment to cells in culture. A great advantage of hydrogel-forming biomaterials is their high versatility: they can be modified to improve mechanical and biochemical properties, so as to better mimic native tissues [24]. In addition, they can be inherently biodegradable, or modified for induced degradability, so that the polymeric network gradually disappears, generating internal space that facilitates cellular activities/function, including ECM production [10,18].

Naturally-derived hydrogels, such as those based on collagen or hyaluronic acid, present intrinsic bioactivity and are typically used as matrices for 3D cell culture. However, the use of single-component hydrogels fails to recreate the high complexity of native ECMs. On the other hand, purified protein substrates are quite expensive. More complex hydrogel formulations are also widely used, namely Matrigel™, a solubilized ECM derived from mouse sarcoma, which contains multiple ECM components and growth factors [23]. Yet, its unknown composition, batch-to-batch variability, and animal origin are undesirable for *in vitro* studies, as they may lead to inconsistencies and poor reproducibility of obtained results [25,26]. Importantly, distinct 3D matrices modulate cell behavior in different ways. For instance, Krause et al. studied mammary gland stromal-epithelial interactions by establishing co-cultures of fibroblasts and epithelial cells in type I collagen and/or Matrigel™ matrices. Formation of branched ducts in collagen, and of both alveoli and ducts in the combined collagen-Matrigel™ matrix were observed. Also, epithelial structures only formed a basement membrane (BM) when cultured in the combined matrix. This experiment shows the effect of matrix features on cell behavior and organization, and highlights the importance of taking this into account when interpreting results and drawing conclusions from 3D studies [27].

Synthetic hydrogels and some non-animal derived natural hydrogels, such as alginate, have also been used, given their biocompatibility and tunability [10,18,27]. Such polymers are advantageous since they offer a “blank slate” that makes room for a range of possible modifications, thus allowing substrate customization [28]. Polymer modifications can range from biochemical alterations, via incorporation of bioactive cues for example, to biomechanical alterations, through modulation of network density/porosity or incorporation of stiff components [29,30]. One drawback of such materials is that they lack cellular recognition domains, such as integrin-binding adhesion sites, thus promoting a low level of interaction with seeded cells [31]. Yet, this can be easily overcome through incorporation of specific biologically active moieties, increasing the similarities with *in vivo* environments, and extending hydrogels’ versatility and applicability [32].

Due to their comparable compliance, hydrogels have been often used as 3D substrates for modeling soft tissues, such as breast tissue [18]. An overview of such applications will be provided in the following section.

2. Breast tissue

The breast is a structure overlying the *pectoralis major* muscles. In females, it corresponds to the mammary gland, mainly composed of white adipose, connective and glandular tissue. When fully developed, the breast has 14-18 glandular lobules, connected to milk ducts, which converge into the nipple (**Figure 1**A). The areola (pigmented skin area surrounding the nipple) contains sweat and sebaceous glands. Histologically, the breast includes two main structures (large ducts and terminal duct lobular units), two epithelial cell types (luminal and myoepithelial cells) and two types of stroma (inter- and intralobular) [33].

The mammary gland is responsible for lactation, i.e. milk production and secretion for infant nourishment and immunologic protection. The functional unit of the mammary gland is the terminal duct lobular unit (TDLU), responsible for the production and drainage of breast milk. The breast undergoes various hormonal changes during puberty, menstruation, pregnancy, breastfeeding and menopause [33]. During pregnancy, breast tissue changes under the influence of estrogen, progesterone and prolactin, which levels vary over time. For example, the increase in estrogen levels leads to blood vessels hyperplasia, as well as to an increase in lobules number and size, and to ductal cells proliferation. Progesterone, on the other hand, leads to lobular cell proliferation. Lastly, in the last weeks of pregnancy and during post-partum, production of prolactin and oxytocin hormones leads to early milk production by the alveolar cells. After delivery, the breast keeps changing according to fluctuating hormonal levels [34].

Later in life, menopause is reported as cessation of ovarian activity and depletion of estrogen and progesterone levels, leading to absence of menstruation [35]. All these changes are accompanied by alterations in tissue composition: during menstrual cycles, women experience alterations in the number and size of acini (larger and more numerous at the late phase of the cycles); after menopause, there is an increase in adipose tissue and elastic fibers, and involution and atrophy of lobules and ducts [36,37].

In periods of such deep changes in tissue organization and properties, it may be difficult to distinguish between normal and tumoral breast. Breast cancer is a pathological condition that involves genetic or epigenetic alterations in ductal or lobular cells (**Figure 1**B). It leads to disorganized cell replication and formation of an aggregate/cell mass, with altered mechanical

and biological properties when compared to healthy breast tissue. The majority of carcinomas are thought to arise from TDLUs, particularly from luminal cells, but also from myoepithelial cells [33]. When tumor formation occurs, several alterations take place, leading to aberrant cellular behavior and loss of ECM organization, and affecting tissue homeostasis (**Figure 1**C) [4].

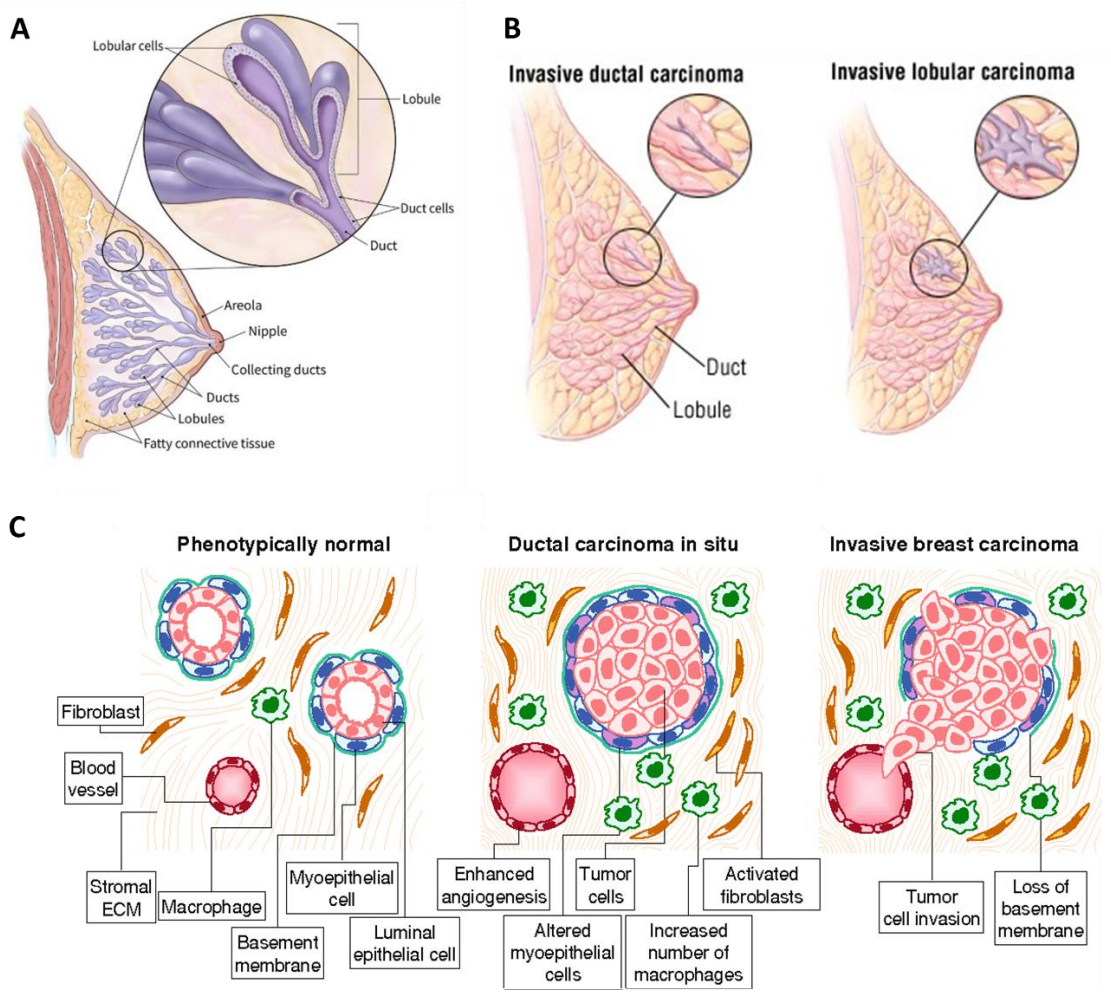

Figure 1 Structural features of breast tissue under **A**) healthy and **B**) tumoral development conditions. **C**) Stromal and epithelial alterations occurring in breast tissue, ranging from a healthy phenotype to cancer development and progression. Adapted from [38–40]

2.1. 3D models of normal mammary gland and breast cancer

Breast tissue is therefore a highly complex and dynamic structure, not easy to replicate *in vitro*. Conventional cell models of breast tissue are based on the use of either cell lines or primary cells, which show distinct patterns in gene expression profiles and signaling pathways. Traditionally, studies have been performed in 2D, that fail to faithfully replicate the *in vivo* events, as already discussed [15,41]. In fact, the first works published on breast tissue only featured epithelial cells cultured on TCPS, and could only barely reproduce breast tissue, as 2D-cultured cells failed to form acini or produce milk in response to lactogenic hormones [42].

The structural complexity of breast tissue, in either healthy or pathological conditions, requires the development of sophisticated 3D *in vitro* culture models. To date, this has been attempted using distinct approaches, [43] often based on the combination of mammary epithelial cells with various types of 3D matrices. These should ideally be able to support epithelial cell growth and function, while allowing mimicry of native pathophysiological microenvironments [41,44]. These are usually based on either ECM-derived hydrogels (e.g. Matrigel™), or hydrogels made of purified proteins, such as type I collagen or fibrin [41]. Such settings generally allow epithelial cells to undergo morphogenesis into acinar-like assemblies and even form typical endogenous structures, such as BM [45]. Seminal work by M. Bissel's team elegantly demonstrated the relevance of using 3D systems to investigate breast cancer mechanisms. First, by postulating that there is a "dynamic reciprocity" between the ECM and cultured cells, in 1982 [46], they started to explain how cells could lose their native properties when cultured as monolayers, due to lack of a more complex environment. The first 3D models, mostly based on Matrigel™, showed how cells could maintain tissue-specific functions and mimic *in vivo* architecture [17,47]. Years later, 3D model refinement led to the use of better characterized substrates, as alternatives to the highly variable Matrigel™. Along the last decades, the work of Bissell and colleagues has been critical in reporting 3D *in vitro* culture systems of breast tissue, and their support in the formation of native-like physiological/pathological 3D structures [48]. To date, various types of hydrogels have been developed as breast tissue models. Some of these studies are briefly described in **Table 1**.

Table 1 Examples of studies using hydrogels as substrates for *in vitro* breast tissue modeling

3D Matrix	Purpose	Main findings	Ref.
Collagen	Study the effect of lactogenic hormones (insulin, cortisol and prolactin) on mouse epithelial cells	Cell cultures acquired ultrastructural and biochemical features of *in vivo* pre-lactating mice mammary tissue, such as secretory profile and accumulation/secretion of casein	[45]
Collagen	Model interactions between MDA-MB-31 TNBC metastatic cells and MC3T3-E1 pre-osteoblasts	MDA-MB-231 cells impair osteoblastic differentiation in MC3T3-E1 cells, suggesting formation of tumor cell configuration in the presence of tumor cells or tumor cell-conditioned medium	[49]
Collagen	Investigate cellular properties of MCF-7 cells	3D substrate induced diversification of cell morphology and proliferation, as well as expression of pro-angiogenic growth factors and MMPs	[50]
Silk-collagen	Recapitulate multidrug resistance of tumor cells *in vitro*, in MCF-7 vs. MCF-7R cell lines	MCF-7R showed increased anticancer drug resistance and higher drug efflux capacity when compared to MCF-7	[51]
RGD-alginate hydrogel	Establish a model to study epithelial-to-mesenchymal transition (EMT) in EpH4 cell line	Formation of acinar-like structures by epithelial cells and generation of intermediate and mesenchymal-like phenotypes upon TGFβ induction	[52]
Alginate-Matrigel™	Build a composite-made model for breast cancer cell culture	MDA-MB-231 showed characteristics of cancer cells, being able to migrate through the gel towards a PCL-gelatin membrane mimicking the vascular wall, suggesting invasive capacity	[53]
Matrigel™	Establish *in vitro* culture of breast carcinoma cells	Reconstituted BM can direct differentiation and morphogenesis of healthy and tumoral cells, which express known patterns of markers, similar to those reported *in vivo*, even though primary cultures and cell lines showed different marker expression patterns	[47]
Methacrylated hyaluronic acid/gelatin	Study the effect of hypoxia on EMT of cancer cell lines 21-PT and 21-MT2	Hypoxia promotes EMT of cancer cell lines without affecting cell viability, even though it delays spheroid formation. Epithelial markers decrease, and mesenchymal markers increase but there is no migratory phenotype	[54]

NOTE: TNBC = triple negative breast cancer; TGF-β = transforming growth factor beta; MDA-MB-231, MCF-7, MCF-7R, EpH4, 21-PT, 21-MT2, MC3T3-E1 = cell lines

2.2. Integration of a stromal compartment in 3D breast tissue models

Along the past decades, the strong influence of the ECM over breast epithelial cells has been acknowledged [55]. In particular, the importance of the breast stromal compartment in maintaining tissue structure and functions is now clear. This has been calling for the refinement

of breast tissue culture models, which should ideally recapitulate the tissue in its full intricacy, as close as possible, by combining stromal and epithelial cells [48,56].

Breast tissue stroma mainly consists of fibroblasts, adipocytes and endothelial cells, which secrete an abundance of enzymes and growth factors, supported by stromal-derived ECM. Stromal components are known to influence the healthy mammary gland, also playing a pivotal role in the breast tumoral environment. Complex remodeling cycles typical of normal breast development (i.e. during pregnancy, lactation or menopause stages) are dictated by stromal cells, which produce ECM components and remodeling enzymes in a highly hormone-regulated manner [55,57].

Apart from cells, research shows that non-cellular components of the tissue microenvironment are also very important during tumor formation and progression. Importantly, it has been shown that resident fibroblasts become activated, overproducing ECM components such as type I collagen, the so-called desmoplasia. The exaggerated fibrillar deposition changes the matrix's relaxed orientation to a highly linearized pattern, altering tissue biomechanics, namely by leading to tissue stiffening [4,5]. This affects the adjacent epithelium, contributing to cancer pathogenesis. Thus, the altered ECM directly impacts cell fate and behavior in different ways, both at biomechanical and biochemical levels. Inversely, ECM alterations produced by stromal and epithelial cells influence stromal constituents [58].

Hence, addition of ECM-producing stromal cells, particularly fibroblasts, to parenchymal cells in 3D *in vitro* models will promote not only heterotypic cell-cell, but also cell-ECM interactions, increasing similarities with *in vivo* conditions [59,60]. For instance, a recent study showed that by coculturing fibroblasts and breast cancer cells in 3D environments, heterogeneous breast tumor-like structures were produced, with fibroblasts migrating towards the tumor edge, rather than the core, and forming what would correspond to the fibrotic capsule encountered *in vivo* [60]. In this sense, an effective way to mimic breast tissue environments or study cancer-related changes in breast tissue would be to combine all the aforementioned tissue components.

This idea matches the most recent paradigm that a full understanding of the intrinsic mechanisms of breast tissue requires engineering of advanced 3D models incorporating various elements of complex native environments. This can be further accomplished *in vitro* by combining the biological factors – cells and associated ECM – with biomaterial-based engineered platforms, which may work as building blocks for the re-creation of this microenvironment. An overview of strategies related to the work developed in this thesis, and of the state-of-the-art of their development will be given in the next section.

3. Building blocks of the proposed breast tissue 3D model

3.1. Tunable alginate-based hydrogels

As already discussed, hydrogels are among the most promising matrices for 3D cell culture. Due to their hydrophilicity, high water content and permeability, they allow easy diffusion of oxygen, nutrients, soluble factors and metabolic waste across the polymeric network. Also, because of their compliance, they closely mimic the biomechanical environment of most soft tissues. Importantly, hydrogels are generally permissive to culture of multiple cell types and can often be formed under mild, cytocompatible conditions [18,61]. One of the most widely used natural, non-animal derived hydrogel is alginate [10]. Alginates are anionic polysaccharides isolated from brown seaweed, mainly composed of (1,4)-linked beta-D-mannuronic acid (M) and alpha-L-guluronic acid (G) residues, which are covalently linked in different sequences or blocks [18]. The blocks composing a polymeric chain can either have similar (-MMMMM- or -GGGGG-) or strictly alternating (-GMGMG-) monomers, and the relative amount depends on the polymer's origin (**Figure 2**A,B). The polymer's structural properties depend on its molecular weight, as well as on monomer composition (M/G ratio) and sequence. G blocks are key for alginate's gelling ability and hydrogel structural properties, and they usually make up 30-70% of natural alginates [61]. A study on neural stem cells found that higher G contents (68%) led to formation of more stable hydrogels and delayed chain dissociation when exposed to low osmolarity solutions [62]. On the other hand, M-rich hydrogels are more permissive for cellular activities and may facilitate motility and function. For instance, a study showed that a low G content (32%) allowed βTC3 cells to experience an increased growth and metabolism, compared with those proliferating in a matrix with 73% G [63].

At neutral pH, alginate has a polyanionic character due to acidic pK_a values of M and G residues, which present a carboxyl group. This, combined with conformational features of alginate chains, results in highly viscous alginate solutions, even at low polymer concentrations. Viscosity is influenced by the ionic strength, temperature and polymer molecular weight [61,64]. Alginate forms viscous solutions when dissolved in monovalent ion solutions (e.g. Na^+), and an increase in polymer concentration leads to an increase in viscosity of the pre-gel solution [65]. This might be interesting for processing and for tuning the stiffness after gelling, but cells may also respond differently to such an environment.

Alginate solutions can produce 3D hydrophilic polymeric networks, when submitted to a gelation process (**Figure 2**C). There are diverse gelation methods, such as ionic or covalent crosslinking, [22] the first being the most common technique: the exchange of Na^+ ions from G

residues with divalent cations, like calcium (Ca^{2+}), barium (Ba^{2+}) or strontium (Sr^{2+}), promotes hydrogel formation [61]. Crosslinking between adjacent monomeric residues leads to establishment of an interconnected molecular network between neighboring alginate chains. Ionic gelation is more frequently promoted through external diffusion of crosslinking agents, but it can also be promoted internally. External gelation uses soluble salts of divalent cations, which diffuse from an external reservoir into the alginate solution. This allows formation of 3D structures of different shapes. While beads are the most common, filaments or fibers can also be obtained using appropriate equipment [61,66]. Gelling conditions, concentration and type of crosslinking agent can also be varied to tune the properties of the resulting hydrogel, including stiffness, swelling and stability, leading to different gelling times or pore size within the network [61,67]. According to Khavari et al., alginate matrices with higher shear moduli (higher stiffness) led to an increased and faster growth of tumoral multicellular aggregates made from metastatic cell lines, proving that confining tumor cells to stiffer environments may promote cell cluster growth [68]. Still, contradictory observations have also been reported. A study from 2016 reported that MCF-7 cells grown in less stiffened hydrogels (150-200 kPa) proliferated and formed spheroids, while in stiffer gels (900-1800 kPa) cells formed smaller aggregates, composed by a lower cell number [69]. This demonstrates that hydrogel properties must be carefully tuned, depending on the cell type and specific application.

Other attractive characteristics of alginate hydrogels as substrates for 3D cell culture are their transparency, useful for microscopic evaluation, and the reversibility of the ionic gelation process. Dissolution of alginate hydrogels can be promoted using chelating agents (e.g. EDTA or sodium citrate) to sequester crosslinking cations, or alginate lyase, which promotes enzymatic cleavage of alginate chains, thus degrading the structured network. Both processes allow easy cell recovery for subsequent analysis [61,70,71].

One of the most valued properties of animal-derived polymers is their cell-driven biodegradability. However, this is not the case for alginate, which derives from algae or bacteria. Therefore, mammalian cells cannot specifically degrade it, as they lack the necessary enzymes [72]. One possible approach for tuning biological degradation of alginate includes modifying the original polymeric chains' structure through incorporation of protease-cleavable and/or hydrolytically degradable links [44]. Nonetheless, under physiological conditions, even unmodified alginate hydrogels will progressively lose stability due to the exchange of crosslinking cations with non-gelling monovalent ions, such as Na^{+}, present in the medium. This results in a slow, irregular degradation, [73] which is difficult to control [74].

Apart from affecting its biodegradability, the inherent bio-inertness of alginate also affects its biological interaction with cells. Alginate does not intrinsically present cell recognition domains and, because of its hydrophilic nature, [75] it discourages protein adsorption to its surface [76]. Therefore, in alginate hydrogels there are no cell adhesion ligands where cells can bind via integrin receptors [77]. Thus, to promote cell anchorage and interaction, alginate hydrogels should be modified with ECM proteins, such as fibronectin, laminin or collagen, [78] or with short amino acid sequences found in those proteins, which are known to specifically mediate cell adhesion and cell-matrix crosstalk [44].

An example is the well-characterized cell adhesion peptide sequence, arginine-glycine-aspartic acid (RGD) and its subtypes, which promote cell attachment, improving cell viability and function [44]. Multiple studies illustrate that the incorporation of RGD or RGD-like peptides into alginate hydrogels promotes cell-substrate interactions, improving alginate potential as a biomimetic 3D matrix. Such modifications positively influence the behavior of diverse cell types [44,79,80].

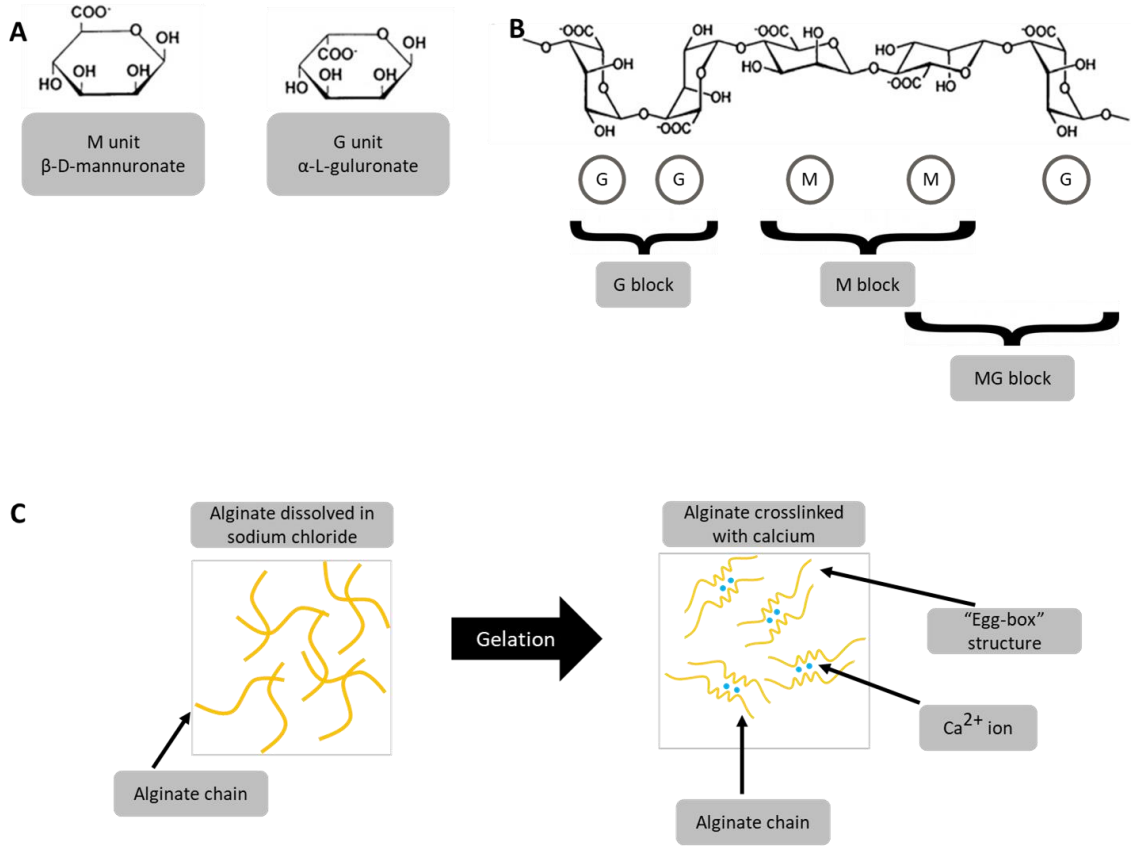

Figure 2 Chemical structure of alginate **A**) essential units, β-D-mannuronate (M unit, left) and α-L-guluronate (G unit, right) and **B**) chains, composed by G blocks, M blocks and combined MG blocks (left to right). **C**) Alginate's external gelation process, from a viscous sodium-dissolved solution to a crosslinked hydrogel with chains forming an "egg-box" structure.

3.2. Processing hydrogels into structured macro-porous 3D structures

The use of 3D *in vitro* models in the investigation of biological processes clearly benefits from a high level of control over material properties, including scaffold architecture, which cannot be provided by traditional processing technologies. Novel biofabrication technologies can be used to build and pattern 3D scaffolds with much higher design flexibility and precision. To improve the knowledge over biological processes, advanced biofabrication techniques have been developed to dynamically replicate cell-cell and cell-matrix interactions with cellular-level resolution [81].

Biofabrication technologies, in the context of 3D modeling, mainly involve printing and assembly strategies, for assembling/patterning cells, biomaterials, bioactive agents and combinations thereof, with predefined spatial organization. 3D scaffolds can be fabricated with different shapes, varying architecture and porosity, requiring precise techniques to reproducibly manufacture complex geometries. 3D printing methodologies are used for additive manufacturing of scaffolds in a computer-controlled and automated layer-by-layer manner, following pre-defined geometrical patterns with high accuracy [82]. Printing technologies can be sub-divided into three main categories: inkjet printing, laser-assisted printing and extrusion printing.

Extrusion printing, the direct extrusion of inks onto a substrate, is the most widely explored technique. Importantly, apart from their biological properties, biomaterials used in extrusion printing approaches must meet specific criteria, depending on the technique and application. Their rheological properties are particularly important, with shear-thinning hydrogels and viscous materials being highly popular choices for scaffold development [81,82].

Therefore, optimization of fabrication processes requires careful consideration of multiple aspects, such as printability, mechanical stability and biological performance of the scaffolds. Printability is highly dependent on the rheological/gelling properties of a material [83]. Ideally, the printing process should generate 3D constructs with high shape fidelity, i.e. that geometrically correspond to the pre-defined design. Changes during/after printing often occur, due to limitations of the ink formulations, ionic crosslinkers or machine accuracy [84,85]. There are studies correlating printing parameters with ink printability and construct mechanical properties, which compare sample dimensions in designed vs. post-fabrication constructs [84].

Importantly, for some applications, printed filaments should be stable enough to maintain structural integrity not only after fabrication, but also when exposed to certain conditions. For example, a hydrogel that is not consistent enough might not be able to preserve

its structure upon lyophilization and re-hydration, which may be needed in some cases [86]. Lastly, biological performance is related to how the printed scaffold interacts with seeded cells [66]. The construct should not be cytotoxic, should support cell adhesion and should not interfere with normal cellular activity/function [84].

Alginate hydrogels qualify as interesting inks for 3D printing for several reasons. Their extrudability, along with their elevated hydration level and gel-forming ability, allows fabrication of 3D structures on-demand, using simple printing set-ups, usually based on polymer extrusion systems. Extrusion-based printing requires that the material exhibits steady flow until deposition, while undergoing rapid stabilization after extrusion onto the support substrate. Also, alginate is widely used as an ink, namely because of its rheological properties, as it forms highly viscous solutions that rapidly crosslink when in contact with divalent crosslinking cations, as already discussed [81].

3.3. Heterotypic models and cell-derived matrices

Even though progress has been made on biomaterials science and processing techniques, replicating the complex ECM composition/structure and dynamic cell-cell and cell-ECM interactions remains a major challenge towards proper mimicry of native cellular microenvironments. In theory, the ideal candidate as scaffolding material would be the native ECM itself. Recent techniques to harvest ECM from tissues or cultured cells have been developed, which involve a decellularization process. Also, co-culture systems may be established, where stromal cells, which are responsible for ECM production, are incorporated along with tissue-specific cells, such as epithelial cells in the case of breast tissue. Such models are called heterotypic, and may include multiple cell types, whose dynamic and reciprocal interactions contribute to homeostasis and disease progression [87]. Considering that breast tissue is highly complex, it makes sense to try and put together a model which includes ECM and tissue-specific cells, namely to study the effect of the stromal compartment on tissue-native cells, and vice-versa.

Co-culture is a long-established methodology for studying heterotypic interactions (**Figure 3**). The literature describes three common methodologies, namely: conditioned media transfer, direct and indirect co-culture [87]. In this work, only direct co-culture was explored. It involves culturing two or more different cell types in close proximity, in the same substrate. The usual goal of such strategy is to unravel not only reciprocal paracrine, but also juxtacrine interactions, which are essential to understand healthy and pathological processes occurring in every tissue. The readout of direct co-culture methods is normally image-based, relying on techniques such as confocal microscopy or histology [87]. More complex models, allowing cell recovery for cell type dissociation/sorting, are needed for cell-specific readouts, such as gene expression analysis. However, it is not easy to obtain such models, and the examples found in the literature are still scarce. In a study by Arrigoni et al., gene expression of bone-seeking breast cancer cells (BOKL) was analyzed after sorting such cells, which had been in direct contact with bone marrow stromal cells (BMSCs), to investigate their crosstalk. However, this study was performed in a 2D setting, thus lacking all the already discussed advantages of 3D systems [88].

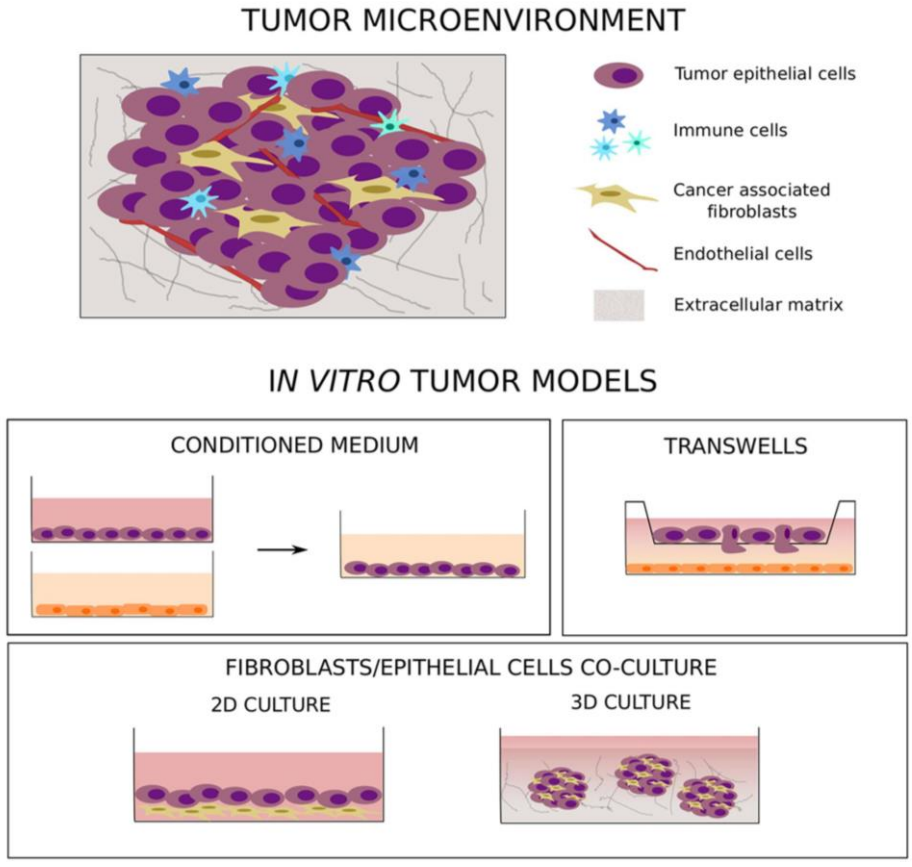

Figure 3 *In vitro* co-culture models of tumor microenvironment (TME) interactions. Focus on indirect co-culture (transwells and cell culture in conditioned medium) and on direct co-culture of fibroblasts and epithelial cells, in both 2D and 3D models. Adapted from [89]

Some studies have tried to produce direct co-culture 3D systems using breast tissue and stromal cells, including fibroblasts or endothelial cells, and have gathered significant data regarding normal/pathological breast tissue mechanisms and breast cancer specific phenotypes. Some of these examples are further detailed in **Table 2**.

Table 2 Heterotypic co-culture models for *in vitro* studies of cell-cell and cell-ECM interactions

3D Substrate	Cells	Purpose	Findings	Ref
Silk fibroin with Matrigel™ and type I collagen	MCF10A, hMFs and hASCs	Study EMT mechanisms underlying embryonic development and carcinogenesis	Triculture system induced structural morphogenesis (ducts and acini) and native-like cell polarization, as well as functional differentiation of epithelial cells (increased mRNA expression of α- and β- forms of casein)	[90]
Silk fibroin	NIH3T3 and EMT6	Study cell interactions related to ECM production and CAFs development from non-tumoral fibroblasts	Significant increase in ECM production by NIH3T3 (fibroblasts); cellular changes related to EMT: downregulation of β-catenin and upregulation of vimentin after fibroblasts addition to the model; CAFs formation from normal fibroblasts, seen through expression of mesenchymal marker CD44	[91]
Alginate	MCF-7 and hDFs	Develop model to study tumor-stroma crosstalk and drug resistance	Observation of epithelial cells phenotypic alterations typical of *in vivo* tumors (migration from capsules and proliferation) under the influence of fibroblasts, which produced increased levels of collagen; such changes were not seen in MCF-7 monocultures	[92]
Matrigel™	MEFs and 4T1	Study epithelial-stromal cell interactions on a basement membrane model	Tumor-associated fibroblasts importance in distribution of factors among epithelial cells, and connections between epithelial cells and between stromal-epithelial cells	[93]
Methacrylated gelatin	CAFs and MCF-7 (or MDA-MB-231)	Study CAFs effects in EMT process of epithelial cells	CAFs have relevant effects in EMT of epithelial cells, enhancing their invasion ability, increase in N-cadherin expression and decrease in E-cadherin expression	[94]
Hyaluronic acid	hMEC-1 and MDA-MB-231	Mimic TME and study cell-cell and cell-ECM interactions	Initial quiescence stage of epithelial cells induced by endothelial cells to restore tumor malignant organization, before further development	[95]

NOTE: hASC = human adipose-derived stem cells; mRNA = messenger ribonucleic acid; CAFs = cancer associated fibroblasts; hDFs = human dermal fibroblasts; CD44 = cluster of differentiation 44; MEFs = mouse embryonic fibroblasts; hMEC-1 = human microvascular endothelial cell line 1; TME = tumor microenvironment; NIH3T3, EMT6, 4T1 = cell lines

To isolate the effect of the ECM present in the stromal compartment, alternative models involving decellularization of an initial culture of stromal cells, followed by culture of tissue-specific cells (i.e. mammary epithelial cells) in the same substrate can also be used. Such cell-derived matrices (CDMs) also provide biologically relevant templates, which can be used to mimic *in vivo* environments for specifically studying ECM-parenchymal cells' interactions.

Decellularization treatments aim to remove the original cells and nuclear material, while preserving, as much as possible, the composition and structure of the matrix component [96]. Studies have shown that CDMs can promote increased cell adhesion, proliferation and migration. In many cases, such matrices are more adequate to guide tissue-specific differentiation towards acquisition of an *in vivo*-like morphology than unspecific commercially available ECM-derived matrices such as Matrigel™ or collagen [97]. CDMs can be prepared from various cell types and cell culture methods, including conventional 2D culture systems, spheroid 3D culture, or scaffold-based 3D culture [96,98].

The decellularization process must be carefully optimized. An effective protocol should lead to successful extraction of cellular/nuclear components, while leaving behind an interconnected network of ECM components. Also, it should maximize uniformity of the obtained matrices. Low heterogeneity of CDMs makes them a superior alternative to conventional allogeneic or xenogeneic matrices, such as Matrigel™, which fails to support cell culture under defined conditions [99–101].

Different variables must be considered when defining a protocol for obtaining decellularized CDMs. According to a review from Hoshiba et al., critical points are related to cell types, culture medium composition, culture substrates and decellularization method [102]. Cell culture prior to decellularization should be done considering the type of ECM to be obtained. Thus, depending on the tissue to be mimicked, a specific cell type should be chosen, and cell density should be optimized to ensure homogeneous coverage of the culture substrate, with significant matrix production, forming a native-like ECM structure. Once the cultured cells have deposited enough ECM, decellularization can be performed. Effective removal of all cellular and DNA traces is generally performed through a combination of chemical, physical and/or biological methods. The choice of the best methods depends not only on the desired outcome, but also on the properties of the original culture, namely cell type and density [103]. Optimal conditions for decellularization should also minimally affect the matrix, by promoting the highest possible retention and preservation of native biochemical and structural features. Significant ECM alterations during the decellularization process may later on affect cells used in dECM re-population [101].

Some studies using CDMs analyzed the distinct roles of the native ECM in different cellular processes, not only in physiological, but also in tumor-related pathological scenarios. For example, one study showed that genetically-modified gastric cancer cells overexpressing specific soluble factors were able to alter the phenotype of stromal cells (i.e. adipose stromal cells, ASCs). These stromal cells are responsible for the deposition of fibrotic/desmoplastic ECM. In turn, once decellularized, this ASC-derived matrix showed to enhance gastric cancer cells proliferation and inhibit cell clustering. This illustrates the complex bi-directional interactions between dECM and repopulating cells [104].

4. Aims of the work

In the field of 3D *in vitro* culture advanced models, strategies that combine the biological relevance of tissue-specific ECM (with or without ECM-producing cells), parenchymal cells, and highly customizable artificial hydrogels are still lacking. To address this unmet need, this work focused on the development of a new 3D *in vitro* model for the study of breast tissue, combining a printed alginate scaffold coated with human mammary fibroblasts and respective ECM, with hydrogel-embedded mammary epithelial cells.

Considering that alginate is a bioinert polymer, where cell-matrix interactions can only be partially recreated through incorporation of a limited number of bioactive moieties [44], the addition of stromal cells and their tissue-specific native ECM will drastically enhance its biological relevance. On the other hand, alginate hydrogels present some advantages that CDMs do not have, including the possibility to fine-tune biochemical/biomechanical properties. Thus, this advanced 3D model is expected to provide a unique tool to study the role of the ECM in mammary epithelial cells behavior, both under physiological and pathological conditions, including cancer (**Figure 4**).

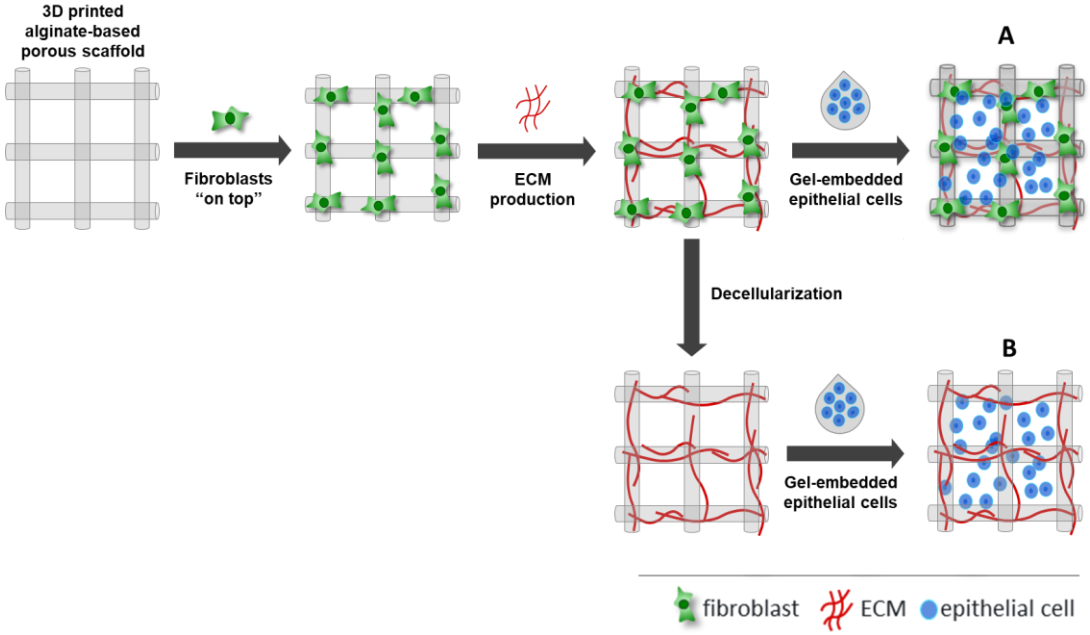

Figure 4 Proposed multi-component 3D heterotypic model. A 3D-printed alginate-hydrogel porous scaffold is seeded with mammary fibroblasts, which proliferate and produce ECM on top of the scaffold, creating a stromal compartment. The pores of the scaffold are filled with a gel-precursor solution laden with epithelial cells, forming a hydrogel where epithelial cells will undergo morphogenesis. Two strategies can be followed: **A**) direct addition of the gel precursor solution to the scaffold colonized with fibroblasts, or **B**) addition of the gel precursor solution to the scaffold, after decellularization. Epithelial cells will be in contact with fibroblasts-derived ECM (CDM), but not with fibroblasts.

This page was intentionally left in blank

MATERIALS AND METHODS

1. Fabrication of the 3D-printed alginate scaffold

1.1. Alginate

Pharmaceutical grade sodium alginate powder with a high content (ca. 70%) of guluronic acid units (LF 20/40, from FMC Biopolymers, Oslo, Norway) was used (hereafter designated as ALG). For some experiments this alginate was purified as described [31]. Briefly, a 1 wt.% alginate solution was prepared by mixing alginate with distilled water and stirring overnight (ON). The solution was then sequentially filtered with 0.8 µm, 0.45 µm and 0.22 µm filters, using a vacuum pump. After filtration was completed, activated charcoal was added and the alginate solution was stirred for 1 h. Next, the solution was vacuum-filtered with a 0.22 µm filter. The filtered solution was frozen at -20°C ON to be lyophilized. The purified alginate (hereafter designated P-ALG) was stored at -20 ºC until used.

1.2. Chemical modification of alginate with RGD peptide

Covalent grafting of the oligopeptidic sequence of (Glycine)4-Arginine-Glycine-Aspartic acid-Serine-Proline (abbreviated as G_4-RGDSP; Peptide International, USA) to alginate was performed according to Bidarra et al [44]. Briefly, MES (Sigma-Aldrich, St. Louis, MO) buffer solution was produced and its pH was adjusted to around 6.5, using NaOH (5 M). Under stirring conditions, 1 g of alginate solution was added to 100 mL of MES buffer solution (1% w/v). This solution was left stirring ON. The day after, sulfo-NHS (27.40 mg per gram of alginate), EDC (48.42 mg per gram of alginate) (Sigma-Aldrich, St. Louis, MO) and RGD peptide (10 mg/mL) were consecutively added very quickly, and the mixture was stirred for 20 h. Finally, the reaction was quenched by adding 18 mg of hydroxyl amine per 1 g of alginate. The modified alginate was purified by dialysis, which was performed along the next 3 days, with decreasing NaCl concentrations. After dialysis was completed, the RGD-modified solution was frozen at -20°C ON, lyophilized and stored at -20°C until used.

1.3. Extrusion-based 3D printing of alginate scaffolds

Alginate was mixed with a solution of sodium chloride (0.9 wt.% NaCl, VWR, Radnor, PA) to a specific concentration, and left stirring ON at room temperature (RT, ≈ 20°C). For different experiments, different types of alginate were used, namely, ALG or P-ALG, with different amounts of RGD (0, 200 µM, 400 µM or 600 µM). The extrusion-based 3D printing setup was mounted (**Figure 5**), and the extrusion pump was connected to it via a 12 mL-syringe containing the printing (sodium alginate) solution (**Figure 5**A). Calcium chloride ($CaCl_2$, VWR, Radnor, PA) crosslinking solution was prepared at 400 mM in 0.9 wt.% of NaCl, diluted accordingly and poured into a Petri dish (v = 50 mL) placed on the printing platform (**Figure 5**B).

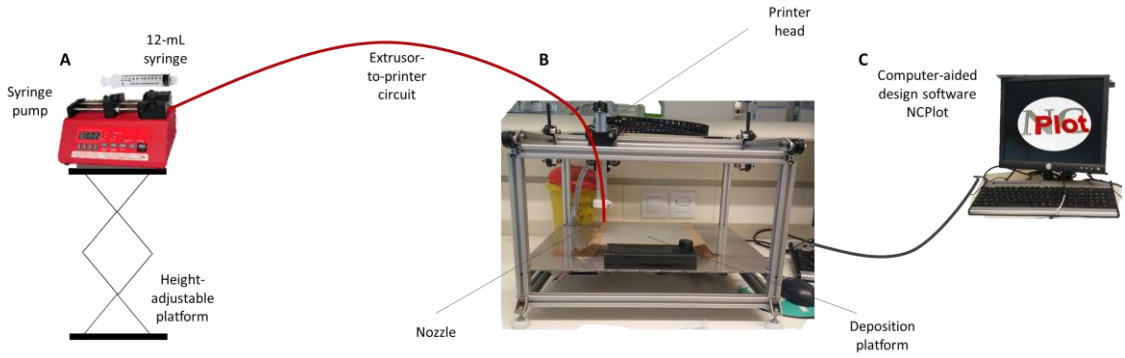

Figure 5 Schematics of the extrusion-based 3D printing system. **A**) Alginate formulation is extruded at a fixed rate through a syringe pump. It flows along the extrusor-to-printer circuit until it reaches **B**), where it is extruded through the nozzle into a crosslinker's solution placed on the deposition platform. **C**) Design of the structure is controlled by a dedicated software.

Briefly, sodium alginate solution was extruded, and the flow stabilized using an extrusion syringe pump (Programmable Aladdin Syringe Pump (AL-1000), NewEra PumpSystems Inc., Farmingdale, NY). The printing code generated using NCPlot (NCPlot Software LLC, Muskegon, MI) was uploaded into RepetierHost software (Hot-World GmbH & Co. KG, Germany). The needle (internal diameter, Ø = 210 µm) was aligned and stabilized inside the $CaCl_2$ solution and printing was initiated. After printing, the 3D-printed alginate scaffold was retrieved from the crosslinking bath. A second crosslinking step was necessary for all scaffolds, to improve mechanical stability and robustness before washes and storage. For this, the scaffolds were soaked in a 20 mM $CaCl_2$ solution for 5-10 min. Afterwards, the scaffolds were washed for 30 s in distilled water, under agitation. From this point on, scaffolds were ready for use, or could be freeze-dried after ON lyophilization (for long-term storage) or through immersion in ethanol (70% v/v) (for short-term storage, over a maximum period of around 2 weeks).

An alternative method for printing scaffolds was tested during the optimization stage. This involved a pre-crosslinking stage prior to printing, where the sodium alginate ink was mixed with a $CaCl_2$ solution with variable concentration (depending on the formulation). In this method, scaffolds were not printed into a crosslinking bath, but instead into a planar plastic platform. Steps performed after printing were the same as previously mentioned. However, due to technical difficulties, this method showed to be unsuitable for its intended use.

1.4. Scaffold analysis

Analysis of 3D-printed scaffolds was performed using the stereomicroscopic system SZX10 (Olympus Life Science Solution, Waltham, MA) connected to a computer. Pictures were taken immediately after i) printing and washing, ii) re-hydration of lyophilized structures and iii) re-hydration in medium after de-hydration with ethanol solutions (70% v/v). For detailed scaffold analysis, namely morphological parameters and pore-size, image processing software ImageJ® (National Institute of Health, USA) [105] was used.

Due to optimization reasons, throughout the cell culture steps, only halves of scaffolds were used, to minimize cell necessities and medium consumption. To obtain miniaturized samples of the scaffolds, whole scaffolds were punched with stainless steel disposable biopsy punchers of 8 mm, 6 mm and 4 mm (Kai Medical, Japan).

2. Cell culture and expansion

2.1. Cell sources and maintenance

Human mammary fibroblasts from primary cultures (hMFs, ScienCell Research Laboratories, Carlsbad, CA) were routinely cultured in high glucose Dulbecco's Modified Eagle Medium GlutaMax™ (DMEM, Gibco® Life Technologies, Carlsbad, CA) supplemented with 10% of Fetal Bovine Serum (FBS, Gibco® Life Technologies, Carlsbad, CA) and 1% of Penicillin-Streptomycin solution (Pen-Strep, Sigma-Aldrich, St. Louis, MO). Cells were maintained in culture until the 10^{th}-12^{th} passage, and re-fed every two days with this medium, according to the ScienCell protocol [106]. Cells used for seeding scaffolds were from passages 5 to 9.

Human mammary gland epithelial cell line (MCF10A, American Type Culture Collection, Manassas, VA) was routinely cultured in DMEM/Ham's F-12 medium (Gibco® Life Technologies, Carlsbad, CA) supplemented with 100 ng/mL cholera toxin, 20 ng/mL epidermal growth factor (EGF), 0.01 mg/mL insulin, 500 ng/mL hydrocortisone, 5% horse serum and 1% Pen-Strep. All growth factors were purchased from Sigma-Aldrich (St. Louis, MO). MCF10A cells were

maintained in culture from passage 28 until passage 34, and re-fed with supplemented medium every two to three days.

2.2. Culture plate coating with pHEMA

To avoid unattached cells to adhere to the bottom of the plates upon seeding on scaffolds, pHEMA-coated wells were prepared. A 10x pHEMA coating solution (120 mg/mL) was prepared by dissolving pHEMA (Sigma-Aldrich, St. Louis, MO) in 95% v/v EtOH and rotating it at 100 rpm in an orbital shaker (37°C, ON). This solution was then diluted 1:10 in 95% v/v EtOH to a concentration of 12 mg/mL and sterilized by filtration (0.22 µm). Culture plates were coated under sterile conditions using a final density of 0.8 mg/cm^2. Plates were placed in the incubator to dry for 48 h at 37°C, to allow a slow evaporation of the coating solution and ensure formation of a uniform layer. After drying, plates were sealed with parafilm and stored at RT. Prior to use, wells were washed with phosphate buffered saline (PBS) solution twice, and with supplemented medium once.

2.3. Fibroblasts culture on top of 3D-printed alginate scaffolds

To establish the fibroblast culture on top of the printed scaffolds, cells were trypsinized from T75 culture flasks and counted. After two washing and centrifugation steps at 1000 rpm (5 min), cell pellets were resuspended in a specific volume, dependent on the cell seeding density.

Sterile RGD-alginate 3D-printed scaffolds were placed in a 24-well plate and cut into halves using a 22 pc. scalpel (FEATHER Safety Razor Co., Ltd, Japan). Before cell seeding, scaffolds underwent 3 consecutive 10-15 min washes, first with unsupplemented medium and then with supplemented high-glucose DMEM GlutaMax™, to remove any traces of ethanol. hMFs resuspended in high-glucose DMEM GlutaMax™ were then seeded onto the scaffolds, at a specific cell density. Scaffolds were incubated for 2 h at 37°C, for cell adhesion. After this time, 700 µL of medium were carefully added to the wells and scaffolds were incubated under standard culture conditions. After 24-48h, scaffolds were transferred to pHEMA-coated wells. Media was changed every 1 or 2 days until the experiment's endpoint (generally 2 weeks after seeding). In some experiments, to enable cell tracking, hMFs were incubated with CellTracker™ (ThermoFisher Scientific, Waltham, MA) with red, green and blue fluorescent dyes, prior to seeding. This protocol involved incubation time with the CellTracker™ dye in unsupplemented medium, according to the manufacturer instructions [107].

2.4. Metabolic activity assay

Metabolic activity quantification was assessed through the resazurin assay, in accordance to the manufacturer's protocol. In brief, a resazurin working solution was made of 20% v/v of resazurin solution from stock (Sigma-Aldrich, St. Louis, MO), with high-glucose DMEM GlutaMax™ (Gibco® Life Technologies, Carlsbad, CA). Each scaffold was covered with 500 µL of working solution in a 24-well plate and placed in the incubator for 2 h (37°C, 5% v/v CO_2), in the dark. Fluorescence, arising from resazurin reduction to the fluorescent compound resorufin, was measured at 530 nm excitation and 590 nm emission using the fluorescence microplate reader Synergy Mx™ (BioTek, Winooski, VT). Results are expressed as relative fluorescence units (RFU).

2.5. Decellularization

For some experiments, decellularized scaffolds were prepared. All steps of the decellularization protocols were performed in the orbital shaker, at 37°C and 80-100 rpm. All decellularization solutions were prepared in Hank's Balanced Salt Solution (HBSS, Gibco® Life Technologies, Carlsbad, CA). Cellularized scaffolds were first rinsed with hypotonic solution of deionized ultrapure water (18 MU, Milli-Q UltraPure Water System, Millipore, Burlington, MA) and then incubated in a detergent solution at 37°C. This could either be sodium dodecyl sulphate (SDS, Merck KGaA, Darmstadt, Germany) or Triton X-100 (Sigma-Aldrich, St. Louis, MO) with 1/740 ammonium hydroxide (NH_4OH, VWR, Radnor, PA), for variable periods of time. After, scaffolds were thoroughly washed with HBSS, they were then kept in 25 U/mL DNAse I solution for a certain time (ThermoFisher Scientific, Waltham, MA) and again rinsed with HBSS. Scaffolds were stored in HBSS until fixation or further processing/analysis.

2.6. Culture of hydrogel-embedded MCF10A cells in 3D-printed alginate scaffolds

Hydrogel-embedded MCF10A epithelial cells were added to the 3D-printed alginate scaffolds with fibroblasts. For this, MCF10A cells were trypsinized, centrifuged (1000 rpm, 5 min), counted and resuspended at an adequate density in sterile 0.9 wt.% NaCl. Cells were then mixed with sterile-filtered (0.22 µm) RGD-modified ultrapure alginate (PRONOVA UP LVG, Novamatrix, FMC Biopolymers, Oslo, Norway) gel precursor solution at a final density of 5×10^6 cells/mL. To promote *in situ* hydrogel formation inside the scaffolds, an internal gelation strategy was followed using calcium as ionic crosslinker, as previously described [44]. A sterile suspension of $CaCO_3$ (Fluka™ Honeywell Research Chemicals, Munich, Germany) in 0.9 wt.% NaCl was mixed with the alginate solution at a Ca^{2+}/-COO^- molar ratio of 0.288, and the gelling process was

triggered through the addition of filtered (0.22 µm) fresh GDL in 0.9 wt.% NaCl at a $CaCO_3$/GDL molar ratio of 0.125 [52]. The process was started with an RGD-modified alginate solution at 1.7 wt.% of alginate and 340 µM of RGD, reaching the final concentration of 1 wt.% alginate with 200 µM of RGD after adding all the previously described components (to the cell suspension) The gel-precursor solution (70 µL) was then quickly applied on top of each fibroblast-seeded alginate scaffold. Hydrogel discs with MCF10A monoculture were also prepared as a control for flow cytometry experiments. These were obtained by dispensing the gel-precursor solution (30 µL-drops) between Teflon plates with 1 mm-thick spacers. The Teflon plates were kept in a Petri dish, while the scaffolds remained in 24-well plates, at 37°C in a 5% v/v CO_2 incubator. 20 to 30 minutes after triggering the gelling process (which started when adding the GDL component [75]), a mixed media (DMEM GlutaMax™ with DMEM/Ham's F-12, 70/30 ratio) was added to the scaffolds. Discs were retrieved from Teflon plates with a spatula, placed in wells and covered by medium (DMEM/Ham's F-12, Gibco® Life Technologies, Carlsbad, CA). Medium was refreshed after 30 minutes.

2.7. Live/Dead assay

To assess cell viability within the 3D-printed alginate structures, scaffolds with cultured hMFs and MCF10A cells were subjected to the Live/Dead assay. Stock solutions of Propidium Iodide (PI, 1 mg/mL in ddH_2O, Invitrogen, Carlsbad, CA) and Calcein AM (1 mg/mL in DMSO, Invitrogen, Carlsbad, CA) were prepared beforehand. Each scaffold was washed with unsupplemented DMEM GlutaMax™ without phenol red and incubated in 500 µL of this medium, containing 2.5 µg/mL of Propidium Iodide and 2.0 µg/mL of Calcein AM stock solutions, at 37 °C for 45 minutes. Then, scaffolds were washed and maintained in fresh medium. Live cells were shown in green fluorescence by Calcein AM (ex/em ≈ 495 nm/≈ 515 nm), and dead cells stained red by aqua-fluorescent reactive dye PI (ex/em ≈ 540 nm/≈ 615 nm). Analysis was carried out by confocal laser scanning microscopy (CLSM, Leica TCS SP5, Wetzlar, Germany) immediately after incubation time.

2.8. Immunofluorescence analysis by confocal microscopy

Scaffolds were fixed at the endpoint of each experiment, and later used for CLSM or histology. For fixation, scaffolds were first washed with HBSS and then fixed with 500 µL of 4% v/v paraformaldehyde (PFA, Sigma-Aldrich, St. Louis, MO) in HBSS, for 20 min at RT. After this, scaffolds were washed and stored at 4°C until used.

For CLSM analysis, different combinations of antibodies were used to perform immunofluorescent stainings on whole-mounted samples (**Table 3**). Scaffolds were first incubated in 1.5% v/v of bovine serum albumin (BSA, Merck KGaA, Darmstadt, Germany) in HBSS blocking buffer, for 30 min at RT, to minimize non-specific adsorption of antibodies. Samples were then incubated in 0.2% w/v Triton X-100 (in HBSS) for cell permeabilization (applicable to intracellular markers) and only then incubated with one or more primary antibodies (**Table 3**) to stain different ECM or cellular components, or with phalloidin (conjugated, laser 488, BioLegend, San Diego, CA) to stain filamentous-actin (F-actin) cytoskeleton filaments (1:100 dilution). Incubation was performed ON, in the dark and at 4 °C.

Table 3 List of primary and secondary antibodies used on confocal microscopy analysis, for staining of hMFs, MCF10A and hMF-derived ECM

	Antibody	Reference	Dilution	Use	Source
Primary antibodies	**Fibronectin** (rabbit)	F3648	1:150	hMFs	Sigma-Aldrich, St.Louis, MO
	E-cadherin 24A10 (rabbit)	31955	1:100	MCF10A	Cell Signaling Technology, Danvers, MA
	Type I collagen (rabbit)	600-401-103-0.1	1:100	hMFs (ECM)	Rockland Immunochemicals, Inc., Pottstown, PA
	Type IV collagen (mouse)	M0785	1:100	hMFs (ECM)	Dako, Glostrup, Denmark
Secondary antibodies	**Goat anti-rabbit 594**	A11072	1:1000	All	Molecular Probes, Eugene, OR
	Chicken anti-mouse 647	A21463	1:1000		

Afterwards, scaffolds were washed 3 times with 1.5 wt.% BSA in HBSS (5 min each). Samples were then incubated with the secondary antibodies, as well as with DAPI, for 1 h in the dark, washed 3 times with HBSS (5 min each), and stored until use. Before use, scaffolds were mounted with VECTASHIELD® Antifade mounting medium (Vector Laboratories, Inc., Burlingame, CA) and analyzed by CLSM on the same day. Different laser wavelengths were used throughout experiments (488, 561 and 633 nm), and the scaffold itself was captured through bright field (BF) imaging. For mosaic images of scaffolds, images were taken at 512x512 resolution and 500 Hz velocity, with a z-step of 9.99 µm. For all other images, resolution was at 1024x1024 and velocity was at 400 Hz. Z-step varied between 1.01 µm and 13.98 µm, depending on the desired image quality.

2.9. Histology

For histological analysis, seeded scaffolds were first embedded in HistoGel™ Specimen Processing Gel (Richard-Allan Scientific™, San Diego, CA) to avoid loss of cells seeded on top. Scaffolds were then processed with the Microm STP 120 Spin Tissue Processor (ThermoFisher Scientific, Waltham, MA) and paraffin-embedded. Subsequently, 6-µm slices were cut transversally with the Leica RM2235 microtome (Leica, Wetzlar, Germany), and these were stained with hematoxylin (for nuclei) and O-safranin (for alginate). Histological analysis was performed with the microscope (ZEISS, Oberkochen, Germany) to assess cell growth and proliferation throughout the alginate scaffolds.

2.10. Flow cytometry

To distinguish hMF and MCF10A populations, flow cytometry (FC) analysis was performed. Since flow cytometry requires cells in suspension, these had to be retrieved from scaffolds. To do this, scaffolds were dissolved in a 0.25% trypsin/50 mM EDTA solution for 5 min, and cells were fixed in 4 % v/v PFA in PBS, and then washed with FACS buffer (2% FBS/PBS). Fixed cells were then blocked with 5 wt.% BSA in PBS (30 min) and stained with conjugated anti-CD90 antibody (laser 647, dilution 1:100, BioLegend, San Diego, CA) for 45 mins. After washing with FACS buffer, cells were permeabilized with 0.2% w/v Triton X-100/PBS for 5 min and stained with anti E-cadherin antibody (dilution 1:200, Cell Signaling Technology, Danvers, MA). After further washes, cells were stained with the secondary antibody for E-cadherin (laser 488, anti-rabbit, dilution 1:1000, Molecular Probes, Eugene, OR) for 30 min, and finally washed and filtered. Cells were analyzed by flow cytometry using BD FACSCanto™ II (BD-BioSciences, San Jose, CA), with FACSDiva software (BD-Biosciences, San Jose, CA). All cells were kept on ice during processing and before FACS. The FC results were analyzed using FlowJo v10.0 1-month trial (FlowJo, Ashland, OR). Optimal experiment settings to facilitate gating and reduce background noise were established by using unstained hMF and MCF10A monocultures and co-cultures, in 2D and 3D, as negative controls; in the other hand, stained hMF and MCF10A monocultures, in 2D and 3D, were used as positive controls for each marker expression.

RESULTS AND DISCUSSION

1. 3D printing of alginate scaffolds

To build a complex 3D model for native tissue *in vitro* replication, we started by optimizing the material properties, according to the main goals of the model and taking into account the selected fabrication technique. Alginate was chosen for both biomaterial components of the combined scaffold (porous scaffold and soft hydrogel). The primary porous scaffold was printed using an extrusion-based 3D printer. Selection of alginate over other hydrogels was mostly based on some of its advantages, namely: i) its bio-inertness, that allows for specific control over cell behavior; ii) its transparency, which facilitates microscopical analysis of cell morphology and growth throughout culture time; iii) the formation of reversible ionically crosslinked hydrogels that allows for hydrogel dissolution using chelating agents, such as EDTA, for easy cell recovery on demand.

1.1. Printability assessment: initial screening

Printability assessment of alginate formulations mainly addressed the evaluation of some key requirements for extrusion printing: capacity to form consistent fibers and acquisition of a cylindrical-like shape after extrusion and screening of different printing strategies. In initial optimization steps, only unpurified alginate (hereafter referred to as ALG) was used.

The first step consisted on testing the material's ability to form filaments in a layer-by-layer fashion, by manually dispensing a pre-crosslinked fluid sodium alginate solution, using calcium (Ca^{2+}) as crosslinking ion, prior to extrusion. Several formulations were tested, with alginate concentrations ranging from 1 to 5 wt.% alginate and concentration of crosslinking solution ranging from 5 to 15 mM $CaCl_2$. In preliminary tests, pre-crosslinked inks were manually dispensed with the same needle to be used in the printing system (ø = 210 µm). Among the different tested conditions, only alginate concentrations between 2 and 3 wt.% formed fibers, when crosslinked with 7.5 and 10 mM $CaCl_2$ solutions, showing a reasonable printability. However, when tested in the printing system, none of these formulations showed printing consistency: alginate filaments lacked shape fidelity, and there was poor reproducibility between consecutive experiments using the same batch of material. Furthermore, persistent clogging of the extrusion system proved these formulations unsuitable for printing (**Figure S 1**, Supplementary Information, SI).

Therefore, a new printing strategy was adopted, which involved extruding non-crosslinked sodium alginate solution directly into a crosslinker bath ($CaCl_2$), leading to immediate crosslinking of the material while printing. As the density of the material was higher than that of the crosslinker solution, the material should become deposited as it was being printed. After reviewing recent literature on the use of alginate-based printing inks, we decided to test solutions with concentrations ranging from 2 to 4 wt.% alginate [108–110]. As in the previous strategy, an initial screening of the alginate solutions was performed through manual dispensing of each ink using the printing needle, to evaluate filament formation in the $CaCl_2$ bath.

Table 4 Filament formation evaluation for various concentrations of alginate and $CaCl_2$

		$CaCl_2$ concentration (mM)				
		7.5	10	12.5	15	20
Alginate concentration (wt.%)	2					
	2.5					
	3					
	3.5					
	4					

NOTE: Dark grey cells indicate inability to form filaments due to increased viscosity (right side) or low viscosity (left side). White cells indicate ink printability and ability to form filaments.

Potentially printable solutions were then tested in the extrusion-based printing system to assess layer-stacking capacity, as well as shape fidelity upon printing. From all the "printable" formulations depicted in **Table 4**, the 4 wt.% ALG solution with 12.5 mM $CaCl_2$ was the only one that produced the desired structures. The printed 3D constructs could be produced with 4 to 8 layers, as desired, maintaining their shape during and after printing. Optimization of critical parameters such as extrusion rate (of the syringe pump), needle flow rate (i.e. writing speed) or the needle height was performed to improve shape fidelity to the original CAD-designed structure. The extrusion rate was set at 2 mL/h: higher rates led to extrusion of too high ink amounts, while lower rates led to extrusion of insufficient ink amounts. Needle flow rate was optimized proportionally to the extrusion rate: the optimal value was set at 170 µm/s. Lower rates led to production of larger filaments, while excessively higher rates led to production of too thin filaments or even droplets. Finally, the chosen formulation was successfully printed into 12 X 12 mm crosshatch 6-layered 3D scaffolds (**Figure 6**).

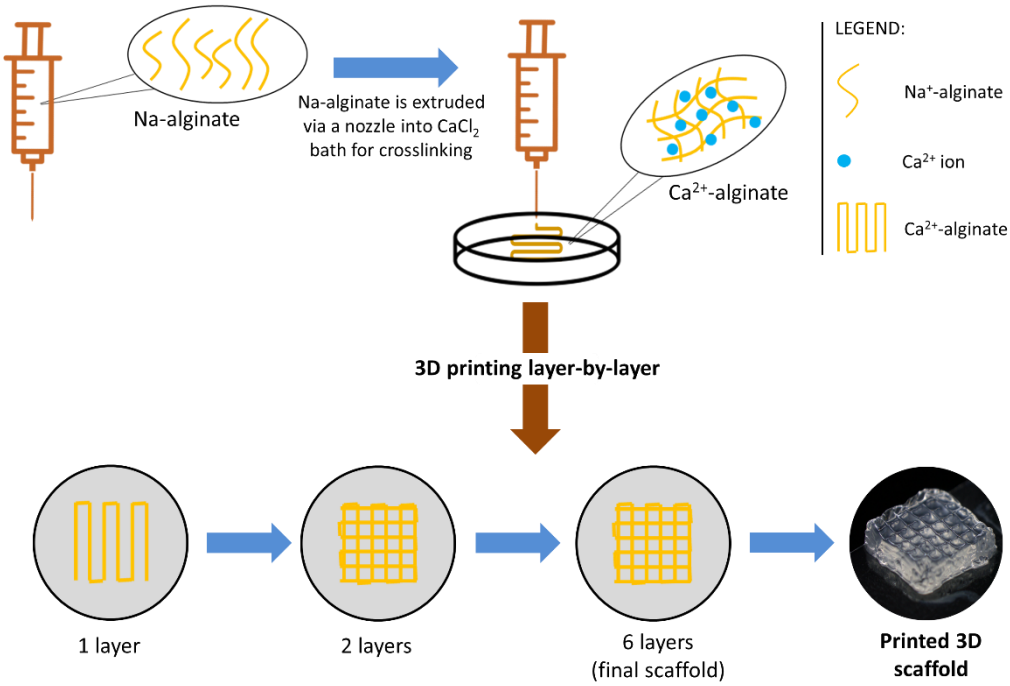

Figure 6 Schematic representation of the strategy used for printing the 3D scaffolds. Sodium alginate is the primary printing ink, which is extruded through a nozzle into a crosslinker bath (with $CaCl_2$). The structure is printed layer-by-layer, until forming a crosshatch 3D scaffold with 6 layers.

Extrusion-printing was chosen over other printing strategies, such as inkjet or laser printing, because it generally allows dispensing of large hydrogel filaments (depending on the needle's diameter, in this case between 200-300 µm, depending on the ink's spreading ratio), instead of droplets. It also presents high deposition and printing speeds, which facilitates scalability and serial scaffold production. Additionally, the printer hardware is affordable, easy to implement and use [111]. The greatest limitation of this technology is reduced resolution, allowing only a minimum feature size of at least 210 µm for this specific case (corresponding to the needle's internal diameter).

1.2. Comparison between alginates

After optimizing printing parameters, it was decided to shift to purified alginate (P-ALG). After purification of the raw pharmaceutical grade alginate (ALG), this was printed using exactly the same settings. Unfortunately, because of its different rheological properties, it did not behave in the same way as ALG, and new optimizations on the printing process had to be performed. Thus, after a second optimization round, printed P-ALG scaffolds were produced. A comparative analysis between both scaffold types (i.e made of ALG or P-ALG) was performed, taking into account the i) easiness of printing and ii) shape fidelity. Easiness of printing was

evaluated based on the ratio between the number of produced scaffolds and the number of attempts to print a scaffold. Shape fidelity was based on lattice measurements and comparison between the inter-filament spacing, as dictated by the CAD software, and as measured on the printed scaffold, according to **Equation 1**. To calculate the % shape fidelity, 5 random pores of representative scaffolds were measured using ImageJ® software [105], and the average pore size was used as "real pore size" [112]. Scaffolds were also evaluated based on their aspect and overall organization (**Figure 7**). Lattice measurements were based on **Figure 7**C,D i).

Equation 1 Percentage of shape fidelity (%)

$$\%\ shape\ fidelity = 1\ -\ \frac{|real\ pore\ size\ -\ theoretical\ pore\ size|}{theoretical\ pore\ size} * 100$$

Table 5 Lattice measurements of ALG and P-ALG scaffolds

Pore size (cm)	ALG	P-ALG
1	0.170	0.148
2	0.161	0.139
3	0.173	0.127
4	0.173	0.166
5	0.175	0.200
Mean	0.170	0.156
Shape fidelity (%)	95.0	87.2

From the measurements, considering "theoretical pore size" to be 0.179 cm, % shape fidelity for the ALG scaffold was 95.0%, while for the P-ALG, this value was 87.2%. Such values were used to support scaffolds' classification regarding the "shape fidelity" parameter in **Table 6**.

Table 6 Comparative table of optimal parameters for printing scaffolds with ALG and P-ALG

	[Alg] (wt.%)	[$CaCl_2$] (mM)	Extrusion rate (mL/h)	Flow rate (μm/s)	Interlayer spacing (mm)	Easiness of printing	Shape fidelity
ALG	4	12.5	2	170	0.2-0.3	5	3
P-ALG	2	7.5	2	200	0.15-0.25	3	1

NOTE: Comparative factor "easiness of printing" is ranked on a scale from 1-5, in which 1 corresponds to 0-20% success in printing scaffolds, 2 corresponds to 21-40%, 3 corresponds to 41-60%, 4 corresponds to 61-80% and 5 corresponds to 81-100%. Comparative factor "shape fidelity" is classified on a scale from 1-3, in which 1 corresponds to less than 90%, 2 corresponds to 90-95% and 3 corresponds to 95-100%.

Regarding the factor "easiness of printing", a score of 5 out of 5 was attributed to ALG, as this formulation was reasonably stable both when flowing through the extrusion system and when printed inside the crosslinking pool. Quantitatively, above 80% of all attempts to print a

scaffold with this formula were successful. Unsuccessful attempts were mainly caused by nozzle clogging, dragging of the structure by the needle or printer technical issues (e.g. when printer loses track of computer's commands). Regarding the "shape fidelity" factor, the ALG formulation was scored with 3 out of 3, as it generally maintained its structure, even though % shape fidelity was 95.0% on average, according to lattice measurements (**Equation 1**).

Regarding the "easiness of printing" of P-ALG formulation, it was scored with 3 out of 5, due to lack of stability during printing (approximately 50% of all printing attempts failed), as well as after printing, which concomitantly affected the "shape fidelity" parameter. There was often loss of the original pore structure and partial clogging of the pores. Thus, this formulation was scored with 1 out of 3 in the "shape fidelity" factor (**Table 6**).

Scaffolds were also analyzed based on their visual aspect and printed pattern. While ALG scaffolds showed a pattern similar to that of the originally designed structure, (**Figure 7**A-C) as well as homogeneously spaced pores, the P-ALG formulation produced highly heterogeneous scaffolds containing irregular patterns (**Figure 7**D). Here, the main purpose of adopting a 3D printing fabrication technique for producing porous scaffolds was to achieve reproducible structures with a specific pattern and architecture. Therefore, the performance of P-ALG formulation was clearly worse than that of ALG. In this work, the quality of scaffolds was a priority, so we decided to use ALG in most experiments. Importantly, ALG is of pharmaceutical grade, which is unsuitable for *in vivo* applications, but suitable for *in vitro* studies.

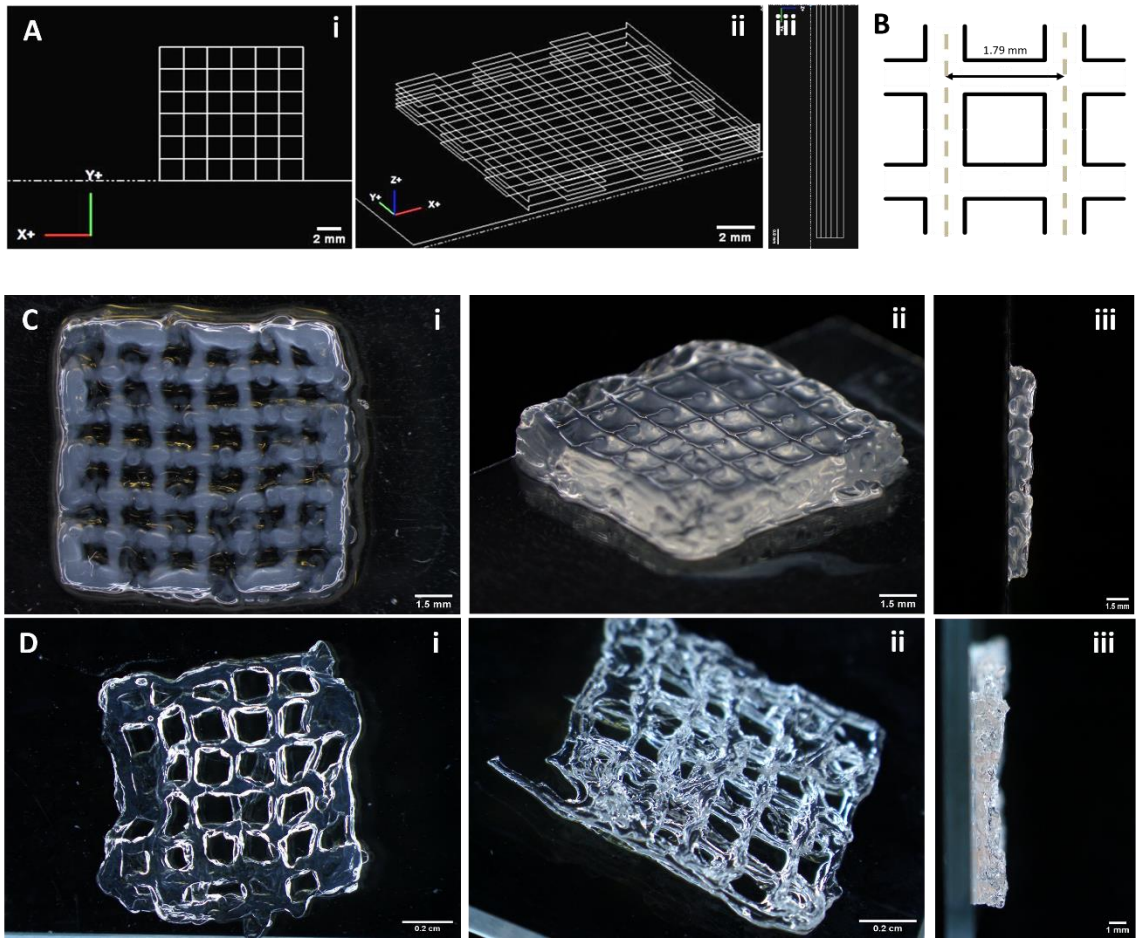

Figure 7 Characterization of alginate 3D scaffolds. **A**) Images showing the original CAD-design of the 3D scaffolds in a i) top view, ii) 3D view and iii) cross-section (lateral) view. **B**) Illustrative image showing the theoretical pore size and shape. Alginate scaffolds produced using: **C**) unpurified alginate (ALG) and **D**) purified alginate (P-ALG): these are also depicted in i) top view, ii) 3D view and iii) cross-section view. Scale bars: 0.2 cm, 1.5 mm, 1 mm or 0.8 mm

2. Cell seeding

2.1. RGD modification

After obtaining the 3D-printed constructs, the second step of our strategy was to optimize the seeding of human mammary fibroblasts (hMFs) onto the porous scaffolds. The aim was to achieve homogeneous colonization of the scaffolds by the initially seeded cells, which should then be able to produce/accumulate an endogenous ECM layer at the scaffolds' surface (**Figure 8**A).

A successful seeding strategy aims at maximizing cellular adhesion to the scaffold, minimizing the number of cells that fail to interact with the scaffold and eventually adhere to the well bottom. Special attention should be given to cell distribution upon seeding, which should be as uniform as possible, throughout the scaffold's surface. Along with that, the seeding

time should be as short as possible, to maximize cell survival and improve reproducibility [113]. Current cell seeding approaches include static and active strategies: static seeding involves pipetting a cell suspension onto the scaffold's top surface and let the cells infiltrate the structure before providing them media [114]. Even though this method induces very little damage to the cells, it generally results in low cell seeding density (high cell loss), especially in scaffolds with larger pores, heterogeneous cell distribution and low reproducibility. Dynamic seeding strategies, involving the application of external forces, namely centrifugation, rotation or even electromagnetic stimuli, might eventually be a better option, and could be explored in future studies [60,115,116].

Herein, to maintain a low degree of complexity, a static seeding strategy was adopted. Optimizable seeding parameters included i) cell density, ii) suspension volume and iii) technique. Alginate scaffolds exhibited a macro-porous patterned architecture, with open and interconnected pores of around 100x the size of a stretched fibroblast [117]. Also**,** as already discussed in the Introduction, unmodified alginate hydrogels are intrinsically non cell-adhesive. [61] Therefore, the material had to be modified with RGD integrin-binding motifs prior to scaffold production, to support cell adhesion.

Preliminary tests were made with P-ALG RGD-modified scaffolds (with 1.6 mm pores), even though such scaffolds were later on discarded, as already explained. Different RGD concentrations were tested, varying from 200 µM to 600 µM (**Table 7**). hMFs seeding was performed with a 30-µL seeding volume on top of each scaffold, at two different cell densities [114,115,118]. Cell metabolic activity along 7 days of culture was assessed through a resazurin assay (**Figure 8**B). Scaffolds were then fixed and stained for CLSM analysis (**Figure 9**).

Table 7 Testing of different RGD concentrations for alginate modification

Cell seeding density (nr cells/scaffold)	RGD concentration (µM)
$2.5x10^5$	200 400 600
$1.5x10^5$	200 400 600

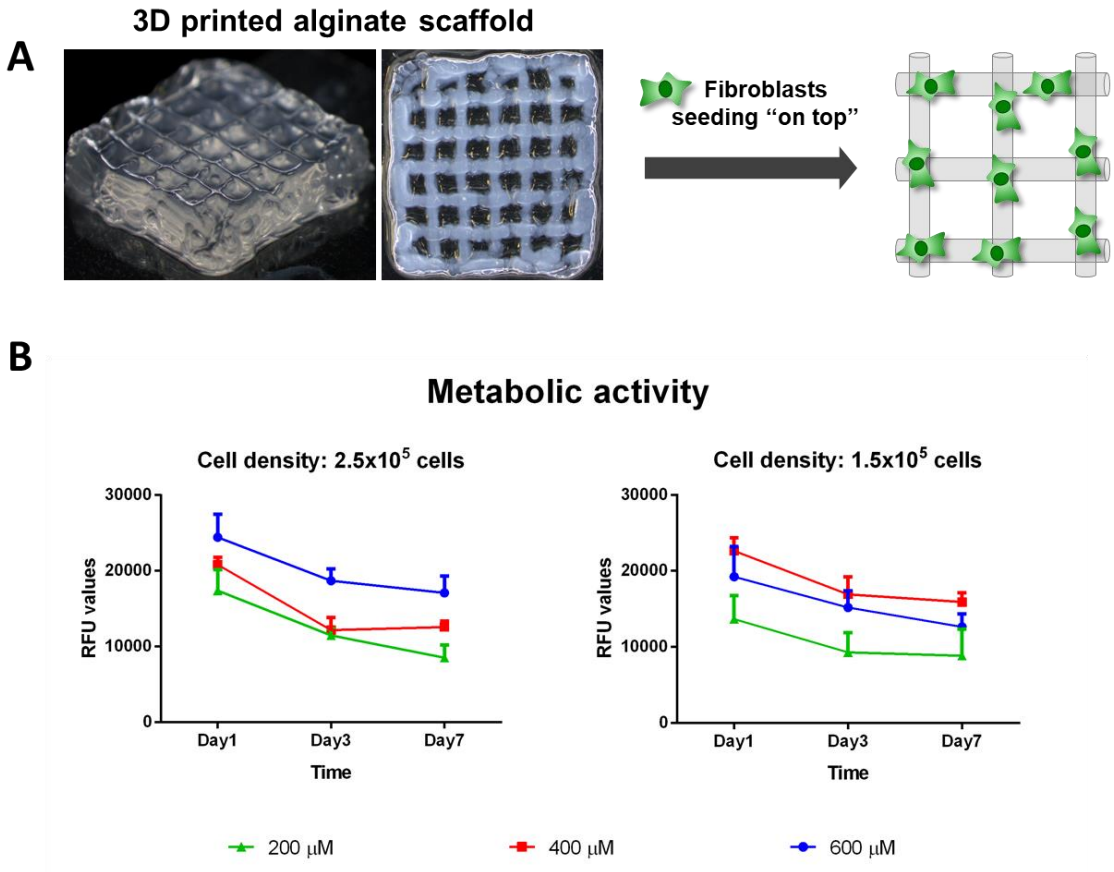

Figure 8 Culture of hMFs on top of printed alginate 3D scaffolds. **A)** Schematic representation of hMF seeding on top of printed scaffolds. **B)** Effect of cell seeding density and RGD amount on the metabolic activity of hMFs along time, measured wih the resazurin assay (3 technical replicates).

In all conditions, a decrease in metabolic activity was observed between days 1 and 3, and then a plateau was reached in almost all situations. The initial decrease was most likely due to cell loss through the scaffold's pores, of large dimensions. Comparing the different RGD concentrations for both cell densities, it can be observed that the amount of 200 µM RGD is the one resulting in lower initial cell adhesion (day 1) and overall metabolic activity. Higher metabolic activity was observed for the two other RGD concentrations. As depicted in **Figure 9**, analysis by CLSM corroborated these findings: cells were overall rounder and clustered in the lowest RGD concentration, while in the other conditions they were more spread and showed ability to assemble a FN meshwork, an essential ECM component (**Figure 9**). By comparing results obtained with 400 µM and 600 µM RGD, which were similar, we decided to use 400 µM in subsequent studies, as it represented a good compromise between cell response and the cost associated with alginate modification. This value also seemed adequate, when compared to values tested in previous studies performed in the group with other cell types [52].

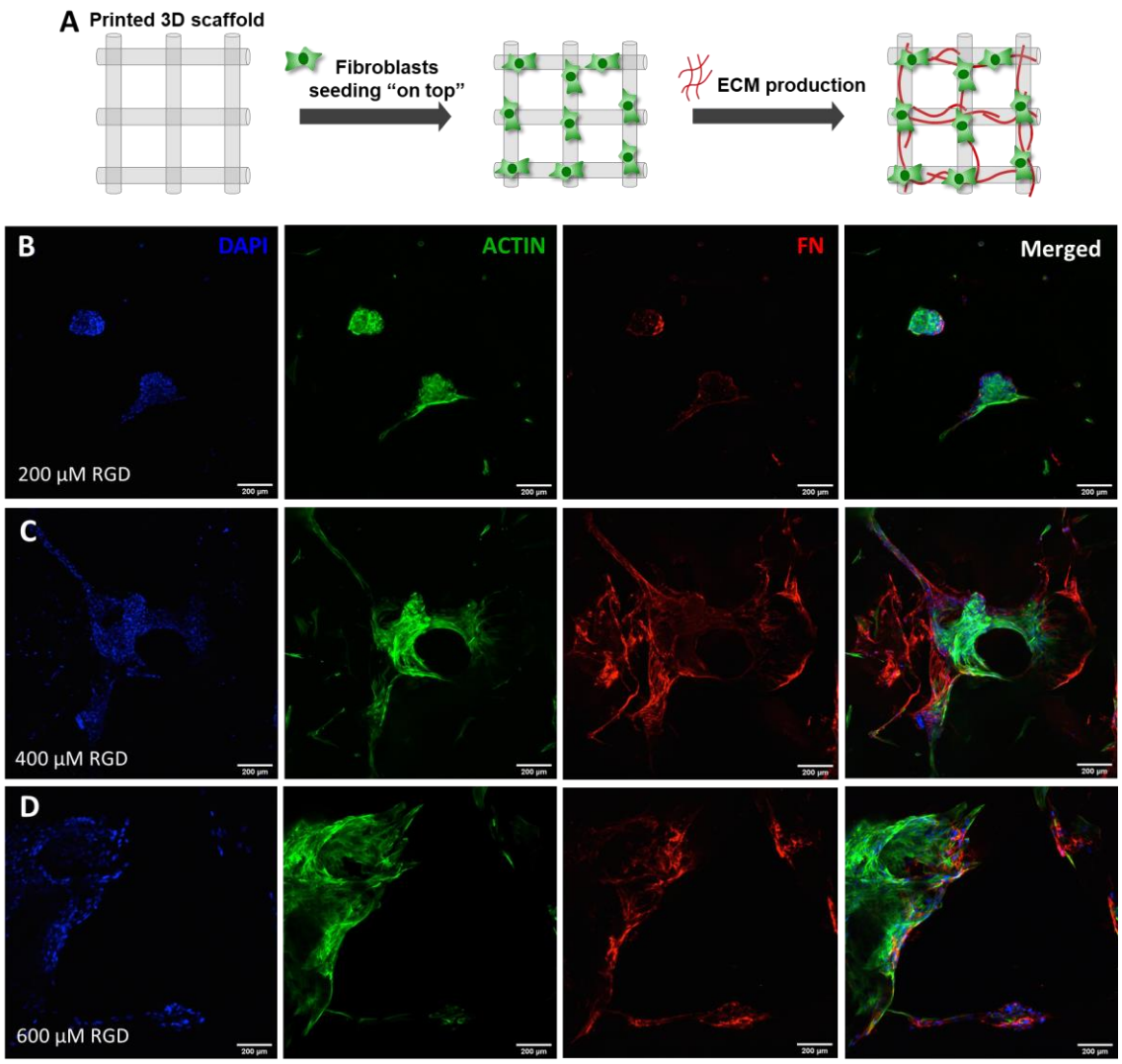

Figure 9 Optimization of the RGD concentration for alginate modification. **A**) 3D model development strategy step-by-step. CLSM representative images of cells seeded onto P-ALG with **B**) 200 µM, **C**) 400 µM and **D**) 600 µM RGD-modified alginate scaffolds, after 7 days of culture. Cytoskeletal organization of fibroblasts grown on the scaffolds at day 7 was demonstrated by F-actin (**green**), fibronectin (**red**) and DAPI (**blue**) staining. Scale bar: 200 µm (10x magnification)

2.2. Effect of porosity and material's properties

The type of material used to fabricate a 3D scaffold, but also its architecture will influence cell response, namely in terms of interactions established with the underlying substrate and with other cells [119]. 3D scaffolds printed with pre-defined geometrical features can have high and uniform porosity. However, the printing strategy used herein only allowed the production of macro-porous structures, with pore size varying from 1.5 mm to 2.0 mm. Such wide pores represent a huge challenge in terms of cell retention during seeding. Thus, different strategies were tested. As scaffold optimization was still ongoing, we used scaffolds of P-ALG with 1.6 mm, and ALG with 2.0 mm pores.

Table 8 Parameters that were varied in the two conditions tested

Condition	Cell seeding density (nr cells)	Alginate type	Pore size (mm)	Surface area (mm^2)
1	$2.5x10^5$ $1.5x10^5$	P-ALG	1.60	92.16
2	$1.5x10^5$ $1.0x10^5$	ALG	2.00	72

The size of the pores impacted the process in two different ways. During cell seeding, larger pores led to loss of a greater portion of seeded cells, which ended up adhering to the bottom of the well. Along culture, fibroblasts proliferated and stretched throughout the structure, populating its surface area, but tended to more easily bridge across smaller pores (condition 1). Thus, while smaller pores (condition 1) decreased initial cell loss, they also often resulted in undesirable formation of a cell monolayer on top of the scaffolds, due to cell bridging across pores. This process was probably facilitated by the fact that condition 1 involved the use of P-ALG scaffolds which, as already described, were poorly patterned with low shape fidelity. So, in this case hMFs did not only grow on top of fibers, but also inside and across the pores (**Figure 10**A). On the other hand, as expected, ALG scaffolds with 2.0 mm pores became more uniformly populated, with cells spreading and growing mainly on fibers, according to pre-defined geometrical features (**Figure 10**B).

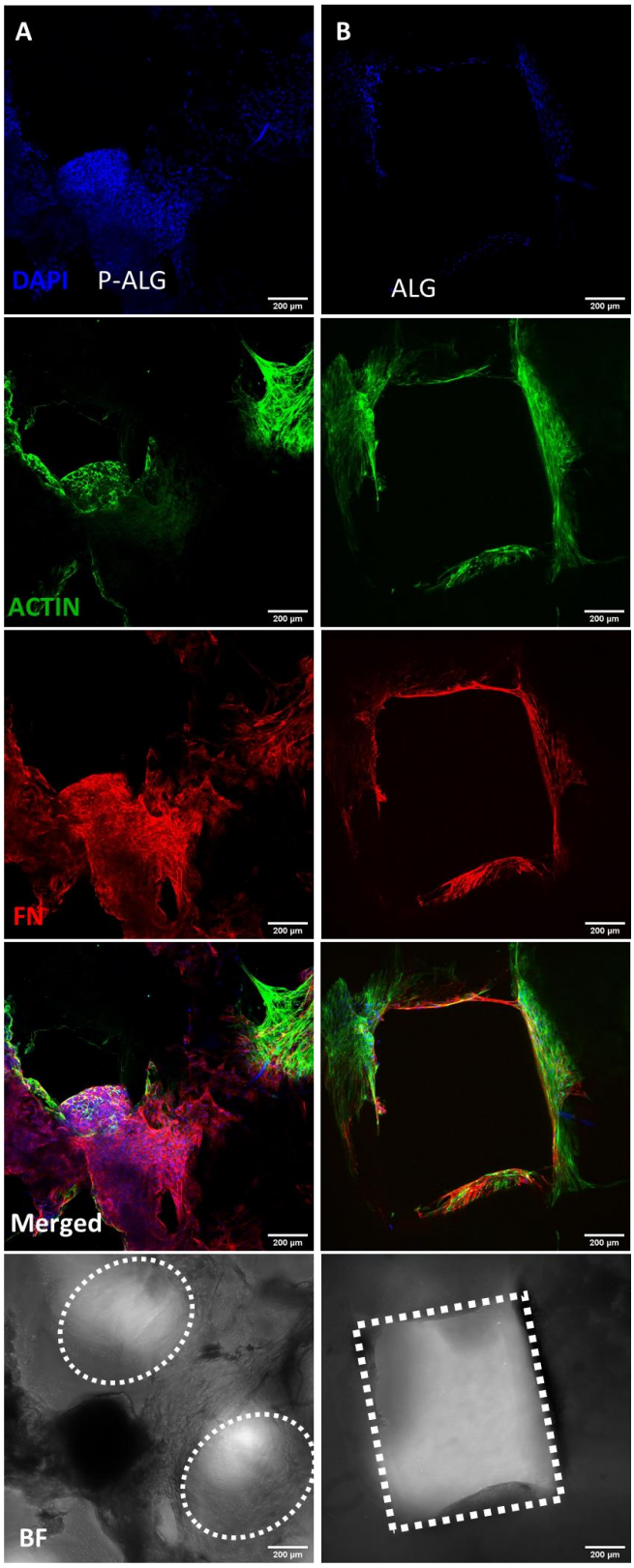

Figure 10 Effect of the type of alginate on hMF distribution/activity around pores of printed scaffolds. **A**) Printed scaffolds fabricated with purified alginate (P-ALG), and **B)** printed scaffolds fabricated with unpurified alginate (ALG). Representative CLSM images with cell nuclei stained in **blue**, F-actin skeleton in **green**, fibronectin (FN) fibers in **red**. Pore details are shown in BF images. Scale bars: 200 µm (10x magnification)

2.3. Effect of cell seeding density

To maximize the amount of adherent cells on the fibers, and not within pores, while minimizing the formation of a fibroblast-layer on top of the scaffolds, cell seeding was optimized using different concentrations, ranging from $1.0x10^5$ to $5.0x10^5$ fibroblasts per scaffold (**Table 9**) [114,118,120]. All scaffolds were produced using 400 µM-RGD ALG, with a 2.0 mm pore size, according to previously optimized conditions. Samples were analyzed by CLSM after different time points (around 2-3 weeks).

Table 9 Cell seeding densities tested for optimization

Condition	Cell seeding density (nr cells per scaffold)
1	$1.0x10^5$
2	$1.5x10^5$
3	$2.5x10^5$
4	$5.0x10^5$

In condition 1, cells were clearly insufficient to populate the whole structure, and did not spread (data not shown), so samples were not further analyzed. In condition 2, despite some initial difficulties in populating the scaffold, fibroblasts reasonably covered the surface of the scaffold after 21 days (**Figure 11**A). However, cell distribution was not uniform, and a portion of the structure was not covered by these cells. In condition 3 (**Figure 11**B), while there was some cell loss during seeding, there was still a reasonable amount of cells that managed to adhere to the scaffold. Along culture, cells were able to uniformly colonize most of the 3D structure throughout the different layers. Still, some portions of the surface were not covered by cells, suggesting that the seeding approach should be further improved. Therefore, a higher cell seeding density was tested (condition 4), to ensure better coverage of the scaffold, while reducing, to a maximum of 2 weeks, the culture time needed for implementing the next steps (addition of epithelial cells or decellularization). So, in condition 4 (**Figure 11**C), $5.0x10^5$ hMFs were seeded per scaffold and cultured for 14 days. Similarly to the other conditions, a portion of cells was lost during seeding, but more cells managed to adhere to the scaffold providing better surface coverage. Analysis of CLSM results showed that cells were well spread, with an organized cytoskeleton (F-actin pseudo-colored in green) and were able to produce ECM (FN mesh pseudo-colored in red). Importantly, the pores were left uncovered, and the open architecture was preserved.

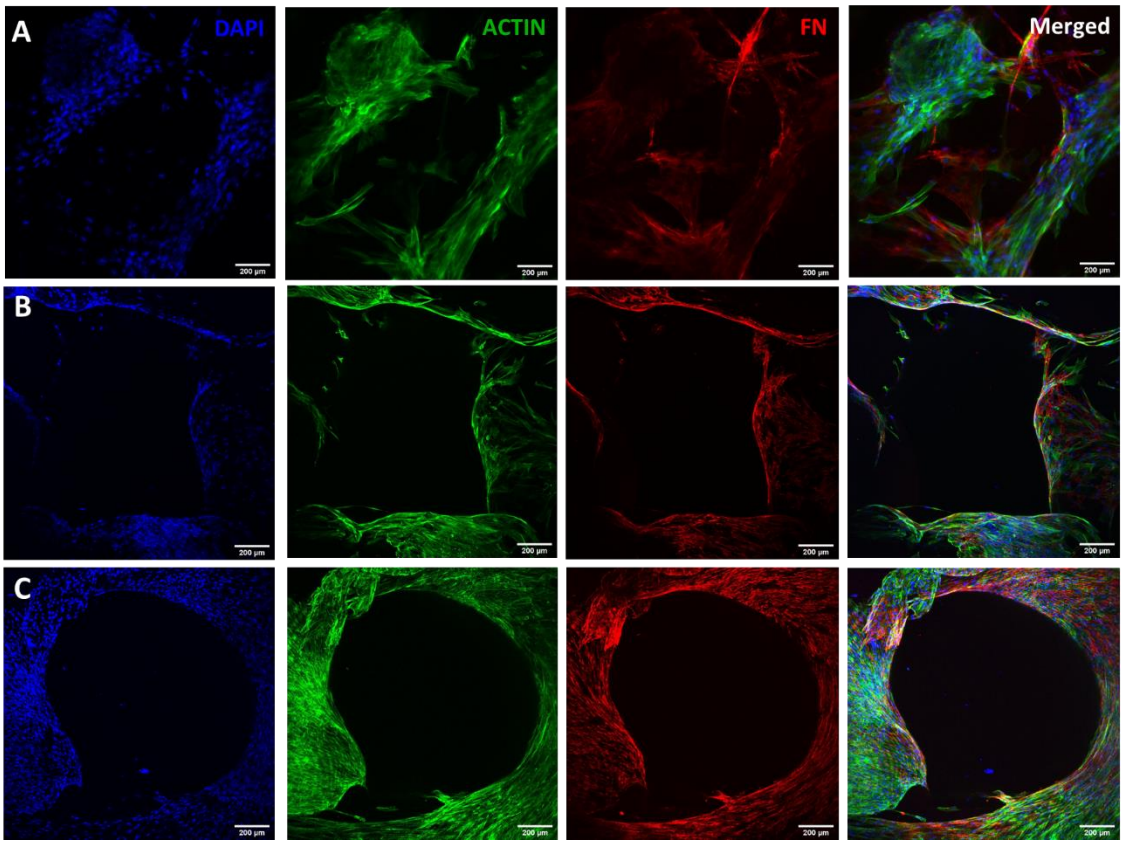

Figure 11 Effect of the seeding density on hMF distribution/activity around pores of printed scaffolds after 14-21 days of culture. Representative CLSM images of alginate scaffolds seeded with **A**) $1.5x10^5$, **B**) $2.5x10^5$ and **C**) $5.0x10^5$ hMFs, with cell nuclei stained in **blue**, F-actin skeleton in **green**, FN fibers in **red**. Scale bar: 200 µm (10x magnification)

To prove that hMFs were not only growing on the top portion of the scaffolds (where seeding was performed) but also on the bottom surface, CLSM images from both sides were obtained. **Figure 12** shows mosaic CLSM images of hMFs colonizing a half-scaffold after all optimizations: 400 µM-RGD ALG scaffolds, with $5.0x10^5$ hMFs, cultured for 14 days.

Some parallel seeding experiments were performed with CellTracker™-stained fibroblasts. Seeding was performed in a phased manner, at three different moments, and cells were pseudo-colored in red, green and blue for each of the seedings. CLSM results allowed to see cell growth across the structure over time, and to evaluate cell spreading starting at each seeding timepoint (**Figure S 2**, SI).

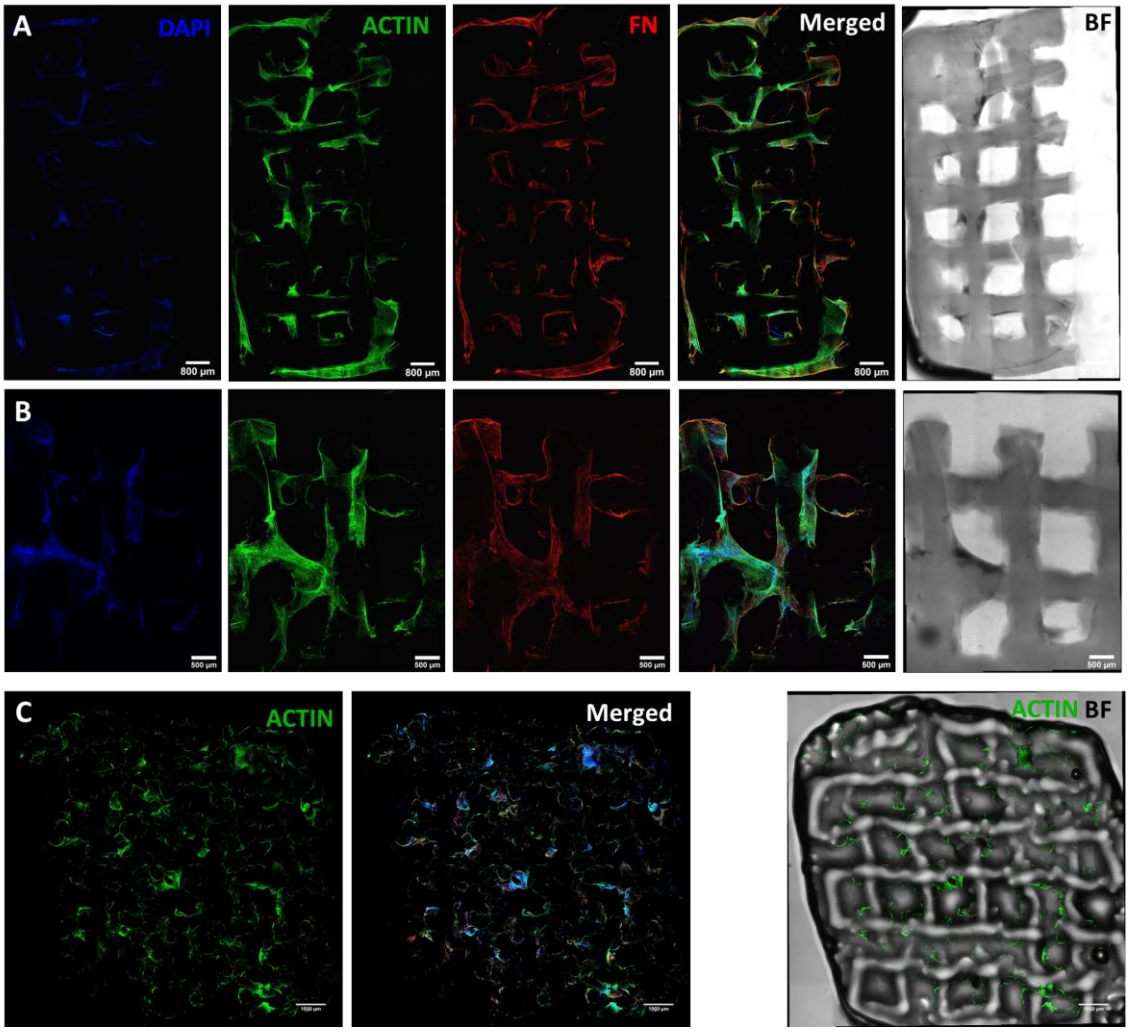

Figure 12 Characterization of optimal hMF-seeded alginate 3D scaffolds. Representative CLSM images of alginate 3D scaffolds (ALG, 400 µM RGD) seeded with $5.0x10^5$ hMFs. **A**) Images of scaffold halves and **B**) magnification showing pores in more detail. **C**) Zoomed-out mosaic image of a whole scaffold cultured with $1.0x10^6$ cells. Fibroblasts grown for 14 days on top of printed scaffolds were able to spread (F-actin, **green**), and produce FN-rich ECM (**red**). Geometry and disposition of pores in the scaffold is depicted by BF imaging. Scale bar: 500 µm or 800 µm (10x and 10x zoomed-out magnification)

Due to optimization purposes, tested scaffolds only included halves of the original structures, as stated above. However, when working with the full 12 X 12 mm scaffolds, the double of the cells should be used to obtain a similar result. This was confirmed by seeding 1 million hMFs onto 12x12 mm 6-layered scaffolds and growing the cells for 2-weeks. Obtained results are shown on **Figure 12**C. Other optimizations were also tested and are presented as SI. These included the optimization of the seeding volume. Namely, to facilitate cell retention and maximize adhesion, cells were seeded in a concentrated suspension, and the construct was maintained in a minimal volume for 2 hours. Only after this time was the remaining media added. The first tests were performed on RGD-modified scaffolds without any cells. Complete

media was pipetted onto the top surface of the scaffolds, to mimic seeding, in various volumes, from 10-50 µL (**Figure S 3**, SI). From that experiment, a volume between 30 µL and 40 µL was considered to be ideal, allowing retention without having excessive fluid flowing through the pores and into the bottom of the well. To promote uniform distribution, addition of cell suspension was done in 10-µL droplets, distributed over different scaffold regions. Even though this was the final optimization performed regarding seeding volume, additional changes could be made. Ideally, a pipetting robot would ensure a more uniform seeding of the cells in each region of each scaffold, avoiding unnecessary user mistakes and deviations, and making the seeding process as uniform as possible.

Some attempts were also made to try to minimize initial cell loss during seeding. For this, cells were suspended in medium containing ALG in order to increase its viscosity (0.10-0.75% w/v alginate) prior to seeding. This method effectively promoted higher retention of cells, but after some days of culture, cells remained arrested in the medium containing ALG, and were thus unable to colonize the surface of the scaffold. The round-shaped cells remained entrapped even after media or well changes. The strategy did not produce the desired result and was therefore abandoned (**Figure S 4**, SI).

2.4. Fibroblast-derived ECM characterization

During optimization steps, it was possible to conclude that hMFs were able to assemble a FN mesh on top of the scaffolds, which is a key component of the ECM. Thereafter, a more detailed characterization of the cell-derived ECM was done by staining scaffolds with specific antibodies for other components, such as type I and type IV collagen [58,121] and analyzing their distribution by CLSM.

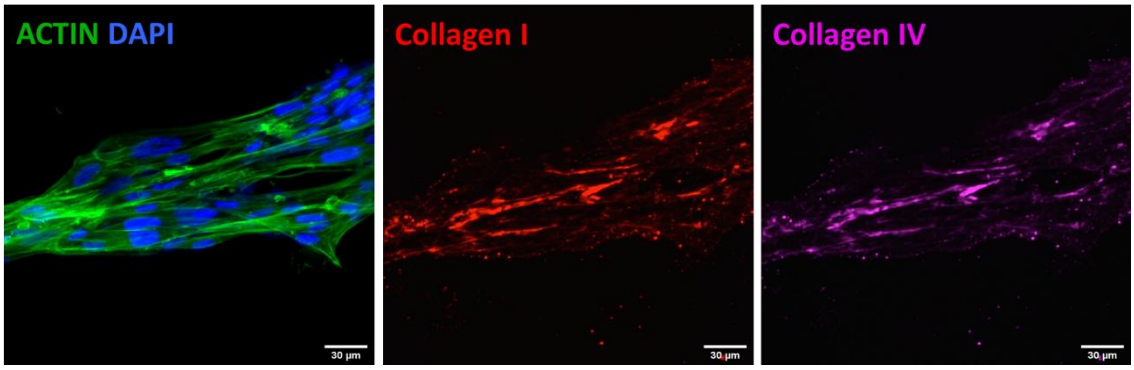

Figure 13 Characterization of hMF-produced ECM. Representative CLSM images of alginate scaffolds seeded with $5.0x10^5$ hMFs. Fibroblasts grown on the scaffolds for 14 days were able to spread (F-actin, **green**) and secrete/accumulate an organized fibrillar ECM, rich in collagen I (**red**) and collagen IV (**pink**), which were co-localized. Scale bar: 30 µm (60x magnification)

Figure 13 shows that ECM components were effectively present, co-localizing with the cell layers, further proving that seeded fibroblasts can produce endogenous ECM on the printed scaffold. Further characterization of the fibroblasts' network distributed over the alginate fibers was performed with histology, using hematoxylin and O-safranin staining. However, due to technical issues during processing of the paraffin-embedded samples, the cellular networks seemed to have detached from the alginate fibers, even though they still maintained a mesh-like structure (**Figure S 5**, SI).

The presence of ECM components is very relevant, as the aim was to recapitulate as much as possible the stromal environment of breast tissue. After addition of the epithelial compartment, these matrix components might not only help epithelial cells acquire their native morphology, but they are also expected to contribute to cell signaling and thus influence cell activity [122].

In future studies, ECM characterization should be assessed at different timepoints of the fibroblasts' culture, to evaluate and quantify matrix production and dynamic alterations throughout time.

3. Adding the parenchymal compartment: hMFs and MCF10A cells co-culture

After establishing the stromal component of the model, epithelial cells were added as the parenchymal compartment of mammary gland tissue. Previous work developed in the group reported the development of an alginate-based 3D *in vitro* model to culture a mouse mammary epithelial cell line. This model successfully mimicked epithelial morphogenesis and documented the formation of acinar-like structures similar to the ones found *in vivo* after 14 days of culture [52]. With our model, we tried to replicate the results previously obtained, but now adding a stromal compartment to enhance the model's complexity, while still supporting epithelial morphogenesis, paving the way for future crosstalk studies under co-culture conditions. Preliminary studies on the direct co-entrapment of fibroblasts and epithelial cells in the hydrogel were not successful, as fibroblasts were unable to spread and accumulate ECM (data not shown). Therefore, cells were combined in a phased manner.

Epithelial cells were combined with hydrogel precursor solution (1 wt.% alginate, 200 µM of RGD) [52] and the fluid mixture was dispensed on top of the scaffolds, so that the gelation process could occur inside the scaffold, forming a hydrogel that filled the pores. Hydrogel-entrapped epithelial cells were grown for 10-14 days, which, according to our previous studies, was enough time for cells to proliferate and undergo epithelial morphogenesis when cultured alone (**Figure 14**A,B) [52].

After culture, scaffolds were analyzed by CLSM. **Figure 14**B,C shows that epithelial cells were distributed throughout the scaffold, namely inside the pores. As depicted in **Figure 14**D, epithelial cells proliferated assembling into spheroids and/or acinar-like structures (**Figure S 6**, SI) similar to the ones documented in [52]. The images also show that these structures (**Figure 14**C,D, red arrows) were in close contact with fibroblasts (**Figure 14**C,D, white arrows), which had been in culture for a period of 28 days.

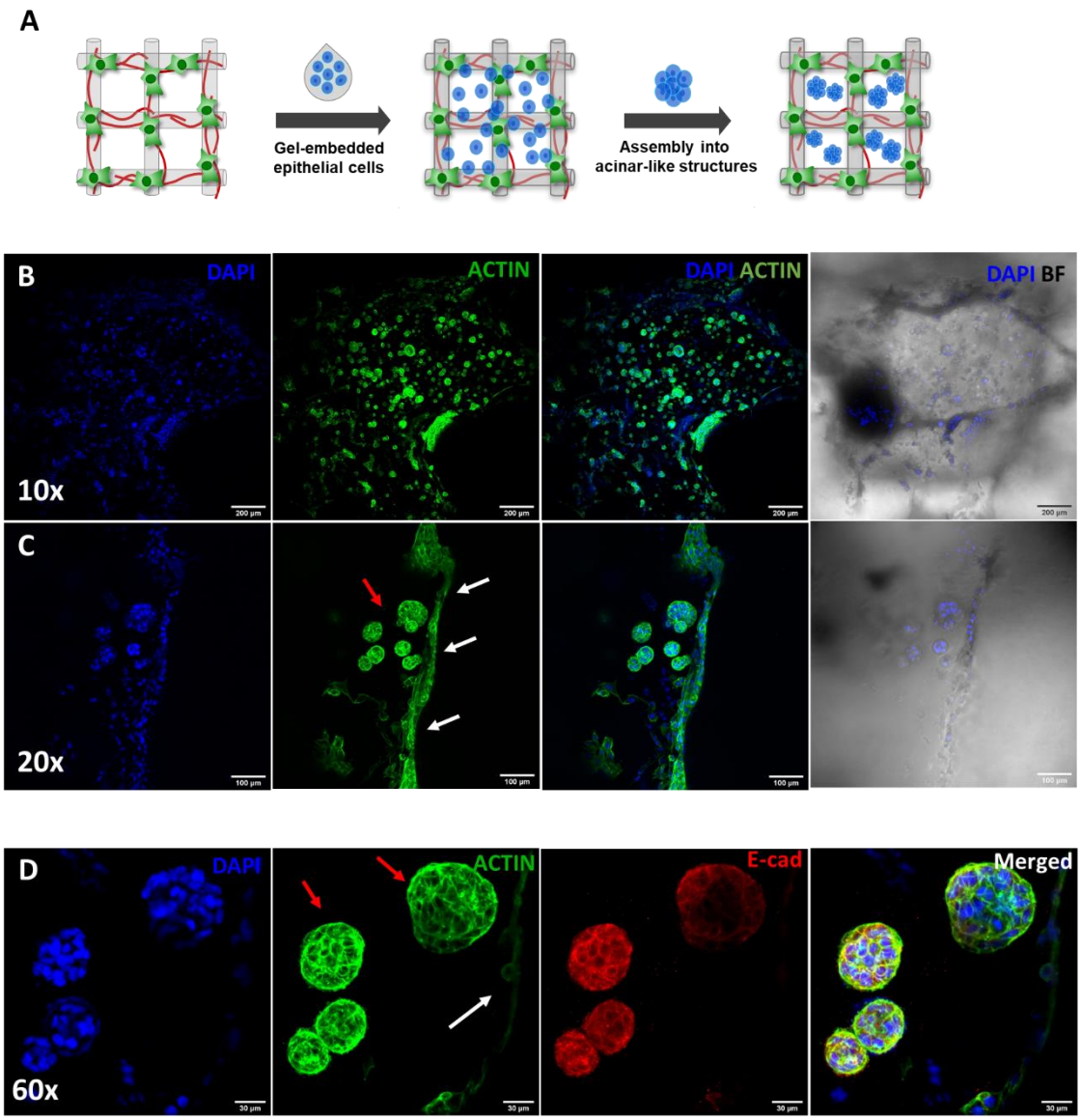

Figure 14 hMF and MCF10A co-culture in alginate scaffolds. **A**) 3D model development strategy step-by-step. Representative CLSM images of alginate scaffolds seeded with $5.0x10^5$ hMFs and $3.5x10^5$ MCF10A. **B**) Organization of co-culture on the scaffolds and of **C**) cellular interactions at day 28 was demonstrated by F-actin (**green**) and DAPI (**blue**) staining. **D**) Epithelial morphogenesis of MCF10A cells was demonstrated by F-actin (**green**), DAPI (**blue**) and E-cadherin (**red**) staining. Scale bar: 200 µm (10x magnification), 100 µm (20x magnification) or 30 µm (60x magnification), respectively

These results were further corroborated by histological analysis with O-safranin and hematoxylin staining. Even though hematoxylin equally stains both cell types, one can partially distinguish them by analyzing cell shape and spatial distribution across the alginate scaffold. **Figure 15** shows one of the scaffold's pores surrounded by alginate (stained in red by O-safranin). Within the pore, there is also alginate, with cell clusters which are, presumably, composed of epithelial cells. The higher magnification image (**Figure 15**B) shows the presence

of spread cells at the interface (pore surface), presumably fibroblasts, some of which still attached to the printed alginate scaffold.

Even though no quantitative assessment was performed along the time, it can be hypothesized that both cell types remained metabolically active by analyzing their behavior throughout the culture period. Fibroblasts first appeared as round cells, but spread and produced ECM along time, while epithelial cells proliferated forming multicellular structures similar to acini found in mammary gland tissue. Still, to prove that cells were effectively alive, a Live/Dead assay was performed on co-cultured scaffolds, at day 28 of culture (**Figure S 7**, SI). In this assay, a large number of both epithelial cells and fibroblasts were stained in green (calcein AM), while very little cells were stained in red (propidium iodide), demonstrating that cells remained viable after 28 days of culture.

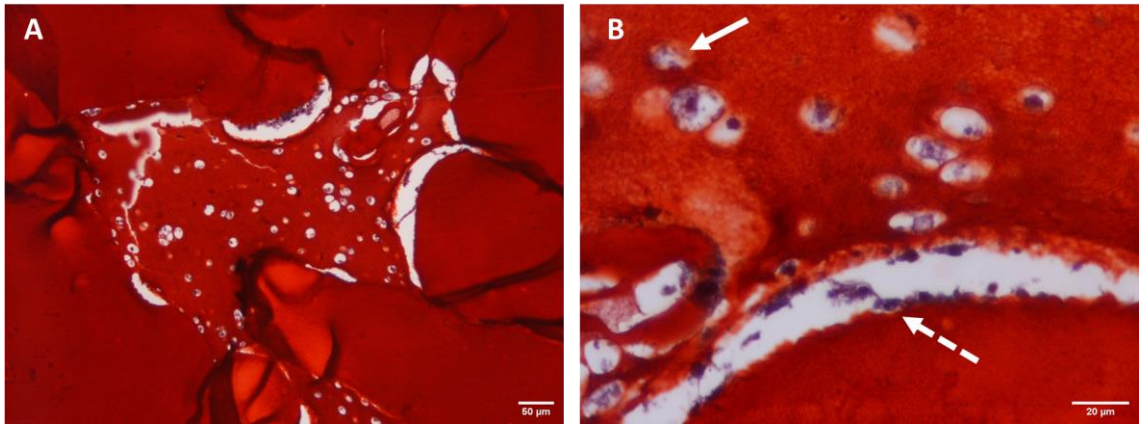

Figure 15 Histologic characterization of co-cultured alginate 3D scaffolds. O-safranin (alginate) and hematoxylin (cell nuclei) staining of paraffin-embedded sections (6-µm), at day 28 (14 days after addition of epithelial cells). **A**) Detail of a pore filled with hydrogel laden with MCF10A epithelial cells, where some of them assembled into spheroid-like structures (scale bar: 50 µm, 10x magnification). **B**) Detail showing that pore walls are populated by cells, presumably hMFs (dashed arrow), which are in close contact with epithelial structures (full arrow) (scale bar: 20 µm, 40x magnification)

Taken together, our results demonstrated the successful establishment of a direct co-culture system, with both stromal and parenchymal compartments, where cells are combined in the same 3D microenvironment. Indirect cellular interactions may occur, mediated by the secretion of growth factors, cytokines and other soluble molecules capable of diffusing throughout the culture system and promoting paracrine signaling [123]. By partially recreating the native breast tissue environment, namely by facilitating heterotypic interactions between stromal and epithelial cells, our 3D model is expected to provide a useful tool to study breast tissue features and alterations, both under healthy or pathological conditions.

4. Model validation: separation of hMF and MCF10A populations after culture

After setting-up the proposed complex 3D model of breast tissue, further validation was required to demonstrate that the model could serve its main purpose: allow the detailed characterization of mammary stromal-epithelial interactions. This should not only include imaging methods such as CLSM and histological analysis, as was previously explored in this work, but also through systematic analysis of gene and protein expression levels after cell-cell and/or cell-ECM interactions along time. For this, the model should allow cells to be retrieved from the construct and separated into different populations. As already discussed, one of the main reasons for selecting alginate as scaffolding material was its ability to form reversible ionically-crosslinked hydrogels, which can be easily dissolved upon addition of a chelating agent.

Thus, herein, cell retrieval after 28 days of culture was promoted by incubating the alginate scaffold in a trypsin/EDTA solution, to reverse the crosslinking of the alginate hydrogels, and disrupt cell-cell and cell-matrix interactions (**Figure S 8**, SI).

The obtained mixed cell suspension was then subjected to flow cytometry (FC) analysis, in an attempt to separate the two cell types. Before that, specific cell markers for fibroblasts and epithelial cells had to be tested and validated. Particularly, CD90 (Thy-1) was tested as a surface marker for fibroblasts, while E-cadherin was tested as an epithelial cell marker. We performed FC analysis using antibodies for these markers to assess their capacity to successfully stain each cell type after monoculture, on both 2D and 3D conditions. These worked as negative (unstained samples) and positive (stained samples) controls, to account for changes in marker expression depending on culture setup (**Figure 16**A).

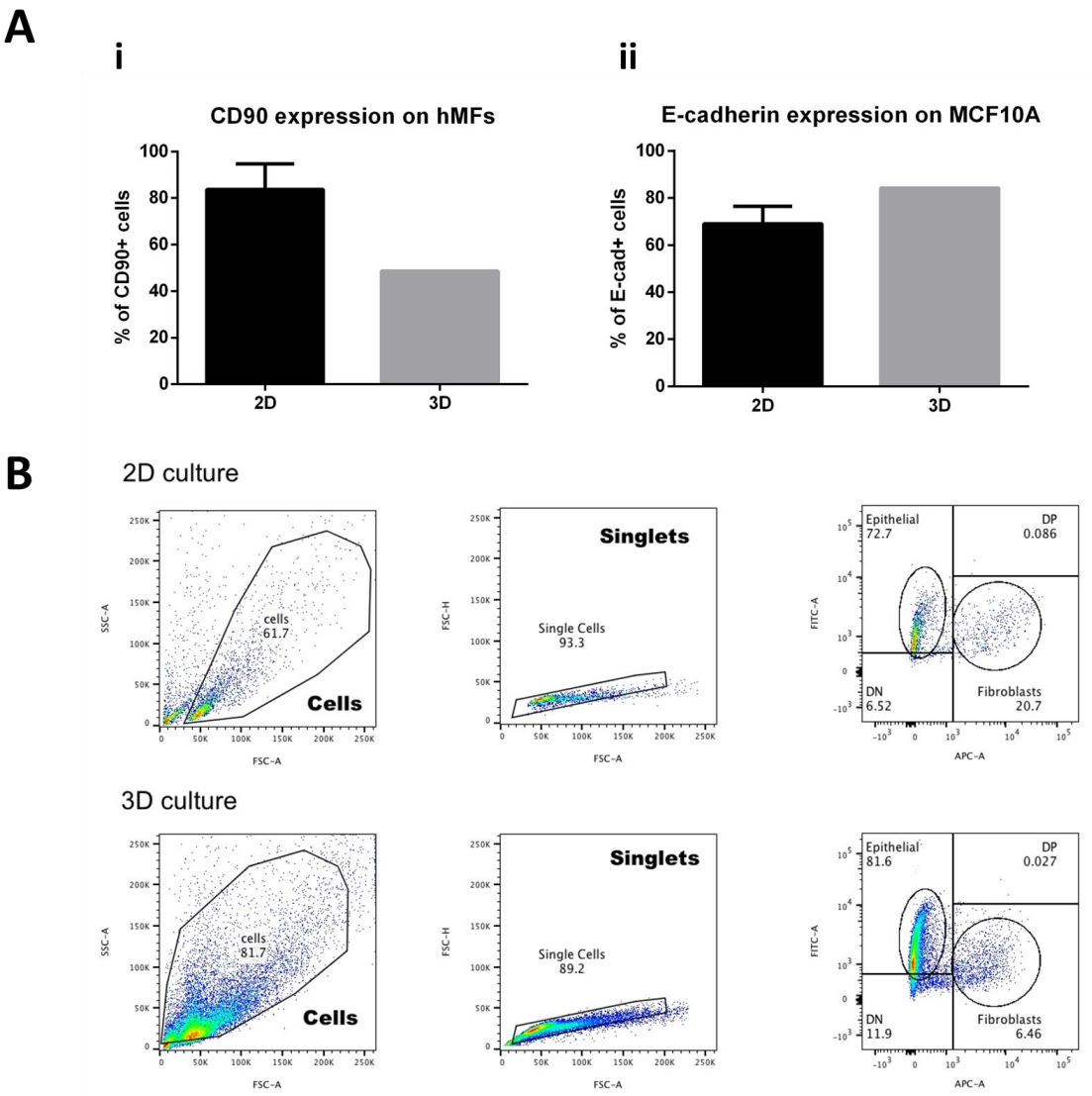

Figure 16 FC analysis of hMF and MCF10A after culture time. **A**) i) hMFs expression of CD90 and ii) MCF10A expression of E-cadherin were validated with flow cytometry. Both cell types were successfully separated with FC, when analyzing mixtures which had been cultured in **B**) 2D and 3D.

Figure 16 shows that fibroblasts were positive for CD90, with expression varying from 80% to 50% on 2D and 3D conditions, respectively. MCF10A epithelial cells stained positive for E-cadherin, with expression leveling to around 85% on 3D conditions. Further analysis of both isolated cell populations (monocultures) on FlowJo revealed that fibroblasts have some auto-fluorescence in the FITC channel (the one on which E-cadherin is shown). This interfered with the results, due to presence of a fibroblastic population in the $FITC^+$ quadrants, and thus led to a marginal error in the percentages of epithelial cells hereby described (**Figure S 9**, SI). However, in future studies, this problem could easily be overcome by using another fluorochrome for E-cadherin (such as PE, or PE-Cy7).

Based on these results, we decided to continue the analysis using these markers to distinguish/separate the two cell populations after co-culture. A mixed suspension was analyzed on the cytometer, to validate the ability to discriminate the two populations: hMFs as $CD90^{+}E\text{-}cad^{-}$, and MCF10A as $CD90^{-}E\text{-}cad^{+}$. **Figure 16**B confirms that the two different cell populations can be successfully separated. On 2D cultured cells the outcome was better, with only 6.52% of events appearing as double negative, 72.7% of events as $CD90^{-}E\text{-}cad^{+}$ (MCF10A), and 21% of events as $CD90^{+}E\text{-}cad^{-}$ (hMFs). On 3D cultured cells, results were less clear, with around 12% of events appearing as double negative, 82% of cells as MCF10A, and only around 7% as fibroblasts.

CD90 is expressed by fibroblasts from different tissues, as well as by mesenchymal stem cells. Alterations on its expression levels have been correlated with cell differentiation/activation stages [124,125]. Thus, one possible reason for the decrease in CD90 expression on 3D cultured fibroblasts may be the fact that these were being stimulated by the 3D environment. Apart from this, the reduced $CD90^{+}$ cell number could be due to fibroblastic loss along the staining process. This could eventually be due to an inefficient trypsin treatment, which might have failed to detach cells from the alginate, therefore leading to lower numbers of these cells in the mixture. On the other hand, E-cadherin is a cell-cell adhesion molecule commonly expressed by epithelial cells, which is known to be one of the main players in maintaining tight junctions between cells when these form acini in breast tissue. So, since MCF10A epithelial cells are stimulated to form these structures when in 3D, it seems reasonable to hypothesize that E-cadherin expression could be slightly increased in 3D, as compared to 2D monocultures [126].

Moreover, it is relevant to mention that during culture, cells are expected to undergo gene and protein alterations, which might lead to variations in expression of different markers. Furthermore, because MCF10A epithelial cells are very plastic, and prone to undergo epithelial-to-mesenchymal transitions [127], for example, this increases the possibility for variations in marker expression, which can make it harder to sort these cells, and can partially explain the variation in expression levels of the analyzed markers. Therefore, it would be recommended to improve the process of discriminating the two populations, by using more than one marker for each cell type. Taking these results together, and although the protocol clearly needs further optimization, our results suggest that in future studies the two cell populations could effectively be sorted by flow cytometry and further analyzed separately, for an efficient use of the 3D model.

5. Preliminary results on 3D model variations

5.1. Decellularization of scaffolds to study interactions between hMF-derived ECM and epithelial cells

One of the possible variations of this 3D model according to **Figure 4** would be to produce a cellular-derived matrix (CDM), through decellularization of the hMF culture on the alginate printed scaffold, before adding gel-embedded epithelial cells on top of the dECM. This would allow isolating the effect of the ECM on epithelial cells, from other interactions with fibroblasts. Decellularization must be optimized for each particular system, to allow for successful cellular/nuclear material removal with minimal ECM damage. Because this is a 3D scaffold, decellularization treatments might be less straightforward than those typically used for 2D cultures, where cells are uniformly distributed throughout a planar substrate. Herein, we started by slightly adapting detergent washing steps from a protocol previously optimized in the group for 2D monolayer cultures, based on Triton X-100 with NH_4OH, and tested some variations, namely increasing the incubation time or using SDS as an alternative detergent (**Figure 17**).

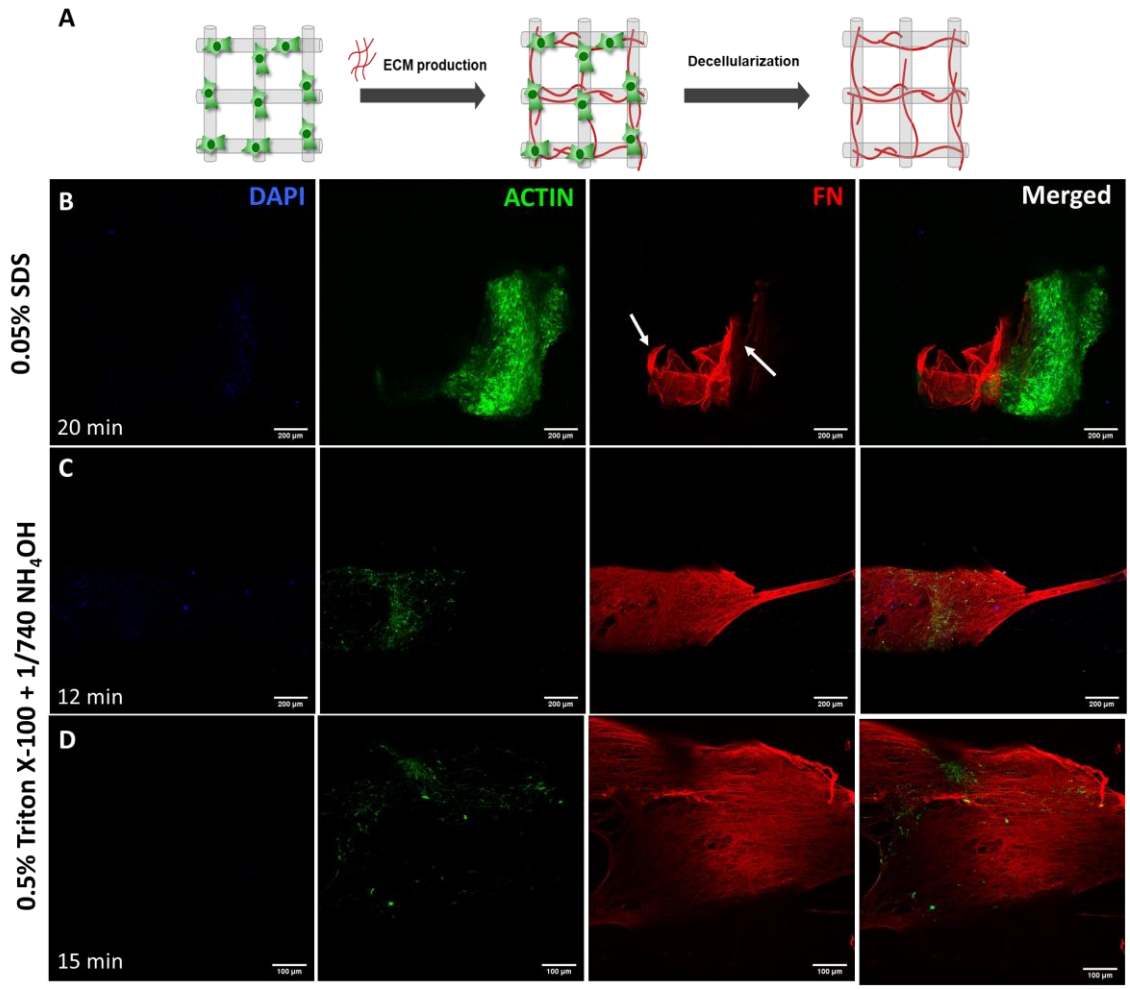

Figure 17 Decellularization preliminary results on 14 day-cultured hMFs. **A**) 3D model development strategy. **B**) Primary experiments with SDS treatment left some F-actin remaining in the scaffolds and disturbed the ECM's normal structure (white arrows). **C**) A 12-min treatment with Triton X-100 and NH_4OH led to better results, with almost no traces of F-actin or DAPI and leaving FN undisturbed. **D**) Treatment timing (for Triton X-100) was increased to 15 min, and results were better. However, some irregularities were noticed, showing intra- and inter-scaffold variability (data not shown).

Figure 17 which depicts CLSM analysis of the decellularized scaffolds, shows that treatment with 0.05% SDS for 20 min was not sufficient for removing all cellular traces (F-actin staining) in the structures, even though nuclear material was not present (DAPI staining). Moreover, while some fibroblast-derived ECM (FN staining) was detected, it appeared extremely folded (**Figure 17**B, white arrows). In future studies it might be worthwhile to vary the SDS incubation time. In parallel, scaffolds were treated with 0.5% Triton X-100 mixed with 1/740 NH_4OH, for 12 min (**Figure 17**C). This led to better results, as compared to SDS, with almost no traces of cellular and nuclear components, and maintenance of a seemingly uniform and well-structured FN mesh. Therefore, after comparing treatment with both detergents, Triton X-100 was chosen over SDS to pursue further optimizations. Because some F-actin traces were still

captured on CLSM images, treatment time was increased by 3 minutes, but no significant changes were seen (**Figure 17**D).

Yet, none of the treatments yielded uniformly decellularized scaffolds, and there was some variation between different regions within the same sample and between samples/procedures. Thus, these preliminary experiments highlighted the difficulties of optimizing a decellularization protocol for our 3D model, showing that much effort would have to be put into this step to achieve a satisfactory result. Other steps requiring optimization are the initial washing step with hypotonic buffer, which leads to membrane bursting and release of cellular contents; and the DNAse I treatment that could be improved to promote better cleavage and elimination of DNA traces [98].

Importantly, even with an optimized decellularization protocol, it would be necessary to first guarantee that the scaffolds themselves are homogeneously populated, to obtain a protocol that works with an efficiency as uniform as possible within the same scaffold. Lastly, after all optimizations, it will be important to establish an adequate methodology to characterize the ECM, before and after decellularization, to assess maintenance of matrix composition after treatment. Apart from CLSM, using antibodies for different ECM components, it would be interesting to perform a quantitative analysis by western blot and/or proteomics, for example. [98] Nevertheless, even though we have not been able to establish an optimal decellularization protocol some preliminary advances have been made.

5.2. Adapting the 3D platform for improved assay throughput

To facilitate the use of the 3D-printed scaffolds and improve the throughput of future assays, we decided to create miniaturized versions of the previously described 3D scaffolds, more adequate for use in 48- or even in 96-well plates. To do this, the original squared scaffolds were punched using stainless steel biopsy punchers of 8 mm, 6 mm and 4 mm. After punching, scaffolds maintained their stability and pore shape while kept in ethanol or medium for a period of at least 10 days (**Figure S 10**, SI). 8-mm punches fitted in 48-well plates, while 6-mm and 4-mm punches fitted in 96-well plates (**Figure 18**A).

We then tried to replicate the seeding conditions that had been optimized for the original scaffolds, on the miniaturized replicates. Therefore, seeding was performed on top of 6-mm punched scaffolds, maintaining the same conditions, except for the cell seeding density, which was adjusted according to the scaffolds' area, from 5.0×10^5 cells (half scaffolds, 72 mm^2 surface area) to 2.0×10^5 cells per scaffold (6.0-mm punched scaffolds, 28.3 mm^2 surface area).

After performing a first experiment, where cells did not grow throughout the structure, forming big clusters soon after seeding, cell density was lowered to $1.5x10^5$ cells and a new seeding experiment was performed. After 14 days, scaffolds were stained and analyzed by CLSM (**Figure 18**B). This showed cells were able to spread throughout the whole scaffold, on both sides, similarly to what was previously seen with half and whole scaffolds. However, when looking at BF images taken by CLSM, pores seemed to have lost their shape, leading to cells distribution all over the scaffold, i.e. also within pores, and not just confined to the alginate fibers. Although the reasons for this remain unclear, perhaps the punching process is not the most effective, affecting the inner pores that become less protected when cutting out the boundaries, and thus making the scaffolds more prone to deformation, especially after addition of cells and media.

Although we have not been able to further optimize the process, it would be worthwhile to test other conditions in future studies. Scaffold miniaturization would allow improvements over the model's features, namely a higher control over seeding and culture, which could take place in 96-well plates, for example using seeding robots. Such system would also be more easily adaptable to current high-content bio-imaging platforms, for example, facilitating the analysis of multiple replicates in the same plate and ensuring higher reproducibility. Furthermore, system miniaturization would reduce reagent consumption, minimize the use of cells and facilitate analysis and trial-and-error combinatorial approaches for testing multiple conditions optimization [128,129].

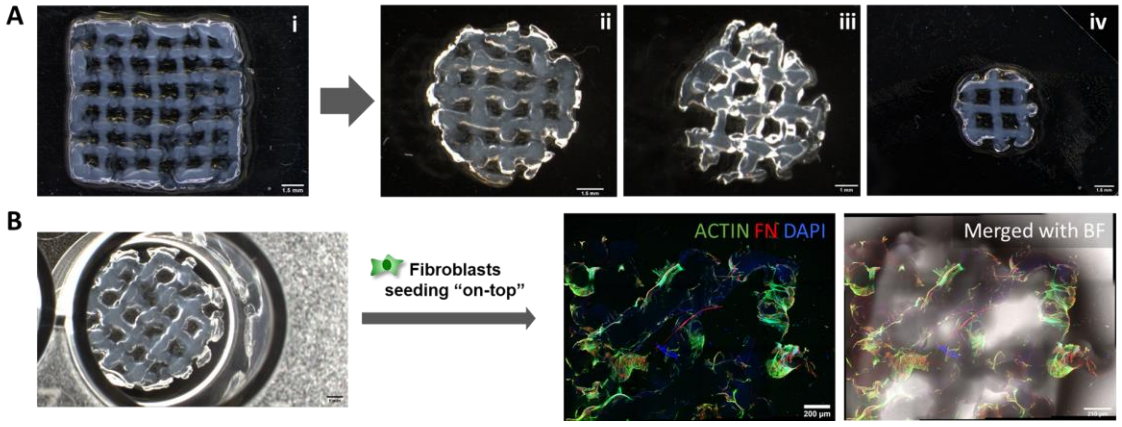

Figure 18 3D model miniaturization strategy. Characterization of the possible miniaturization strategy by **A**) producing smaller scaffolds, using ii) 8-, iii) 6- or iv) 4-mm biopsy punchers, to be able to culture cells in **A** ii) 48- or **A** iii, iv) 96-well plates, in a high-throughput system. **B**) Preliminary optimization experiments on hMF culture on 6-mm punched scaffolds, inside 96-well plates, stained for F-actin (**green**), DAPI (**blue**) and FN (**red**). Scale bar: 1.5 mm or 1.0 mm on Figure 18A; 1.0 mm, 210 µm or 200 µm on Figure 18B.

CONCLUDING REMARKS AND FUTURE PERSPECTIVES

The breast is a highly complex tissue, characterized by dynamic interactions between its constituting cell types and the ECM, further exacerbated by the profound alterations occurring during a woman's life. From physiological menstruation cycles to menopause, and to pathological breast carcinomas formation, mammary cells are influenced by many factors, which are still poorly characterized. According to various studies, there is an essential crosstalk between mammary gland epithelial cells and stroma-producing cells, namely fibroblasts. Such interactions play a central role in both healthy and pathological processes occurring in breast tissue, but adequate *in vitro* models to dissect associated mechanisms are still scarce.

Up to now, most *in vitro* studies are overly focused on simplistic 2D *in vitro* models, which fail to adequately recapitulate cell-cell and cell-ECM interactions. On the other hand, studies using *in vivo* animal models are frequently too complex to use and analyze, as they do not allow isolating specific processes. More recently, the scientific community started to change the paradigm by recognizing the advantages of 3D culture models, which somehow fill the gap between the two previous model types. Adoption of innovative tissue and cellular engineering approaches, as well as biofabrication tools, has helped with the creation of advanced 3D models, that more faithfully mimic native *in vitro* environments. Yet, there are still very few breast tissue models that integrate its distinct constituents, namely for studying heterotypic cellular communication and the effect of the ECM on cells.

To address this unmet need, this work was focused on developing a complex, multicomponent, breast tissue 3D model for the study of healthy and pathological processes. Firstly, we developed a multi-layered 3D-printed alginate scaffold produced by customized design. This scaffold was obtained by extrusion-based 3D printing, which allowed fabrication of stable porous scaffolds, with reasonable shape fidelity. Pharmaceutical-grade alginate was used as scaffolding biomaterial and was chemically modified with integrin-binding RGD peptides to promote cell adhesion and facilitate scaffold colonization.

In a first step, optimized scaffolds were seeded with ECM-producing mammary fibroblasts. Seeding and culture processes were both improved, by varying different parameters such as RGD concentration, cell seeding density or alginate type, to achieve acceptable and uniform coverage of the scaffolds with cells and native ECM, without clogging the pores. Under optimal conditions, fibroblasts effectively adhered, spread and populated the scaffold in its full depth and produced endogenous ECM covering the alginate fibers and leaving the scaffold's

pores empty, as desired. Different components of the ECM were detected, including fibronectin and collagen type I and IV.

To study heterotypic interactions between stromal and parenchymal cells, human breast epithelial cells were added within a cell-laden alginate gel-precursor solution, also added on top of the structure. The solution filled the pores of the printed scaffold, forming a hydrogel inside, which promoted epithelial morphogenesis of these cells into spheroids and acinar-like structures. These structures become in close contact with fibroblasts and their ECM, as was clearly shown by CLSM analysis, allowing for cellular interactions.

To further demonstrate the potential of the proposed 3D model, which should allow performing a detailed characterization of both cell types after culture, a strategy was developed to retrieve cells from the scaffold and discriminate the different populations. Alginate was dissolved after reversing the crosslinking process with a chelating agent, and the recovered cells were stained with specific markers for flow cytometry analysis. Specific cell markers were tested for hMF and MCF10A cells, namely CD90 and E-cadherin, respectively. Although the process has not been fully optimized, this possibility is particularly interesting for future studies, as it will allow a much more comprehensive analysis of cellular interactions. Such achievement allows analysis to be performed by using imaging techniques, which do not require the scaffold to be dissolved, but it also clears the path for other types of methodologies for analyzing cells, at protein and gene expression levels, for example. Depending on the application, it will be very interesting to study how cells react to other cells and to the ECM, both under physiological and pathological settings.

Additionally, preliminary results were obtained on scaffold decellularization after fibroblast culture. This would allow the creation of a second model, which would not include coculturing hMFs, but using their matrix, working as a CDM where epithelial cells could be cultured and, again, cell-ECM interactions could be studied on an easily solubilized biomaterial substrate. Lastly, by downsizing the printed scaffolds, we started to develop a miniaturized version of the same model, where cells are not cultured onto whole scaffolds, but in punched round scaffolds. These scaffolds fit into 48-well or 96-well plates, depending on the puncher diameter and can greatly improve the throughput of the analysis.

Although significant achievements have been made during this work, further refining and optimization of this 3D model could be performed in the future, namely to improve the model's reproducibility. Furthermore, molecular and functional studies should be performed on the cultured cells to validate the purpose of this model, which is to investigate biological

processes occurring in breast tissue, related to both healthy and pathological conditions. Processes like the epithelial-to-mesenchymal (EMT) transition could be studied and correlated with contact between stromal and epithelial cells, to evaluate the effect of heterotypic communication on this metastasis-related process.

Importantly, this bioengineered platform could also be adapted for mimicking other tissues, with different cell types, to study other specific processes. It could also be used to culture patient-derived cells, serving as a personalized medicine *in vitro* platform for advanced study of different biological processes, which vary at the individual level.

This page was intentionally left in blank

REFERENCES

1 Lodish, H. *et al.* (2000) Integrating Cells into Tissues. In *Molecular Cell Biology* (4th edn) W. H. Freeman

2 Griffith, L.G. and Swartz, M.A. (2006) Capturing complex 3D tissue physiology in vitro. *Nat. Rev. Mol. Cell Biol.* 7, 211–224

3 Lee, J. *et al.* (2008) Three-Dimensional Cell Culture Matrices: State of the Art. *Tissue Eng. Part B Rev.* 14, 61–86

4 Frantz, C. *et al.* (2010) The extracellular matrix at a glance. *J. Cell Sci.* 123, 4195–4200

5 Lu, P. *et al.* (2012) The extracellular matrix: A dynamic niche in cancer progression. *J. Cell Biol.* 196, 395–406

6 Bhowmick, N.A. *et al.* (2004) Stromal fibroblasts in cancer initiation and progression. *Nature* 432, 332–337

7 Levental, K.R. *et al.* (2009) Matrix Crosslinking Forces Tumor Progression by Enhancing Integrin Signaling. *Cell* 139, 891–906

8 Erler, J.T. *et al.* (2006) Lysyl oxidase is essential for hypoxia-induced metastasis. *Nature* 440, 1222–1226

9 Kaplan, N.A. *et al.* (2009) Epithelial polarity: interactions between junctions and apical-basal machinery. *Genetics* 183, 897–904

10 Duval, K. *et al.* (2017) Modeling Physiological Events in 2D vs. 3D Cell Culture. *Physiology (Bethesda).* 32, 266–277

11 Rappel, W.-J. and Edelstein-Keshet, L. (2017) Mechanisms of Cell Polarization. *Curr. Opin. Syst. Biol.* 3, 43–53

12 Mak, M. *et al.* (2016) Single-Cell Migration in Complex Microenvironments: Mechanics and Signaling Dynamics. *J. Biomech. Eng.* 138, 021004

13 Tibbitt, M.W. and Anseth, K.S. (2009) Hydrogels as extracellular matrix mimics for 3D cell culture. *Biotechnol. Bioeng.* 103, 655–663

14 Kapałczyńska, M. *et al.* (2016) 2D and 3D cell cultures – a comparison of different types of cancer cell cultures. *Arch. Med. Sci.* 14, 910–919

15 Haycock, J.W. (2011) 3D Cell Culture: A Review of Current Approaches and Techniques. In *Methods in molecular biology (Clifton, N.J.)* 695pp. 1–15

16 Moran, C.J. *et al.* (2016) The benefits and limitations of animal models for translational research in cartilage repair. *J. Exp. Orthop.* 3, 1

17 Roskelley, C.D. *et al.* (1994) Extracellular matrix-dependent tissue-specific gene expression in mammary epithelial cells requires both physical and biochemical signal transduction. *Proc. Natl. Acad. Sci. U. S. A.* 91, 12378–82

18 Augst, A.D. *et al.* (2006) Alginate Hydrogels as Biomaterials. *Macromol. Biosci.* 6, 623–633

19 Hinderer, S. *et al.* (2016) ECM and ECM-like materials — Biomaterials for applications in

regenerative medicine and cancer therapy. *Adv. Drug Deliv. Rev.* 97, 260–269

20 Uchida, N. *et al.* (2016) Nanometer-sized extracellular matrix coating on polymer-based scaffold for tissue engineering applications. *J. Biomed. Mater. Res. Part A* 104, 94–103

21 Qian, Y. *et al.* (2015) The effect of hyaluronan on the motility of skin dermal fibroblasts in nanofibrous scaffolds. *Int. J. Biol. Macromol.* 79, 133–143

22 Bidarra, S.J. *et al.* (2014) Injectable alginate hydrogels for cell delivery in tissue engineering. *Acta Biomater.* 10, 1646–1662

23 Knight, E. and Przyborski, S. (2015) Advances in 3D cell culture technologies enabling tissue-like structures to be created in vitro. *J. Anat.* 227, 746–56

24 Huang, X. *et al.* (2012) Microenvironment of alginate-based microcapsules for cell culture and tissue engineering. *J. Biosci. Bioeng.* 114, 1–8

25 Sodunke, T.R. *et al.* (2007) Micropatterns of Matrigel for three-dimensional epithelial cultures. *Biomaterials* 28, 4006–4016

26 Campbell, J.J. and Watson, C.J. (2009) Three-dimensional culture models of mammary gland. *Organogenesis* 5, 43–9

27 Krause, S. *et al.* (2008) A Novel 3D *In Vitro* Culture Model to Study Stromal–Epithelial Interactions in the Mammary Gland. *Tissue Eng. Part C Methods* 14, 261–271

28 Caliari, S.R. and Burdick, J.A. (2016) A practical guide to hydrogels for cell culture. *Nat. Methods* 13, 405–414

29 Ladewig, K. (2011) Drug delivery in soft tissue engineering. *Expert Opin. Drug Deliv.* 8, 1175–1188

30 Zhou, K. *et al.* (2015) Preparation and characterization of hydroxyapatite–sodium alginate scaffolds by extrusion freeforming. *Ceram. Int.* 41, 14029–14034

31 Fonseca, K.B. *et al.* (2011) Molecularly designed alginate hydrogels susceptible to local proteolysis as three-dimensional cellular microenvironments. *Acta Biomater.* 7, 1674–1682

32 Chwalek, K. *et al.* (2014) Glycosaminoglycan-based hydrogels to modulate heterocellular communication in in vitro angiogenesis models. *Sci. Rep.* 4, 4414

33 Hall, John E. (John Edward), G. (2015) Female physiology before pregnancy and female hormones. In *Textbook of medical physiology* (13th edn) pp. 1145, Elsevier

34 Yu, J.H. *et al.* (2013) Breast diseases during pregnancy and lactation. *Obstet. Gynecol. Sci.* 56, 143

35 Dalal, P.K. and Agarwal, M. (2015) Postmenopausal syndrome. *Indian J. Psychiatry* 57, S222-32

36 White, E. *et al.* (1998) Variation in Mammographic Breast Density by Time in Menstrual Cycle Among Women Aged 40-49 Years. *JNCI J. Natl. Cancer Inst.* 90, 906–910

37 Farahmand, S. and Cowan, D.F. (1991) Elastosis in the normal aging breast. A histopathologic study of 140 cases. *Arch. Pathol. Lab. Med.* 115, 1241–6

38 Cichon, M.A. *et al.* (2010) Microenvironmental Influences that Drive Progression from Benign Breast Disease to Invasive Breast Cancer. *J. Mammary Gland Biol. Neoplasia* 15,

389–397

39 American Cancer Society (2018), Breast Density and Mammogram Reports | Dense Breast Tissue [Online]. Available: https://www.cancer.org/cancer/breast-cancer/screening-tests-and-early-detection/mammograms/breast-density-and-your-mammogram-report.html. [Accessed: 20-Apr-2019]

40 A Medium Corporation (2018), Breast Cancer: Invasive Ductal Carcinoma (IDC) [Online]. Available: https://medium.com/@indianflagco/breast-cancer-invasive-ductal-carcinoma-idc-19fc57e3743d. [Accessed: 20-Apr-2019]

41 Guiro, K. and Arinzeh, T.L. (2015) Bioengineering Models for Breast Cancer Research. *Breast Cancer (Auckl).* 9, 57–70

42 Bissell, M.J. (1981) The Differentiated State of Normal and Malignant Cells or How to Define a "Normal" Cell in Culture. *Int. Rev. Cytol.* 70, 27–100

43 Sanyal, S. (2014) Culture and Assay Systems Used for 3D Cell Culture. *Corning Cult. Assay Syst. Used 3D Cell Cult.*

44 Bidarra, S.J. *et al.* (2011) Injectable in situ crosslinkable RGD-modified alginate matrix for endothelial cells delivery. *Biomaterials* 32, 7897–7904

45 Emerman, J.T. *et al.* (1977) Hormonal effects on intracellular and secreted casein in cultures of mouse mammary epithelial cells on floating collagen membranes. *Proc. Natl. Acad. Sci. U. S. A.* 74, 4466–70

46 Bissell, M.J. *et al.* (1982) How does the extracellular matrix direct gene expression? *J. Theor. Biol.* 99, 31–68

47 Petersen, O.W. *et al.* (1992) Interaction with basement membrane serves to rapidly distinguish growth and differentiation pattern of normal and malignant human breast epithelial cells. *Proc. Natl. Acad. Sci. U. S. A.* 89, 9064–8

48 Nelson, C.M. and Bissell, M.J. (2005) Modeling dynamic reciprocity: engineering three-dimensional culture models of breast architecture, function, and neoplastic transformation. *Semin. Cancer Biol.* 15, 342–52

49 James-Bhasin, M. *et al.* (2018) A three-dimensional dense collagen hydrogel to model cancer cell/osteoblast interactions. *J. Funct. Biomater.* 9, 72

50 Chen, L. *et al.* (2012) The enhancement of cancer stem cell properties of MCF-7 cells in 3D collagen scaffolds for modeling of cancer and anti-cancer drugs. *Biomaterials* 33, 1437–1444

51 Ding, Y. *et al.* (2018) Three-dimensional tissue culture model of human breast cancer for the evaluation of multidrug resistance. *J. Tissue Eng. Regen. Med.* 12, 1959–1971

52 Bidarra, S.J. *et al.* (2016) A 3D in vitro model to explore the inter-conversion between epithelial and mesenchymal states during EMT and its reversion. *Sci. Rep.* 6, 27072

53 Cavo, M. *et al.* (2018) A new cell-laden 3D Alginate-Matrigel hydrogel resembles human breast cancer cell malignant morphology, spread and invasion capability observed "in vivo." *Sci. Rep.* 8, 5333

54 Wang, Y. *et al.* (2018) 3D hydrogel breast cancer models for studying the effects of hypoxia on epithelial to mesenchymal transition. *Oncotarget* 9, 32191–32203

55 Lochter, A. and Bissell, M.J. (1995) Involvement of extracellular matrix constituents in

breast cancer. *Semin. Cancer Biol.* 6, 165–173

56 Cunha, G.R. (1994) Role of mesenchymal-epithelial interactions in normal and abnormal development of the mammary gland and prostate. *Cancer* 74, 1030–44

57 Ghajar, C.M. and Bissell, M.J. (2008) Extracellular matrix control of mammary gland morphogenesis and tumorigenesis: insights from imaging. *Histochem. Cell Biol.* 130, 1105–18

58 Oskarsson, T. (2013) Extracellular matrix components in breast cancer progression and metastasis. *The Breast* 22, S66–S72

59 Arendt, L.M. *et al.* (2010) Stroma in breast development and disease. *Semin. Cell Dev. Biol.* 21, 11–8

60 Jaganathan, H. *et al.* (2014) Three-dimensional in vitro co-culture model of breast tumor using magnetic levitation. *Sci. Rep.* 4, 6468

61 Andersen, T. *et al.* (2015) 3D Cell Culture in Alginate Hydrogels. *Microarrays* 4, 133–61

62 Purcell, E.K. *et al.* (2009) Alginate composition effects on a neural stem cell-seeded scaffold. *Tissue Eng. Part C. Methods* 15, 541–50

63 Stabler, C. *et al.* (2001) The effects of alginate composition on encapsulated betaTC3 cells. *Biomaterials* 22, 1301–10

64 Haug, A. (1964) *Composition and properties of alginates*, Norwegian Institute of Seaweed Research.

65 LeRoux, M.A. *et al.* (1999) Compressive and shear properties of alginate gel: effects of sodium ions and alginate concentration. *J. Biomed. Mater. Res.* 47, 46–53

66 Sarker, M. *et al.* (2018) Influence of ionic crosslinkers (Ca^{2+} /Ba^{2+} /Zn^{2+}) on the mechanical and biological properties of 3D Bioplotted Hydrogel Scaffolds. *J. Biomater. Sci. Polym. Ed.* 29, 1126–1154

67 Dimonie, D. *et al.* (2013) Parameters influencing the properties of layered shaped ionotropic alginate hydrogels designed for soft tissue engineering. *Dig. J. Nanomater. Biostructures* 8, 1727–1738

68 Khavari, A. *et al.* (2016) Composite alginate gels for tunable cellular microenvironment mechanics. *Sci. Rep.* 6, 30854

69 Cavo, M. *et al.* (2016) Microenvironment complexity and matrix stiffness regulate breast cancer cell activity in a 3D in vitro model. *Sci. Rep.* 6, 35367

70 Chueh, B. *et al.* (2010) Patterning alginate hydrogels using light-directed release of caged calcium in a microfluidic device. *Biomed Microdevices* 12, 145–151

71 Zhu, B. *et al.* (2016) Enzymatic Hydrolysis of Alginate to Produce Oligosaccharides by a New Purified Endo-Type Alginate Lyase. *Mar. Drugs* 14, 108

72 Schneider, G.B. *et al.* (2004) The effect of hydrogel charge density on cell attachment. *Biomaterials* 25, 3023–3028

73 Lansdown, A.B. and Payne, M.J. (1994) An evaluation of the local reaction and biodegradation of calcium sodium alginate (Kaltostat) following subcutaneous implantation in the rat. *J. R. Coll. Surg. Edinb.* 39, 284–8

74 Kong, H.J. *et al.* (2004) Controlling Degradation of Hydrogels via the Size of Crosslinked Junctions. *Adv. Mater.* 16, 1917–1921

75 Lee, K.Y. and Mooney, D.J. (2012) Alginate: Properties and biomedical applications. *Prog. Polym. Sci.* 37, 106–126

76 Jeong, S.I. *et al.* (2010) Electrospun Alginate Nanofibers with Controlled Cell Adhesion for Tissue Engineering. *Macromol. Biosci.* 10, 934–943

77 Smetana, K. (1993) Cell biology of hydrogels. *Biomaterials* 14, 1046–50

78 Livingston, S. (2017) Cell Attachment to Alginate Hydrogel Structures. *J. Undergrad. Res.*

79 Rowley, J.A. and Mooney, D.J. (2002) Alginate type and RGD density control myoblast phenotype. *J. Biomed. Mater. Res.* 60, 217–23

80 Taketa, H. *et al.* (2015) Peptide-modified Substrate for Modulating Gland Tissue Growth and Morphology In Vitro. *Sci. Rep.* 5, 11468

81 Moroni, L. *et al.* (2018) Biofabrication strategies for 3D in vitro models and regenerative medicine. *Nat. Rev. Mater.* 3, 21–37

82 Zhang, Y.S. *et al.* (2018) Three-Dimensional Bioprinting Strategies for Tissue Engineering. *Cold Spring Harb. Perspect. Med.* 8, a025718

83 Paxton, N. *et al.* (2017) Proposal to assess printability of bioinks for extrusion-based bioprinting and evaluation of rheological properties governing bioprintability. *Int. Soc. Biofabrication* 9, 044107

84 Chung, J.H.Y. *et al.* (2013) Bio-ink properties and printability for extrusion printing living cells. *Biomater. Sci.* 1, 763

85 Ouyang, L. *et al.* (2016) Effect of bioink properties on printability and cell viability for 3D bioplotting of embryonic stem cells. *Biofabrication* 8, 035020

86 Wang, L. *et al.* (2012) Design and fabrication of a biodegradable, covalently crosslinked shape-memory alginate scaffold for cell and growth factor delivery. *Tissue Eng. Part A* 18, 2000–7

87 Regier, M.C. *et al.* (2016) Progress towards understanding heterotypic interactions in multi-culture models of breast cancer. *Integr. Biol. (Camb).* 8, 684

88 Arrigoni, C. *et al.* (2014) Direct but not indirect co-culture with osteogenically differentiated human bone marrow stromal cells increases RANKL/OPG ratio in human breast cancer cells generating bone metastases. *Mol. Cancer* 13, 238

89 Gambar, G. *et al.* (2018) From chemotherapy to combined targeted therapeutics: In vitro and in vivo models to decipher intra-tumor heterogeneity. *Front. Pharmacol.* 9, 1–18

90 Wang, X. *et al.* (2010) A complex 3D human tissue culture system based on mammary stromal cells and silk scaffolds for modeling breast morphogenesis and function. *Biomaterials* 31, 3920–9

91 Dondajewska, E. *et al.* (2017) Heterotypic breast cancer model based on a silk fibroin scaffold to study the tumor microenvironment. *Oncotarget* 9, 4935–4950

92 Estrada, M.F. *et al.* (2016) Modelling the tumour microenvironment in long-term microencapsulated 3D co-cultures recapitulates phenotypic features of disease progression. *Biomaterials* 78, 50–61

93 Li, L. and Lu, Y. (2011) Optimizing a 3D culture system to study the interaction between epithelial breast cancer and its surrounding fibroblasts. *J. Cancer* 2, 458–466

94 Zhang, G. *et al.* (2017) A simple 3D cryogel co-culture system used to study the role of CAFs in EMT of MDA-MB-231 cells. *RSC Adv.* 7, 17208–17216

95 Kassim, Y.L. *et al.* (2017) Three Dimensional Tumor Engineering by Co-Culture of Breast Tumor and Endothelial Cells Using a Hyaluronic Acid Hydrogel Model. *J. Clin. Exp. Oncol.* 06, 6–13

96 Hoshiba, T. *et al.* (2010) Decellularized matrices for tissue engineering. *Expert Opin. Biol. Ther.* 10, 1717–1728

97 Cukierman, E. *et al.* (2001) Taking Cell-Matrix Adhesions to the Third Dimension. *Science.* 294, 1708–1712

98 Harris, G.M. *et al.* (2018) Cell-derived decellularized extracellular matrices. *Methods Cell Biol.* 143, 97–114

99 Nagaoka, M. *et al.* (2010) Culture of human pluripotent stem cells using completely defined conditions on a recombinant E-cadherin substratum. *BMC Dev. Biol.* 10, 60

100 Serban, M.A. *et al.* (2008) Effects of extracellular matrix analogues on primary human fibroblast behavior. *Acta Biomater.* 4, 67

101 Fitzpatrick, L.E. and McDevitt, T.C. (2015) Cell-derived matrices for tissue engineering and regenerative medicine applications. *Biomater. Sci.* 3, 12–24

102 Hoshiba, T. (2017) Cultured cell-derived decellularized matrices: a review towards the next decade. *J. Mater. Chem. B* 5, 4322–4331

103 Crapo, P.M. *et al.* (2011) An overview of tissue and whole organ decellularization processes. *Biomaterials* 32, 3233–3243

104 Lourenço, B.N. *et al.* (2018) CD44v6 increases gastric cancer malignant phenotype by modulating adipose stromal cell-mediated ECM remodeling. *Integr. Biol.* 10, 145–158

105 Rueden, C.T. *et al.* (2017) ImageJ2: ImageJ for the next generation of scientific image data. *BMC Bioinformatics* 18, 529

106 Laboratories, S.R. (2012) Human Mammary Fibroblasts Culture - Protocol. 20, 2–4

107 invitrogen (2018) CellTracker ™ Fluorescent Probes - Product Information Sheet.

108 Hinton, T.J. *et al.* (2015) Three-dimensional printing of complex biological structures by freeform reversible embedding of suspended hydrogels. *Sci. Adv.* 1, e1500758

109 Freeman, F.E. and Kelly, D.J. (2017) Tuning Alginate Bioink Stiffness and Composition for Controlled Growth Factor Delivery and to Spatially Direct MSC Fate within Bioprinted Tissues. *Sci. Rep.* 7, 17042

110 Li, H. *et al.* (2016) Rheological study on 3D printability of alginate hydrogel and effect of graphene oxide. *Int. J. Bioprinting* 2, 163–175

111 Ozbolat, I.T. and Hospodiuk, M. (2016) Current advances and future perspectives in extrusion-based bioprinting. *Biomaterials* 76, 321–343

112 Das, S. *et al.* (2015) Bioprintable, cell-laden silk fibroin–gelatin hydrogel supporting multilineage differentiation of stem cells for fabrication of three-dimensional tissue

constructs. *Acta Biomater.* 11, 233–246

113 Tan, L. *et al.* (2012) A 1-min Method for Homogenous Cell Seeding in Porous Scaffolds. *J. Biomater. Appl.* 26, 877–889

114 Shi, L. *et al.* (2018) Three-dimensional printing alginate/gelatin scaffolds as dermal substitutes for skin tissue engineering. *Polym. Eng. Sci.* 58, 1782–1790

115 Chen, C.-Y. *et al.* (2015) 3D Porous Calcium-Alginate Scaffolds Cell Culture System Improved Human Osteoblast Cell Clusters for Cell Therapy. *Theranostics* 5, 643–655

116 Dar, A. *et al.* (2002) Optimization of cardiac cell seeding and distribution in 3D porous alginate scaffolds. *Biotechnol. Bioeng.* 80, 305–312

117 Freitas, R.A. (1999) Volume I: Basic Capabilities. In *Nanomedicine* (1st edn) pp. 523, Landes Bioscience

118 Vitacolonna, M. *et al.* (2013) Effect of static seeding methods on the distribution of fibroblasts within human acellular dermis. *Biomed. Eng. Online*

119 Lim, E.-H. *et al.* (2014) Nanotechnology Biomimetic Cartilage Regenerative Scaffolds. *Arch. Plast. Surg.* 41, 231

120 Levin, A. *et al.* (2018) The importance of factorial design in tissue engineering and biomaterials science: Optimisation of cell seeding efficiency on dermal scaffolds as a case study. *J. Tissue Eng.* 9, 1–14

121 Kumar Jena, M. *et al.* (2018) Role of extracellular matrix in breast cancer development: a brief update. *F1000 Res.* 7, 274

122 Sadlonova, A. *et al.* (2005) Breast fibroblasts modulate epithelial cell proliferation in three-dimensional in vitro co-culture. *Breast Cancer Res.* 7, R46-59

123 Roy, S. and Kornberg, T.B. (2015) Paracrine signaling mediated at cell-cell contacts. *Bioessays* 37, 25–33

124 Moraes, D.A. *et al.* (2016) A reduction in CD90 (THY-1) expression results in increased differentiation of mesenchymal stromal cells. *Stem Cell Res. Ther.* 7, 97

125 Sanders, Y.Y. *et al.* (2007) Enhanced Myofibroblastic Differentiation and Survival in Thy-1(−) Lung Fibroblasts. *Am. J. Respir. Cell Mol. Biol.* 36, 226–235

126 Andrews, J.L. *et al.* (2012) The role and function of cadherins in the mammary gland. *Breast Cancer Res.* 14, 203

127 Cichon, M.A. *et al.* (2015) Regulation of Epithelial-Mesenchymal Transition in Breast Cancer Cells by Cell Contact and Adhesion. *Cancer Inform.* 14, 1

128 Montanez-Sauri, S.I. *et al.* (2015) Microscale screening systems for 3D cellular microenvironments: platforms, advances, and challenges. *Cell. Mol. Life Sci.* 72, 237–249

129 Joshi, P. and Lee, M.-Y. (2015) High Content Imaging (HCI) on Miniaturized Three-Dimensional (3D) Cell Cultures. *Biosensors* 5, 768–790

SUPPLEMENTARY INFORMATION

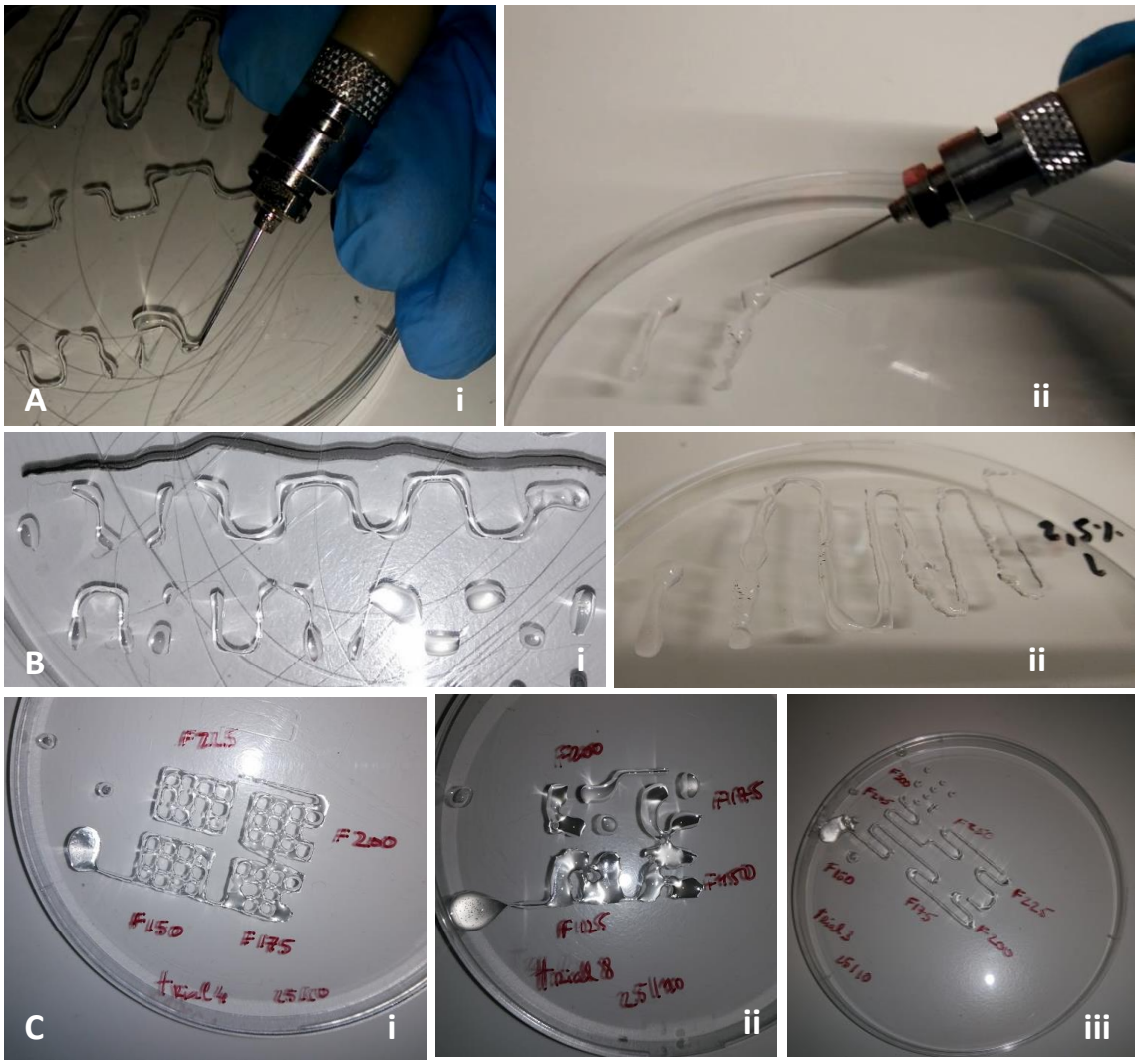

Figure S 1 Manual testing of alginate formulations with the 210 µm-printing needle. **A**) 3 wt.% ALG crosslinked with 7.5 mM $CaCl_2$. **B**) 2.5 wt.% ALG crosslinked with 10 mM $CaCl_2$. **C**) Loss of shape of alginate filaments after printing

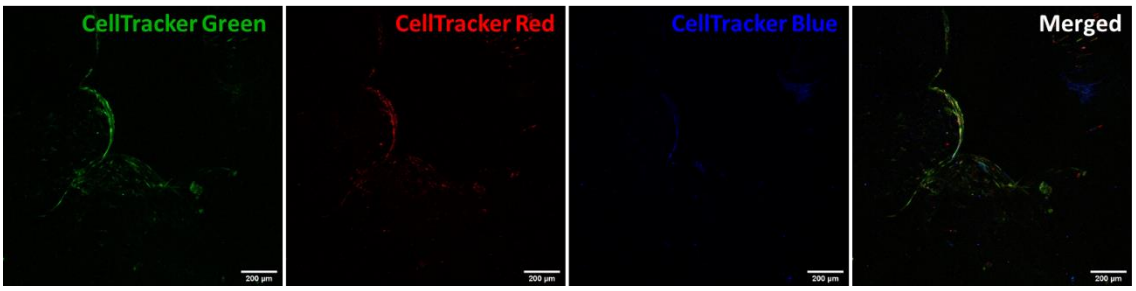

Figure S 2 Phased cell seeding experiment with CellTracker™-stained human mammary fibroblasts, to analyze cell growth throughout time. CLSM image taken at day 10 after CellTracker™ Green-stained cells seeding, day 7 after CellTracker™ Red-stained cells seeding and day 4 after CellTracker™-Blue stained cell seeding. Scale bar: 200 µm, 10x magnification

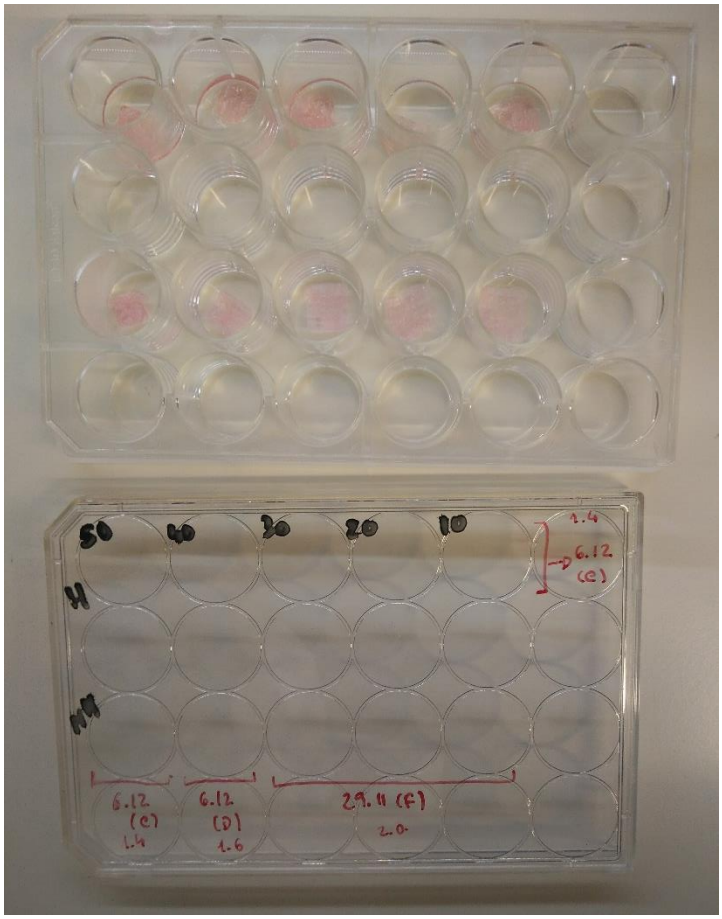

Figure S 3 Optimization of hMF seeding volume performed with pre-hydrated and de-hydrated structures (simulating the lyophilized and non-lyophilized scaffolds). From left to right, seeding volume decreases from 50 µL to 10 µL. First row of scaffolds is only comprised of hydrated replicates, while the second row is only non-hydrated (lyophilized) ones

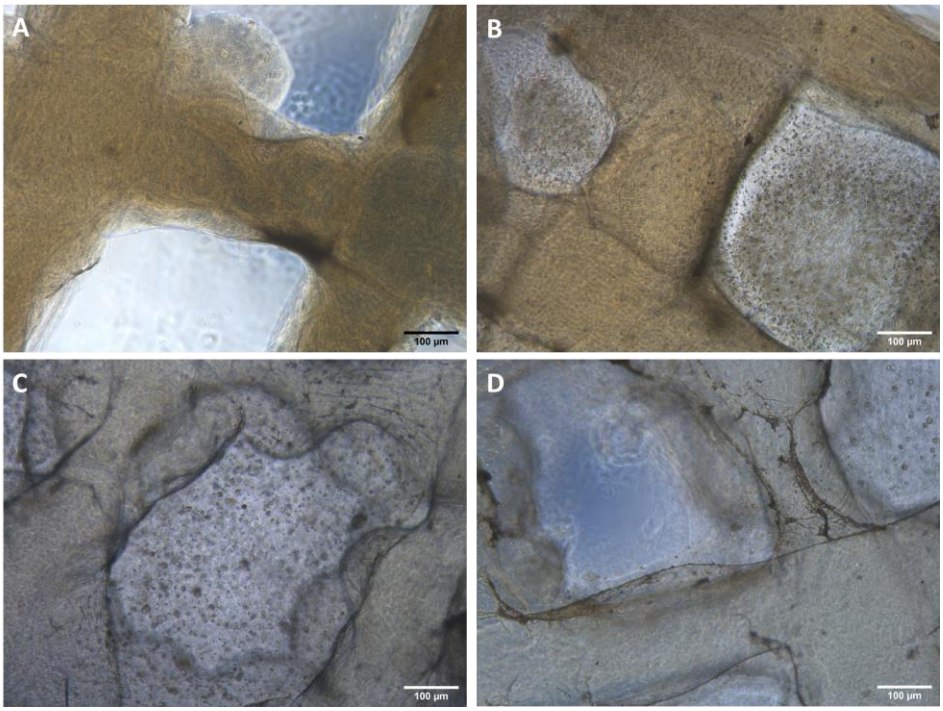

Figure S 4 Optimization of hMF seeding by entrapping hMFs within non-modified alginate-thickened cell culture medium. Alginate concentrations in DMEM GlutaMax™ varied: **A**) 0.1% w/v, **B**) 0.25 % w/v, **C**) 0.5% w/v, **D**) 0.75% w/v. In each of these concentrations, hMFs were found entrapped hours and days post-seeding, which means they could not escape from this thickened media to adhere to the scaffolds. Scale bar: 100 µm, 10x magnification

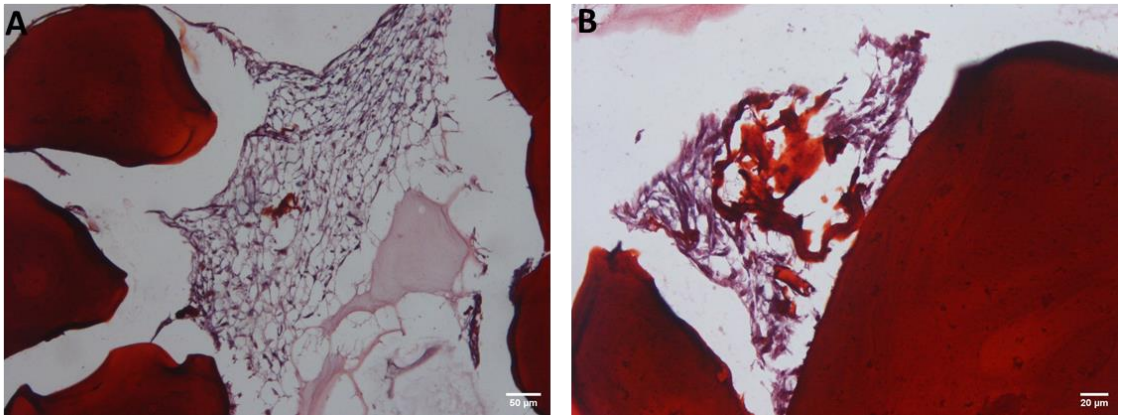

Figure S 5 Histologic characterization of hMFs cultured on alginate scaffolds. 6-µm vertical histologic cuts stained with safranin and hematoxylin. Alginate is stained in red (O-safranin) while nuclei are stained in purple (hematoxylin). **A**) shows the cross-section of the alginate structure with the hMFs network surrounding the alginate fibers (10x magnification), **B**) shows a close-up on the fibroblast-mesh with 20x magnification. Scale bars: 50 µm and 20 µm

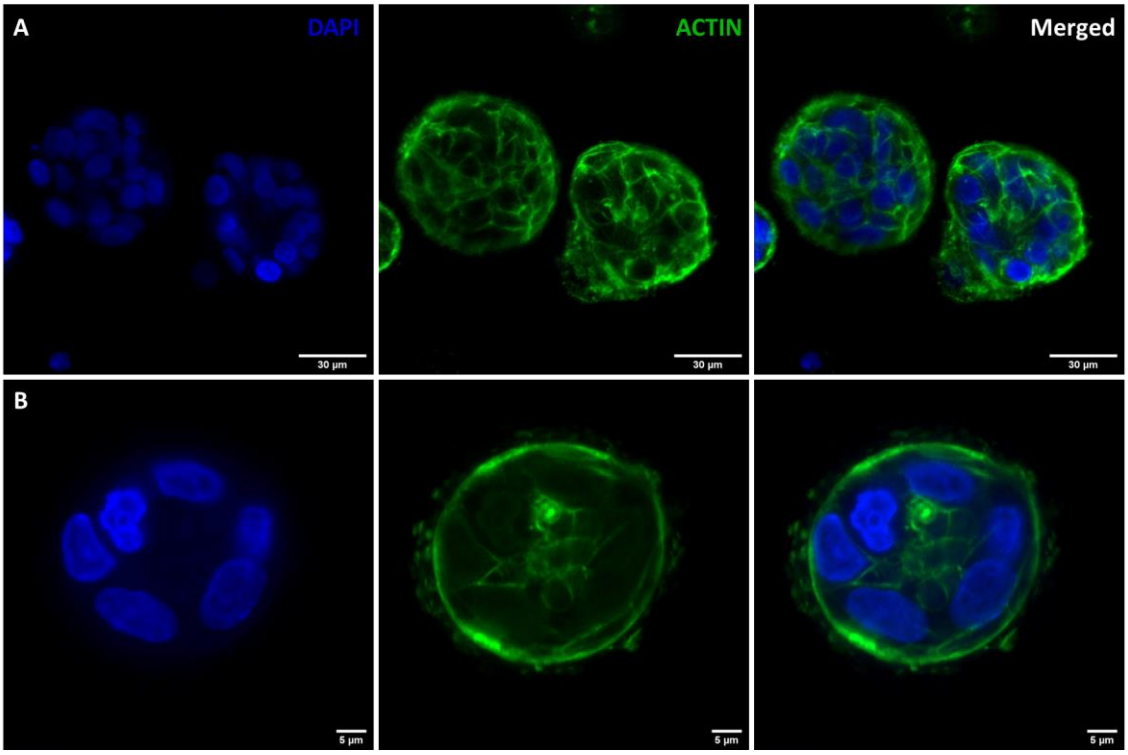

Figure S 6 Representative CLSM images of MCF10A epithelial cells forming acinar-like structures when cocultured with hMFs in an alginate environment. **A**) 63x magnification of two acini on different stages of development. Right: formation of luminal-like architecture inside the acinar structure; Left: cells dividing/organizing inside the acinus. **B**) 63x magnification, 4x zoomed-in image of a single acinar-like structure, seemingly going through lumenization. Scale bar: 30 µm and 5 µm

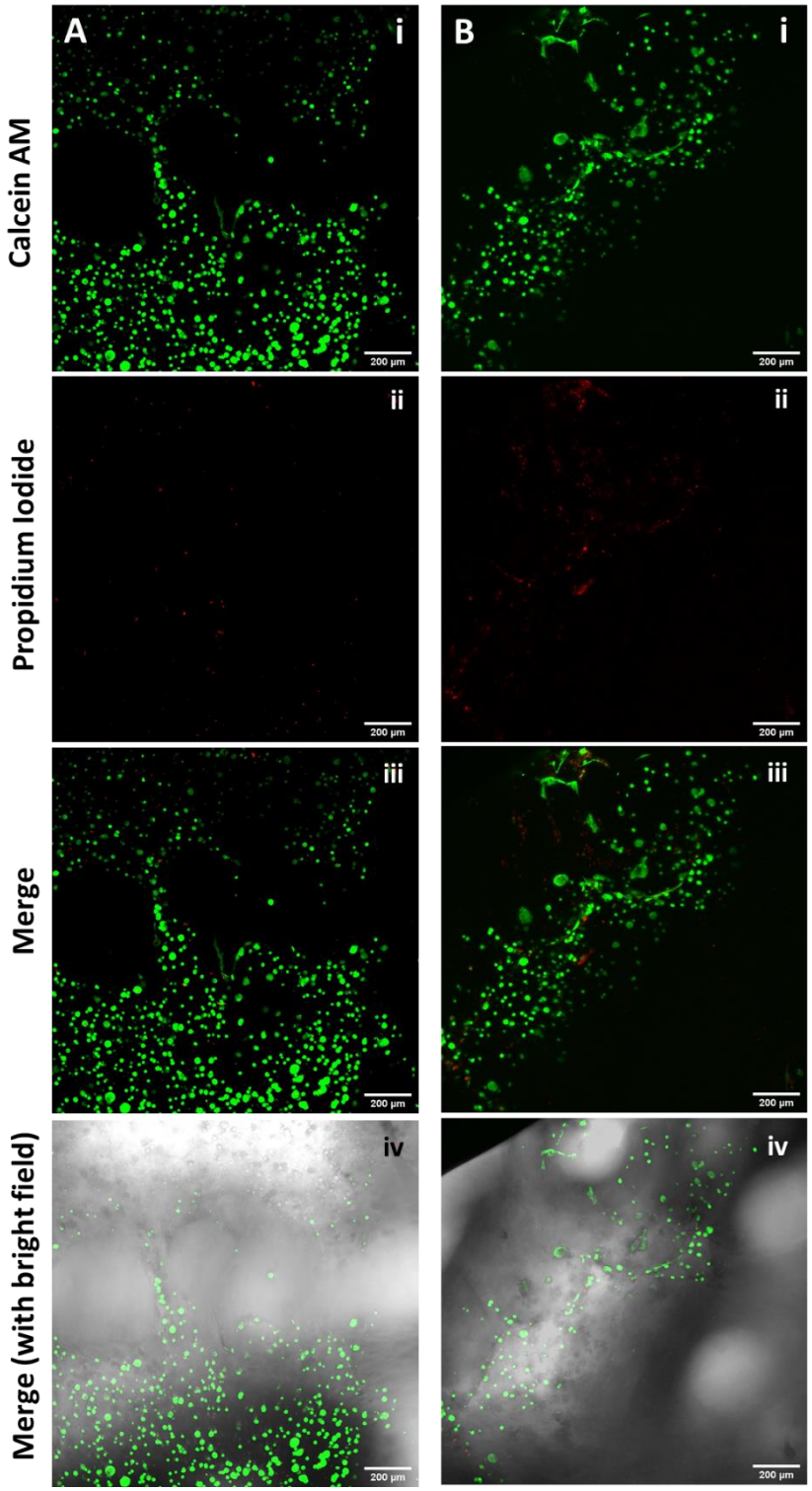

Figure S 7 Live/Dead assay of fibroblasts (hMFs) and epithelial cells (MCF10A) incubated on top of ALG scaffolds after 28 days of culture. **A** and **B** show two different scaffold areas, where live cells are represented in green and dead cells in red. Scale bar: 200 µm, 10x magnification

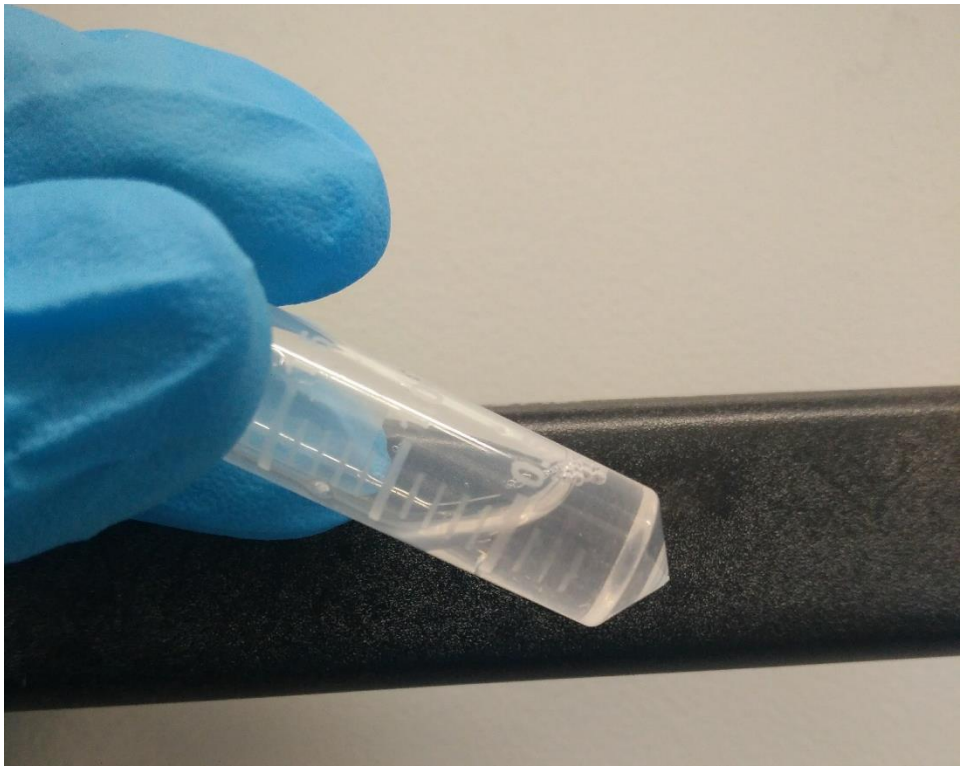

Figure S 8 Alginate scaffold dissolved after 5 minutes in trypsin/EDTA solution

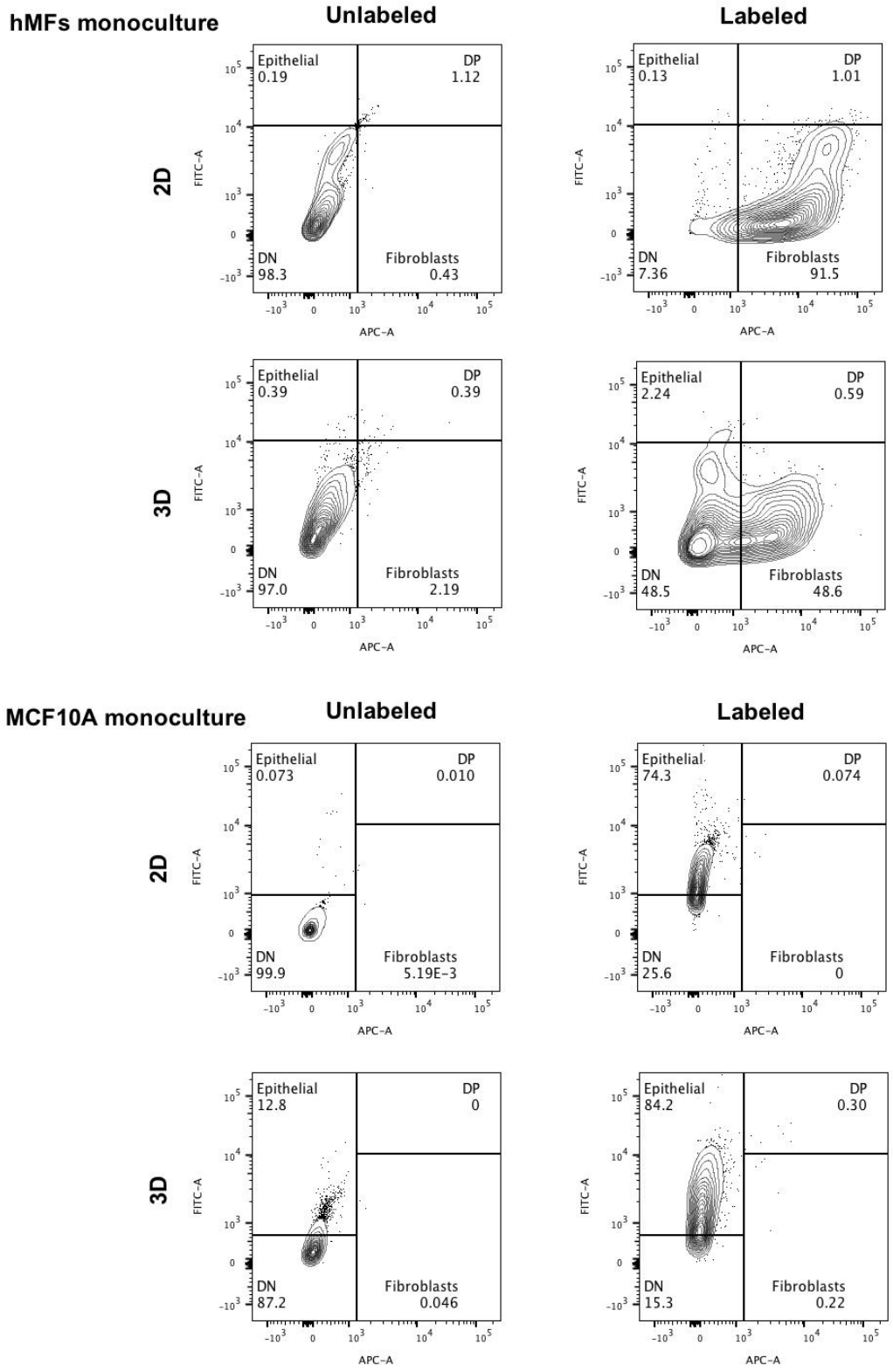

Figure S 9 FACS gating strategy of hMFs (top plots) and MCF10A (bottom plots) monocultures. Fibroblasts show auto-fluorescence going into the FITC channel. To avoid an "epithelial" population on the hMF monocultures, the gate for double-negative (DN) cells was elevated. 3D culture does not show as high auto-fluorescence as in 2D. Gates for MCF10A monocultures were adjusted to epithelial populations.

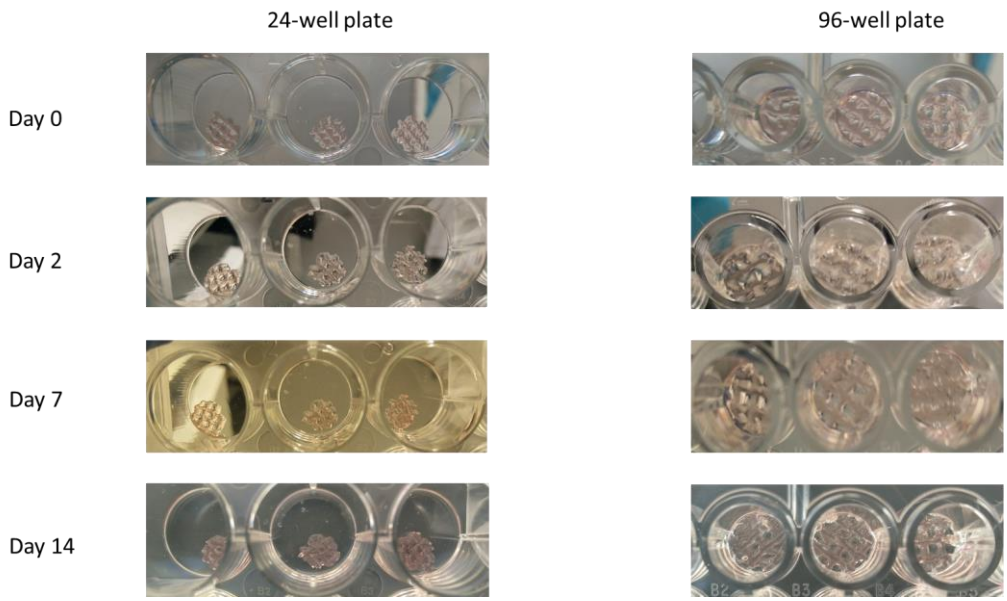

Figure S 10 Testing of miniaturized scaffolds' response to immersion in media during the period of culture time. Pictures of the scaffolds were taken at days 0, 2, 7 and 14 after media immersion, and media was changed every 2 days, to mimic cell culture conditions. Scaffolds were kept in a 24- and a 96-well plate for comparison reasons, to see if the well size had any repercussion on the maintenance of the scaffold's structure.